

**CATALYTIC PYROLYSIS OF HEAVY DISTILLATE FROM PLASTIC  
WASTE INTO A DIESEL RANGE FUEL**

**BY  
OKINO JASPER**

A Thesis Submitted to the School of Engineering, Department of Mechanical,  
Production and Energy Engineering in Partial Fulfilment of the Requirements for the  
Award of Degree of Master of Science in Energy Studies (Renewable Energy)


Moi University

**2023**

## DECLARATION

### Declaration by Candidate

This thesis is my original work and has not been presented for a degree at any other University. No part of this thesis may be reproduced without the prior written permission of the author and/or Moi University.


Okino Jasper ..... 

Date: 3<sup>rd</sup> August 2023

MS/MES/5506/21


### Declaration by the Supervisors

This thesis has been submitted with our approval as University Supervisors.

Prof. Zachary Otara Siagi .....  Date: 3<sup>rd</sup> August 2023

Department of Mechanical, Production and Energy Engineering,

Moi University, Eldoret, Kenya

Prof. Anil Kumar .....  Date: 3<sup>rd</sup> August 2023

Department of Chemical and Process Engineering,

Moi University, Eldoret, Kenya

## DEDICATION

This thesis is dedicated to my mother, **Esther Acen**; father, **Charles Ojok**; wife, **Vicky Atworo**; son, **Emmanuel Ojok**, daughter, **Praise Acen**, and my beloved family members.

## ACKNOWLEDGEMENTS

Firstly, I thank the Almighty God for the protection and good health throughout my graduate studies. I deeply acknowledged my supervisors **Prof. Zachary Otara Siagi** and **Prof Anil Kumar** whose constant invaluable guidance, encouragement, constructive comments, and research expertise enhanced my piecing and prolific write-up of this thesis work.

I am most indebted to the **Mobility for Innovative Renewable Energy Technologies (MIRET)** project under the Intra Africa Academic Mobility Scheme of the European Union for the scholarship awarded to me through the Africa Center of Excellence II in Phytochemicals, Textiles and Renewable Energy (ACE II PTRE), Moi University that fully supported this degree program financially. Special thanks go to **Prof Henry Kirimi Kiriamiti**, Lead Coordinator – MIRET and **Prof Ambrose Kiprop**, Centre Leader – ACE II PTRE, and **Dr. Stephen Talai** -Postgraduate Coordinator – Department of Mechanical, Production and Energy Engineering, Moi University for their invaluable support and guidance during my stay at the university.

I extend my sincere appreciation to my father, **Charles Ojok**, and my mother, **Esther Acen** for their love and comfort rendered to me during this research work. I also extend brotherly gratitude to **Agnes Apio, Moses Odul, Alex Awio, Morrish Okori, Kevin Ayugi, Felix Ongora, Dina Awidi**, and **Florence Atala** for generous love given to me during my studies.

Lastly, I deeply acknowledged my lovely wife, **Vicky Atworo**, dear son, **Emmanuel Ojok** and daughter, **Praise Acen** who pricelessly accepted me out of the family circle, and gave me a strong moral support and constant love toward the success of this research work.

## ABSTRACT

Heavy distillate is a heavy fraction of plastic pyrolysis characterized by high viscosity, long-chain hydrocarbons which makes it low-graded biproduct. Catalytic pyrolysis is amongst the promising upgrading techniques which has greater comparative advantage over thermal pyrolysis in cost control and lowering reaction temperature/time. Clay-based catalyst has not been adequately assessed in enhancing HD pyrolysis product yield and there is limited knowledge on HD thermal characteristics. The main objective of this study was to upgrade HD from plastic waste into a diesel range fuel through catalytic pyrolysis. The specific objectives were to: characterize HD from plastic waste; produce diesel-like product from HD through catalytic pyrolysis; analyse effects of catalyst ratio and operating temperatures on product yield; and characterize the properties of fuel produced. The HD was obtained from Alternative Energy Systems Limited, Thika – Kenya. The thermal properties of HD were analyzed with simultaneous thermal analyzer at heating rates (5,10,15,20 °C/min) and ascertained using modified Coats Redfern method. A central composite design - response surface methodology was employed on a batch reactor with design matrix: reaction temperatures (350,375,400 °C), heating times (90,120,150 mins) during thermal pyrolysis; catalyst ratios (5,10,15%) added during catalytic pyrolysis. Kaolin was used as a catalyst to boost product yield. Design Expert and Minitab software were employed to analyze effects of process parameters on product yield. The HD and pyrolytic liquid oils (PLOs) were characterized based on Fourier transform infrared (FTIR), physical properties, elemental and gas chromatography-mass spectroscopy (GC-MS) analyses. At respective heating rates, derivative thermogravimetric curves indicate that HD structures break at 285.77, 290.63, 327.02, 343.46 °C, and fully decompose at 365.83, 391.38, 412.42, 424.40 °C; activation energy values during decomposition phase (63.04, 61.52, 70.16, 65.57 kJ/mol) were slightly lower than heavy crude oils (50-177 kJ/mol). The FTIR spectra of HD&PLOs showed presence of symmetric and asymmetric stretching modes for methyl/CH<sub>3</sub>, methylene/CH<sub>2</sub>, and methylidyne/C-H. The oil yields (73.28, 70.13, 20.50, 28.50 wt%) obtained with catalytic pyrolysis matrix (400 °C,5%,150 min; 400 °C,15%,150 min; 350 °C,5%,150 min; 350 °C,5%,150 min) were higher than those without catalyst (18.88, 63.63 wt%) from process matrix (350 °C,150 min; 400 °C,150 min). The Pareto, normal and surface plots divulged that oil yields largely depended on temperature as compared to catalyst ratio, heating time, and factor interactions. GC-MS results established heavy carbon range (>C<sub>23</sub>) noticeably decreased in area percentages from HD (41.82 wt%) to without catalyst (10.03 wt%) and with catalyst (8.88 wt%) where more diesel range organics (C<sub>6</sub>-C<sub>23</sub>) were produced. The density (864, 779, 788 kg/m<sup>3</sup>), viscosity (14.00, 2.63, 2.88 cSt), and calorific value (44.52, 46.62, 47.23 MJ/kg) of HD, PLOs without and with catalyst, respectively compares favorably to diesel heating value (46 MJ/kg), elemental compositions increased in carbon contents (77.21, 83.24, 84.83 wt%) and decreased in hydrogen, nitrogen, sulphur and oxygen contents. In conclusion, the kaolin had a substantial role to enhance oil yields during pyrolysis than thermal pyrolysis and oil products are potential substitute for diesels. Further studies on desulfurization and dehalogenation of PLOs are suggested to obtain better diesel fuel.

## TABLE OF CONTENTS

DECLARATION .....	ii
DEDICATION .....	iii
ACKNOWLEDGEMENTS .....	iv
ABSTRACT.....	v
TABLE OF CONTENTS.....	vi
LIST OF FIGURES .....	xii
LIST OF PLATES .....	xv
ABBREVIATIONS AND ACRONYMS .....	xvi
DEFINITIONS OF TERMS .....	xvii
<b>CHAPTER ONE .....</b>	<b>1</b>
<b>INTRODUCTION.....</b>	<b>1</b>
1.1 Background of the Study .....	1
1.2 Statement of the Problem.....	5
1.3 Objectives .....	5
1.3.1 Main Objective.....	5
1.3.2 Specific Objectives .....	6
1.4 Justification of the study .....	6
1.5 Significance of the Study .....	7
1.6 Research Questions .....	7
1.7 Scope of the Study .....	7
1.8 Limitations .....	8
<b>CHAPTER TWO .....</b>	<b>9</b>
<b>LITERATURE REVIEW .....</b>	<b>9</b>
2.1 Introduction.....	9
2.2 Plastics Waste Scenario .....	9
2.3 Plastic Waste Management Techniques.....	10

2.4 Heavy Distillate from Plastic Pyrolysis .....	12
2.5 Upgrade of Heavy Oil .....	13
2.6 Heavy Distillate Degradation .....	15
2.7 Chemistry of Heavy Distillate .....	16
2.8 Thermal Decomposition of Heavy Distillate .....	17
2.8.1 Saturates .....	18
2.8.2 Aromatics .....	18
2.8.3 Resins .....	19
2.8.4 Asphaltenes .....	20
2.9 Chemistry of Catalytic Cracking of Heavy Distillate .....	21
2.10 Kinetics of Polymer Substance .....	22
2.10.1 Estimation of Activation Energy from thermal analysis.....	25
2.10.2 Thermodynamics parameters analysis of Polymer Sample .....	26
2.11 Kaolin clay catalyst for Heavy distillate Pyrolysis .....	27
2.12 Heavy oil properties .....	28
2.12.1 Density .....	28
2.12.2 Kinematic viscosity .....	29
2.12.3 Pour and cloud points.....	29
2.12.4 Flash Point .....	30
2.12.5 Calorific value.....	30
2.13 Types of Pyrolysis.....	31
2.13.1 Thermal Pyrolysis .....	31
2.13.2 Catalytic Pyrolysis .....	32
2.13.3 Microwave pyrolysis.....	33
2.14 Common Factors affecting process reactors .....	33
2.14.1 Types of pyrolysis reactors .....	33
2.14.1.1 Batch and semi-batch reactors .....	33

2.14.1.2 Fixed bed reactors.....	34
2.14.1.3 Fluidized-bed reactors .....	34
2.14.1.4 Spouted bed reactors.....	35
2.14.1.5 Screw kiln reactors .....	35
2.14.2 Catalysts used.....	36
2.14.2.1 Homogeneous catalysts .....	37
2.14.2.2 Heterogenous catalysts .....	37
2.14.3 Operating temperatures.....	38
2.14.4 Residence and heating times.....	39
2.15 Common Analytical techniques for heavy distillate and oil product analysis.....	40
2.15.1 Gas chromatography-mass spectroscopy technique .....	40
2.15.2 Infrared spectroscopy .....	41
2.15.3 Nuclear magnetic resonance spectroscopy .....	42
2.15.4 Scanning Electron Microscopy and Energy Dispersive X-ray .....	42
2.16 Thermal Analysis of Polymer Substance.....	43
2.16.1 Thermogravimetric Analysis (TGA).....	43
2.16.2 Differential Thermal Analysis (DTA) .....	44
2.16.3 Differential Scanning Calorimetry.....	44
2.16.4 Simultaneous Thermal Analyzer (STA) .....	45
2.17 Analytical Techniques Suitable for Kaolin Characterization .....	45
2.17.1 Atomic Absorption Spectrometry (AAS) Analysis .....	45
2.17.2 X-Ray Fluorescence Spectrophotometer (XRFS) Analysis.....	46
2.17.3 X-Ray Diffraction (XRD) Analysis.....	46
2.18 Design of Experiment (DOE) .....	47
2.19 Literature Summary .....	48
<b>CHAPTER THREE</b> .....	<b>50</b>
<b>MATERIALS AND METHODS</b> .....	<b>50</b>



3.1 Introduction.....	50
3.2 Materials Used .....	50
3.2.1 Collection and preparation of HD sample .....	50
3.2.2 Kaolin collection, preparation and characterization .....	50
3.2.2.1 Moisture content of fresh Kaolin.....	51
3.2.2.2 XRF Analysis of Kaolin Clay.....	51
3.3 Equipment Used.....	52
3.4 Experimental Procedure.....	55
3.5 Experimental Design.....	58
3.5.1 Statistical Analysis of Selected Process Parameters .....	61
3.6 Characterization of heavy distillate from plastic waste .....	61
3.6.1 Physical properties .....	61
3.6.1.1 Determination of density of heavy distillate.....	62
3.6.1.2 Determination of Calorific (Heating) Value.....	62
3.6.1.3 Determination of kinematic and dynamic viscosities.....	63
3.6.2 Elemental Analysis .....	63
3.6.3 Thermal Properties.....	64
3.6.3.1 Thermogravimetric Analysis (TGA) .....	64
3.6.3.2 Heat flow profiles .....	65
3.6.4 FTIR Analysis.....	65
3.6.5 GC-MS Analysis.....	66
3.7 Characterization of Fuel Properties .....	67
3.7.1 Determination of Density.....	67
3.7.2 Flash point Determination.....	67
3.7.3 Freezing and Pour points Determination .....	67
3.7.4 Determination of pH .....	67
3.8 Data Analysis .....	68

3.9 Methodology Summary .....	69
<b>CHAPTER FOUR</b> .....	70
<b>RESULTS AND DISCUSSION</b> .....	70
4.1 Introduction.....	70
4.2 Kaolin Clay Characterization.....	70
4.2.1 Moisture Content of Kaolin Clay.....	70
4.2.2 XRF Analysis Results of Kaolin from Eburru Hill.....	71
4.3 Heavy Distillate Characterization .....	73
4.3.1 FT-IR Analysis results .....	74
4.3.2 Kinetic analysis results for heavy distillate .....	77
4.3.3 Activation Energy and other thermodynamic behaviors of HD .....	78
4.3.4 Rate constant and Half-life of Heavy distillate.....	81
4.3.5 Weight Loss of HD at the various Heating rates .....	82
4.3.6 Decomposition of Heavy Distillate at different Heating Rates .....	84
4.3.7 Derivative Thermogravimetric (DTG) Curves of HD .....	85
4.3.8 Heat Flow of HD at various heating rates.....	86
4.4 Thermal and catalytic pyrolysis experimental results.....	87
4.5 Length of pyrolysis time effect on oil yield.....	92
4.6 Analyzing the effects of process parameters on Oil yield .....	95
4.6.1 Analysis of variance for PLO yield .....	95
4.6.2 Pareto plot of oil yield from thermal pyrolysis of heavy distillate .....	101
4.6.3 Normal Plot of standardized effects on oil yield from thermal pyrolysis.....	102
4.6.4 Contour Plots of oil yield generated from TP and CP .....	104
4.6.5 RSM of Diesel Oil yield from Thermal Pyrolysis of Heavy distillate.....	105
4.7 Characterization results for Fuel Properties.....	107
4.7.1 Physical Properties.....	108
4.7.2 Elemental analysis results .....	110

4.7.3 GC-MS analysis results of HD and PLOs.....	111
<b>CHAPTER FIVE</b> .....	115
<b>CONCLUSION AND RECOMMENDATIONS</b> .....	115
5.1 Conclusion .....	115
5.2 Recommendations.....	116
5.3 Research Contribution .....	116
<b>REFERENCES</b> .....	118
<b>APPENDICES</b> .....	138
Appendix A: Kaolin Preparation and Sieving .....	138
Appendix B: Heavy Distillate sample and Pyrolysis of HD into Diesel Fuel .....	139
Appendix C: GC-MS Analysis results of HD and PLOs.....	141
Appendix D: GC-MS Spectra of heavy distillate and pyrolytic liquid oils .....	149
Appendix E: Activation energy of HD with MCRM at various phases .....	151
Appendix F: Rate constants of HD from slope of $\ln(1-x)$ against time .....	153
Appendix G: Calculation of thermodynamics parameters of HD.....	155

## LIST OF FIGURES

Figure 2.1: Flow Chart showing production of HD from plastic pyrolysis .....	13
Figure 2.2: The Components of Heavy Distillate .....	17
Figure 2.3: Structure depiction for resins, saturates, asphaltenes and aromatics.....	17
Figure 2.4: The Chemistry of Catalytic Cracking of Heavy Distillate .....	22
Figure 2.5: Natural logarithm of residual mass against reciprocal Temperature.....	24
Figure 3.1: Flowchart showing description of modified brick electric furnace.....	54
Figure 3.2: Pyrolysis setup showing cross-section of a Batch Reactor .....	56
Figure 3.3: Flow Chart showing methodology overview .....	69
Figure 4.1: FTIR Spectra of Heavy Distillate and pyrolytic liquid (Diesel) Oils.....	76
Figure 4.2: MCRM curve of heavy distillate at different heating rates .....	81
Figure 4.3: Plot for Determination of Rate Constant and Half-Life of HD.....	82
Figure 4.4: Thermogram of HD sample at different heating rates.....	84
Figure 4.5: Derivative Thermogram of HD sample at different heating rates.....	86
Figure 4.6: Heat Flow Curve of HD Sample at various heating rates .....	87
Figure 4.7: Formation of diesel-like oil with time during TP.....	94
Figure 4.8: Formation of diesel-like oil with time during CP.....	94
Figure 4.9: Comparison of Predicted and actual oil yields from TP and CP.....	98
Figure 4.10: Pareto plots (a, b) on oil yield from TP and CP of heavy distillate.....	102
Figure 4.11: Normal plots (a, b) on oil yield from TP and CP of heavy distillate.....	104
Figure 4.12: Contour Plots on oil yield from TP and CP of Heavy Distillate .....	105
Figure 4.13: RSM plot on oil yield from TP of Heavy distillate .....	107
Figure 4.14: RSM plot on oil yield from CP of heavy distillate.....	107
Figure 4.15: Distribution of hydrocarbon groups in HD and PLOs .....	113
Figure D. 1: GC-MS Spectra of Heavy distillate .....	149
Figure D. 2: GC-MS Spectra of Pyrolytic liquid oil (without catalyst).....	149
Figure D. 3: GC-MS Spectra of Pyrolytic liquid oil (with catalyst).....	150
Figure E. 1: Dehydration phase of HD at various heating rates with MCRM.....	151
Figure E. 2: Decomposition phase of HD at various heating rates with MCRM .....	151
Figure E. 3: Condensation phase of HD at various heating rates with MCRM.....	152
Figure F. 1: Dehydration phase of HD from $\ln(1-x)$ vs. time .....	153
Figure F. 2: Decomposition phase of HD from $\ln(1-x)$ vs. time.....	154
Figure F. 3: Condensation phase of HD from $\ln(1-x)$ vs. time .....	154

## LISTS OF TABLES

Table 2.1: Plastic Group and Source.....	10
Table 2.2: The Summary of Selected Literatures .....	49
Table 3.1: Specifications of Modified Brick Electric Furnace .....	55
Table 3.2: Number of Factors and $\alpha$ Value for TP experiment .....	59
Table 3.3: Number of Factors and $\alpha$ Value for CP experiment .....	60
Table 3.4: Design Matrix for DOE for Thermal pyrolysis .....	60
Table 3.5: Design Matrix for DOE for Catalytic Pyrolysis .....	60
Table 4.1: XRF analysis result of Kaolin from Eburru Hill .....	73
Table 4.2: Band Assignment for Infrared Spectra of HD and PLOs .....	77
Table 4.3: Activation Energy and other thermodynamic Properties of HD .....	82
Table 4.4: Thermogravimetric Analysis of HD showing remaining weight percent...83	83
Table 4.5: Decomposition of HD at different heating rates.....	85
Table 4.6: TP experimental results .....	91
Table 4.7: CP experimental results .....	92
Table 4.8: Sequential model sum of squares of PLO yield from TP .....	99
Table 4.9: Sequential model sum of squares of PLO yield from CP.....	99
Table 4.10: ANOVA for quadratic model of PLO yield from TP .....	100
Table 4.11: ANOVA for quadratic model of PLO yield from CP.....	100
Table 4.12: Coefficients for the quadratic model of PLO yield from TP .....	101
Table 4.13: Coefficients for a quadratic model of PLO yield from CP.....	101
Table 4.14: Physical properties of HD and PLOs.....	108
Table 4.15: Elemental composition of HD and PLOs .....	111
Table 4.16: Carbon distribution and heavy carbon (>C23) in HD and PLOs.....	111
Table A. 1: Moisture Content of Kaolin Clay.....	138
Table B. 1: Density of Heavy Distillate.....	140
Table C. 1: GC-MS analysis results of organic compounds identified in HD.....	141
Table C. 2: GC-MS Analysis of PLO obtained from thermal pyrolysis.....	143
Table C. 3: GC-MS Analysis of PLO obtained from catalytic pyrolysis .....	145
Table G. 1: Activation energy of HD from MCRM at 5 oC/min .....	155
Table G. 2: Frequency factor of HD at 5 °C/min from MCRM at respective phases	155
Table G. 3: Entropy changes of HD at 5 °C/min from MCRM at respective phases	155
Table G. 4: Enthalpy and Gibbs Free Energy changes of HD at 5 °C/min.....	156

Table G. 5: Activation energy of HD from MCRM at 10 °C/min .....	156
Table G. 6: Frequency factor of HD at 10 °C/min from MCRM.....	156
Table G. 7: Entropy changes of HD at 10 oC/min from MCRM .....	157
Table G. 8: Enthalpy and Gibbs Free Energy changes of HD at 10 oC/min .....	157
Table G. 9: Activation energy of HD from MCRM at 15 °C/min .....	157
Table G. 10: Frequency factor of HD at 15 °C/min from MCRM.....	158
Table G. 11: Entropy changes of HD at 15 °C/min from MCRM.....	158
Table G. 12: Enthalpy and Gibbs Free Energy changes of HD at 15 °C/min.....	158
Table G. 13: Activation energy of HD from MCRM at 20 °C/min .....	159
Table G. 14: Frequency factor of HD at 20 °C/min from MCRM.....	159
Table G. 15: Entropy changes of HD at 20 °C/min from MCRM.....	159
Table G. 16: Enthalpy and Gibbs Free Energy changes of HD at 20 °C/min.....	159

**LIST OF PLATES**

Plate A. 1: Sundrying of Kaolin Clay .....	138
Plate A. 2: Sieving of Kaolin .....	138
Plate A. 3: Kaolin sieved to 400 $\mu\text{m}$ .....	138
Plate B. 1: Heavy Distillate Sample from AESL.....	139
Plate B. 2: Pyrolysis setup .....	139
Plate B. 3: Monitoring with Power Meter and Electronic Balance.....	139
Plate B. 4: Diesel oil from HD pyrolysis .....	140

**ABBREVIATIONS AND ACRONYMS**

AESL	Alternative Energy Systems Limited
API	American Petroleum Institute
ASTM	American Society for Testing and Materials
CP	Catalytic Pyrolysis
e.g.	for example
EAC	East African Community
EPRA	Energy and Petroleum Regulatory Authority
HD	Heavy Distillate
HDP	Heavy Distillate Pyrolysis
IEA	International Energy Agency
IRENA	International Renewable Energy Agency
ISO	International Organization for Standardization
IUCN	International Union for Conservation on Nature
KAM	Kenya Association of Manufacturers
MEF	Ministry of Environment and Forestry
MSW	Municipal Solid Waste
OECD	Organization for Economic Cooperation and Development
PLOs	Pyrolytic Liquid Oils
TP	Thermal Pyrolysis
WEF	World Economic Forum
wt.%	weight percent



## DEFINITIONS OF TERMS

**Catalytic Pyrolysis** - Involves thermal degradation of polymer substance with catalyst.

**Cracking** - A process of breaking into smaller units, especially the process of splitting a large heavy hydrocarbon molecule into smaller, lighter components.

**Heavy distillate** - A byproduct obtained during pyrolysis of plastic waste.

**Plastic waste** - Any discarded plastic (organic, or synthetic, material derived from polymers, resins or cellulose) generated by any industrial process, or by consumers.

**Pyrolysis** - A process by which a solid (or a liquid) undergoes thermal degradation into smaller volatile molecules, without interacting with oxygen or any other oxidants.

**Thermal Pyrolysis** - Involves thermal degradation of polymer substance without catalyst.

## **CHAPTER ONE**

### **INTRODUCTION**

#### **1.1 Background of the Study**

Plastic products are essential part of everyday human activities which results into vast production with over 300 million tons of annual production globally (Miandad, Rashid; Mohammad et al., 2019). Plastics are mostly produced in China (28%), North America (19%), and Western Europe (19%) with only 5% in Africa of the total global production (Sadan & De Kock, 2022). Experts project that 26 billion tonnes of plastics may be generated by year 2050, of which utmost percent would be landfilled or scattered both on lands and in oceans (Geyer et al., 2017; Papari et al., 2021). Around 6.3 billion tonnes of waste plastics has been generated, 9% recycled, 12% incinerated, and 79% landfilled or in natural environment (Geyer et al., 2017). This waste mostly accumulates due to poor waste management and low recycling facilities and it is anticipated to account for about 20 percent of the total oil consumption in the world coupled with 15 percent of the annual carbon budget by 2050 (WEF, 2016). This could be further exacerbated as nearly 50 percent of global plastic waste is made up of plastic packaging (disposable or single-use plastics) intended for a single use only before being disposed or recycled. Packaging is the world's largest plastic sector accounting for about 25 percent of the market with approximately one million of these plastic bottles being purchased every minute (OECD, 2018). Geyer *et al.* (2017) highlight that around 54 percent of plastics from packaging leave use in the same year of its production; hence resulting in more plastic waste which calls for searching for better solutions to curb and reverse the current trend.

Plastic waste production is projected to still increase by 40 percent in the next ten years amidst ban on plastic use by other countries (Kenya inclusive) and even current efforts

to reduce, reuse, and recycle plastic products (Ellen MacArthur Foundation, 2017; WEF, 2016). In Kenya, over 98% of the country's plastic consumed is imported as a product or raw plastic (IUCN et al., 2020; MEF, 2021). Around 73% of all waste plastics in Kenya is uncollected, 27% collected (8% recycled, 19% disposed of in unclean landfills or dumpsites) and 92% mismanaged (IUCN et al., 2020). There is no proper disposal of waste in Kenya as a result of no sanitary landfills and incineration facilities (MEF, 2021). Therefore, non-recycled plastic waste is prone to leakage and mismanagement. IUCN et al. (2020) reported that 37,000 tons of plastic leak into the ocean yearly. This is only a small portion of the mismanaged waste, which reaches 465,000 tons per year. Waste generation patterns vary sharply between urban and rural areas of Kenya which are on average 30 kg/capita/year and 4 kg/capita/year respectively (MEF, 2021). The common practice even in city centers include littering and burning of waste. There are however low collection rates in rural areas and informal settlements. The urban areas of Kenya possess 20% to 72% collection rates with the average rate of 27%. IUCN *et al.* (2020) report that the annual leakage of mismanaged waste is 35,139 tonnes while that from sea fishing gears and overboard litter is 14 tonnes. Nearly 67% of waste leakage emanates from urban areas due to high per capita waste generation (IUCN et al., 2020).

Despite Kenya's 2017 plastic bags ban, this policy has not been fully implemented in the country due to some pressures. Behuria (2019) highlights that the plastic bag bans implementation policy is mediated by three kinds of pressures: business power, local and external (Behuria, 2019). In business power; the active plastic bag producers, their associations, and local manufacturing groups organize pressure groups, as they offer business investment and employment in addition to paying government taxes. The second set of pressures is the local where some scholars (Clapp & Swanston, 2009)

urged that the anti-plastic bag norm “emerged primarily for locally specific reasons and this has been largely a bottom-up simultaneous occurrence for Kenya where the strength of the local movements are not salient. The third set of pressure is external which include the involvement of civil society group in anti-plastic bag activism (Clapp & Swanston, 2009), alignment of government services-based development strategy toward prioritizing plastic bag with external actors (Goodfellow, 2014), and engagement in regional cooperation such as East African Community (EAC) where priorities are set for plastic bag ban regionally by signing some bill in achieving it (Behuria, 2019).

Nearly 18% of municipal solid waste (MSW) of Thika Municipality [Kenya] is of plastic-type (Mugo Ephantus et al., 2015), with plastic in MSW ranging between 9-15% (Kenya Association of Manufacturers (KAM), 2019). Plastic waste is useful alternative source of energy (Nugroho et al., 2018). This waste has lately fascinated greater consideration for various sources of energy such as solid, liquid, and gaseous fuels (Miandad et al., 2019). Alternative Energy System Limited (AESL) based in Thika, Kenya is the first firm in Kenya to utilize plastic wastes via pyrolysis to produce useful products like synthetic oil, carbon black, and heavy distillate with a proportion of 55, 20, and 25% respectively. The firm produces 7000 liters of fuel by recycling 12 tons of plastic waste daily (Takouleu, 2018).

About 2.3-46.6% of the plastic waste input from pyrolysis of plastic waste remained in solid form which is mainly the heavy wax content (Choi et al., 2022). In a typical plastic waste recycling plant, heavy distillate/wax is usually interleaved into the pyrolysis reactor or used as a heat source due to its low value. This residue sometimes piles up in the recycling plants due to its less desirability in the market (Kasar &

Ahmaruzzaman, 2022). Furthermore, heavy waxy oil is a highly viscous oil with, tar-like nature, high asphaltene, waxy content, and low value that makes it difficult to burn (Zhao et al., 2021). It is also composed of large molecular weights (heavy hydrocarbons) and contain heterocyclic compounds including sulfur, nitrogen, oxygen, and organo-metallic compounds (A. Demirbas et al., 2015). The oxide of sulphur, nitrogen and carbon from such heterocyclic compounds are basically air pollutants that evolved from transport fuels, industrial furnaces, and thermal power plants. Pyrolysis is one of the common upgrading technologies for heavy distillate due to its simplicity in operation and cost (Ayhan Demirbas et al., 2016). Catalytic pyrolysis is a promising way for the production of light products such as gasoline and diesel from low-valued heavy oil (Almeida & Marque, 2015; Fadillah et al., 2021). Pyrolyzed liquids are mostly aromatic components which signifies high degree of pyrolysis with catalyst (Meng et al., 2006). Catalytic pyrolysis has greater comparative advantages due to its effectiveness in lowering reaction temperatures, reaction time, and cost control (Fadillah et al., 2021; Miandad et al., 2019; S. Wang et al., 2021). The mechanism for reaction of the heavy oil during catalytic pyrolysis is complex as it undergoes many reactions for instance cracking, hydrogen transfer, aromatization, isomerization, alkylation, and dimerization (LIU et al., 2007). Heavy oil catalytic pyrolysis depends on type and pore size of the catalyst used and catalyst upgrading is necessary for fast-forward production (Soni, 2020), however upgrading of catalyst is associated with an extra cost which makes it not practically possible in real life applications and this necessitates the search for low-cost catalysts. There is also a need for more research in heavy distillate to build a full knowledge of heavy oil combustion characteristics due to its complex nature and obtain improve physiochemical properties, combustion efficiency, and emissions control.

## **1.2 Statement of the Problem**

Heavy distillate is heavy fraction of plastic pyrolysis characterized by high viscosity, heavy hydrocarbons, waxy content which makes it a low-valued biproduct (Motawie et al., 2015). This requires upgrading to improve its mobility (viscosity) and quality (Zhao et al., 2021), obtain better market value (Sun et al., 2021), improves pyrolysis economics (Choi et al., 2022) and meets rapidly growing concerned for circular economy and sustainability (Al-salem & Dutta, 2021). There is still limited knowledge on the thermal characteristics of heavy distillate derived from plastic waste. The upgrade and characterization of heavy distillate, and optimization of its operating process parameters are not adequately assessed to the best of authors' knowledge. One of the promising upgrading techniques is catalytic pyrolysis and this can be done by employing clay-based catalyst during pyrolysis process. The development of suitable clay-based catalysts for the upgrading of heavy wax is of current interest to reduce the reaction temperature and residence time of the feedstock in the reactors (Ore & Adebisi, 2021). Clay-based catalyst has received little attention for pyrolysis processes and its use has not been adequately ascertained (Fadillah et al., 2021). This study has therefore put effort to convert heavy distillate into diesel range fuel with the use of kaolin as the catalyst to enhance product oil yield, pyrolysis economics and reserve the carbon neutrality resources.

## **1.3 Objectives**

### **1.3.1 Main Objective**

The main objective of the study was to upgrade heavy distillate from plastic waste into a diesel range fuel through catalytic pyrolysis.

### **1.3.2 Specific Objectives**

The specific objectives of this study were:

- i. To characterize heavy distillate from plastic waste
- ii. To produce light diesel-like product from heavy distillate through catalytic pyrolysis
- iii. To analyze the effects of catalyst ratio and operating temperatures on product yield
- iv. To characterize the properties of fuel produced from heavy distillate

### **1.4 Justification of the study**

Energy consumption during transportation, industrial, and households applications increases as population grow yet fossil fuels reserves are rapidly diminishing (Kumar et al., 2011); this creates a serious energy concern for future use if no alternative energy sources exist (Nugroho et al., 2018). Additionally, the demand for petroleum continues to grow every time, and in developing countries like Kenya there is high demand for petroleum fuel, yet the country relies heavily on imports to meet these requirements for instance the light diesel oil demand increased by 5 percent after 2.08 million tons in 2015 to 2.198 million tons in 2019 (EPRA, 2020). These are likely to strike consumers in Kenya due to high demand and low supply of petroleum fuels (Amadala, 2021). Hence, alternative fuels like light diesel oil products obtained from heavy distillate would be desirable. The plastic-to-fuel competitiveness is anticipated to grow significantly in the coming years as a response to meet rising energy demands. More research on the heavy distillate could be helpful in cautiously selecting the most suitable approach in order to avert environment and economical risks (Ore & Adebisi, 2021). The study would also help to create value-added products from heavy distillate thus increasing market value which can reduce pressure on conventional petroleum fuels.

Kaolin is one of the clay-based catalysts which can provide greater catalytic effect toward enhancing pyrolysis product yield and quality due to its silica-alumina ratio (Luo et al., 2021), and it is low-cost local clay catalyst with low surface acidity which encourages intermediate cracking or formation hence suitable for liquid yield compared to other clay catalysts (Gandidi et al., 2018a; Hakeem et al., 2018) and is locally available in the developing countries like Kenya.

### **1.5 Significance of the Study**

The study is helpful to obtain diesel fuels from HD which can help reduce over reliance on conventional fuels. The study would help industries to improve operational performance by increasing the value of their products from HD using clay-based catalysts. This study is also paramount in waste management to meet energy, economic and environmental demands.

### **1.6 Research Questions**

- I. What are the physiochemical properties of heavy distillate from plastic waste and its products?
- II. What hydrocarbon compounds and functional groups are present in heavy distillate from plastic waste?
- III. What is the kinetics of the heavy distillate pyrolysis process?
- IV. How does optimization with response surface methodology of selected operating parameters during heavy distillate pyrolysis describe process conditions?

### **1.7 Scope of the Study**

The up-gradation of heavy distillate was done with the use of kaolin as a catalyst through the pyrolysis process and thermal pyrolysis was taken as a control experiment



without using catalyst. The response surface methodology with central composite design was employed as experimental design for selected process parameters during pyrolysis of heavy distillate.

### **1.8 Limitations**

The study was particularly limited to heavy distillate generated from the plastic recycling industry obtained from pyrolysis of polyethylene (PE), polypropylene (PP), low-density polyethylene (LDPE) and high-density polyethylene (HDPE) mixture as feedstocks. Heavy distillate generated from other plastic sources was not possible for this study due to no plants currently under operation with such plastics in Kenya. There were no practical engine tests with the diesel oil products produced from HD upgrading. The variation of factors in selecting operating process parameters may affect the process conditions of the pyrolysis process conducted by the use of response surface methodology.

## **CHAPTER TWO**

### **LITERATURE REVIEW**

#### **2.1 Introduction**

This chapter presented heavy distillate production, upgradation techniques, chemistry and thermal decomposition characteristics, heavy oil properties, different pyrolysis processes, catalyst used during pyrolysis, kinetics, and analytical characterization techniques.

#### **2.2 Plastics Waste Scenario**

Plastics are polymeric materials that has intrinsically instigated as tough, light in weight, chemically and physically molded, non-degradable and applicable in packaging, construction, transportation, and industrial sectors. Non-utilization of disposable plastics and its transformation to circular economy is the greatest dismay in the world. Plastics are exacerbated as havoc in environment (Sharma et al., 2021). The increasing quantity of plastic wastes is terrifying soil environment, freshwater, marine system, and perhaps the safety of the entire food chain system. While plastics are universal in use, exterminating plastics pollution requires stride from all users to revitalize appropriate ways for sustainable plastics utilization such as reduce consumption and curb plastic wastes. According to World Bank, the generation of waste plastics worldwide in 2025 would be about 9-13% of total municipal solid waste which varies for every country. Several attempts have been made to eradicate the unfavorable effect of plastic wastes, one of these is by promoting plastic wastes recovery through recycling. Only Europe has succeeded in recovering plastic waste up to 50%, the rest is discarded into landfills (Sharma et al., 2021). Recycling of plastic wastes is more costly than landfilling and incineration practices. Further substitutes which are worthwhile are vital to boost recycling plastic waste. Society of plastic

industry (SPI) categorized a framework that partitions plastics into associated seven groups dependent on the substance structure and applications as shown in Table 2.1 (Rathod, 2020). Of them, Alternative Energy Systems Limited (AESL) based in Thika - Kenya utilizes soft plastics like polyethylene (PE), polypropylene (PP), Low-Density Polyethylene (LDPE), and High-Density Polyethylene (HDPE) mixture as feedstocks through pyrolysis technology to produce synthetic oil, carbon black, and heavy distillate.

**Table 2.1: Plastic Group and Source**

S/N	Plastic Group	Plastic Source
1	PET ((Polyethylene Terephthalate)	Plastic water bottles, sports drinks
2	HDPE (High-Density Polyethylene)	Milk, water and juice containers, laundry soap
4	PVC (Polyvinyl Chloride)	Bottles with handles
5	LDPE (Low-Density Polyethylene)	Shopping bags, bread bags, plastic sheeting
5	PP (Polypropylene)	Food containers
6	PS(Polystyrene)	Egg cartons, cups, plates
7	Others	Specialized packaging products

### 2.3 Plastic Waste Management Techniques

Many techniques and approaches have been employed to eliminate plastic waste and these include adsorption, photocatalytic degradation, coagulation and microbial decomposition (Pandey et al., 2023). Adsorption technique utilize absorbent solid materials which adsorbed pollutants from the water or gaseous phase on its surface, and it favours removal of organic and inorganic pollutants such as microplastics from water and waste water (Pandey et al., 2023), work best for plastic size greater than 5  $\mu\text{m}$ , limited to remove microplastics from oceans and also has very low regeneration (Pandey et al., 2023). The photocatalysis technique can be used to handle micro/nano

plastics waste. In this technique, a suitable light energy stimulates nanostructured semiconductors leading to exciton pairs creation, and then react with surrounding water/moisture to produce highly reactive species such as superoxides and hydroxyl radicals that oxidize organic species like polymers (Tofa et al., 2019). Some of the photocatalysts used include ZnO nanorod (Tofa et al., 2019), copper phthalocyanine (CuPc) sensitized with TiO<sub>2</sub> (Shang et al., 2003). Coagulation involves removal of solid particles from water through chemical method by introducing small and highly charged molecules into the water to manipulate the electrostatic charges of the suspended particles in water (Pandey et al., 2023). The use of microbes such as bacteria and fungi has also been reported to degrade polymer materials (Shen et al., 2019), lab engineered bacteria are useful to degrade plastic waste (Espinosa et al., 2020), but the method is slowest among all removal methods which can take several days for degradation and also depends on the characteristics of plastic waste including its physical and chemical nature as well as environmental factors such as temperature, sunlight, ultraviolet rays, and atmospheric humidity (Yuan et al., 2020). Plastic waste has also been landfilled and incinerated (Z. Yang et al., 2021), managed by 3R approach i.e., reduce, reuse and recycle (Pandey et al., 2023), with recycling reported as effective way of managing plastic waste (Maitlo et al., 2022). There is stricter limitation for land filling as imposed by government as a result of its being unsustainable disposal method (Acomb et al., 2014). Incineration typically decrease the volume of plastic waste (Kibria et al., 2023), and can reduce waste by 80 to 90% (Yogalakshmi & Singh, 2020), however it emits hazardous emissions and detrimental constituents such as particulate matter, dioxins, CO, furans, metals and volatile organic chlorides (Dadario et al., 2023; Maitlo et al., 2022). The primary recycling method for plastic waste is mechanical recycling, which encompasses heating, shredding, and remolding (Lange, 2021; Maitlo et al., 2022;

Ragaert et al., 2017), however the method produces plastic with inferior properties by decreasing its tensile strength (Ragaert et al., 2017), which thus requires other waste management alternatives. Pyrolysis and gasification of plastic waste are most suited for plastic waste conversion into valuable products, in addition to being environment-friendly and requires less space for plant installation (Maitlo et al., 2022). Gasification generates mainly synthesis gas such as CO, H<sub>2</sub>, and CH<sub>4</sub> (Acomb et al., 2014), but involves air being used as a gasifying agent resulting in a decrease in the calorific value of produced syngas (Maitlo et al., 2022). Pyrolysis produces high quality hydrocarbons which can be utilized as fuel (Maitlo et al., 2022), favours formation of liquid fuels (Mibei et al., 2023), and thus necessitates its choice for this study to obtain diesel fuels from heavy distillate derived from plastic waste.

#### **2.4 Heavy Distillate from Plastic Pyrolysis**

Heavy distillate (HD) from AESL is obtained during plastic pyrolysis as illustrated in the flow chart in Figure 2.1. The heavy distillate commonly called heavy wax is usually collected from the cyclone as a byproduct. The threaded polymers are fed from the top of the pyrolyzer with temperature maintained between 680-700 °C. The plastic then undergoes complex chemical transformation from raw oil into fine oil. The liquid vapour from the pyrolyzer is condensed from 240 °C to 40 °C. The combustible gases are recovered from the pyrolysis process and used in the gas heating system during heat recovery to provide additional heat for pyrolysis. The heat source at around 721 °C is supplied to pyrolyzer, vapours at 172 °C are released from the pyrolyzer to pass tangentially through the cyclone, the HD are trapped with the cyclone and then collected beneath the cyclone with a barrel. The collected HD is manually charged back into a pyrolysis reactor or utilized as a heat source in a pre-heater. About 25% of the output pyrolysis products from AESL consisted of heavy distillate. There is a huge

potential to convert HD into a valuable energy source and improve the pyrolysis economics of the plastic recycling plant. However, it is still hard to understand the exact chemical reactions that take place within the process and how much heat is required which requires understanding thermal properties of cracking process.

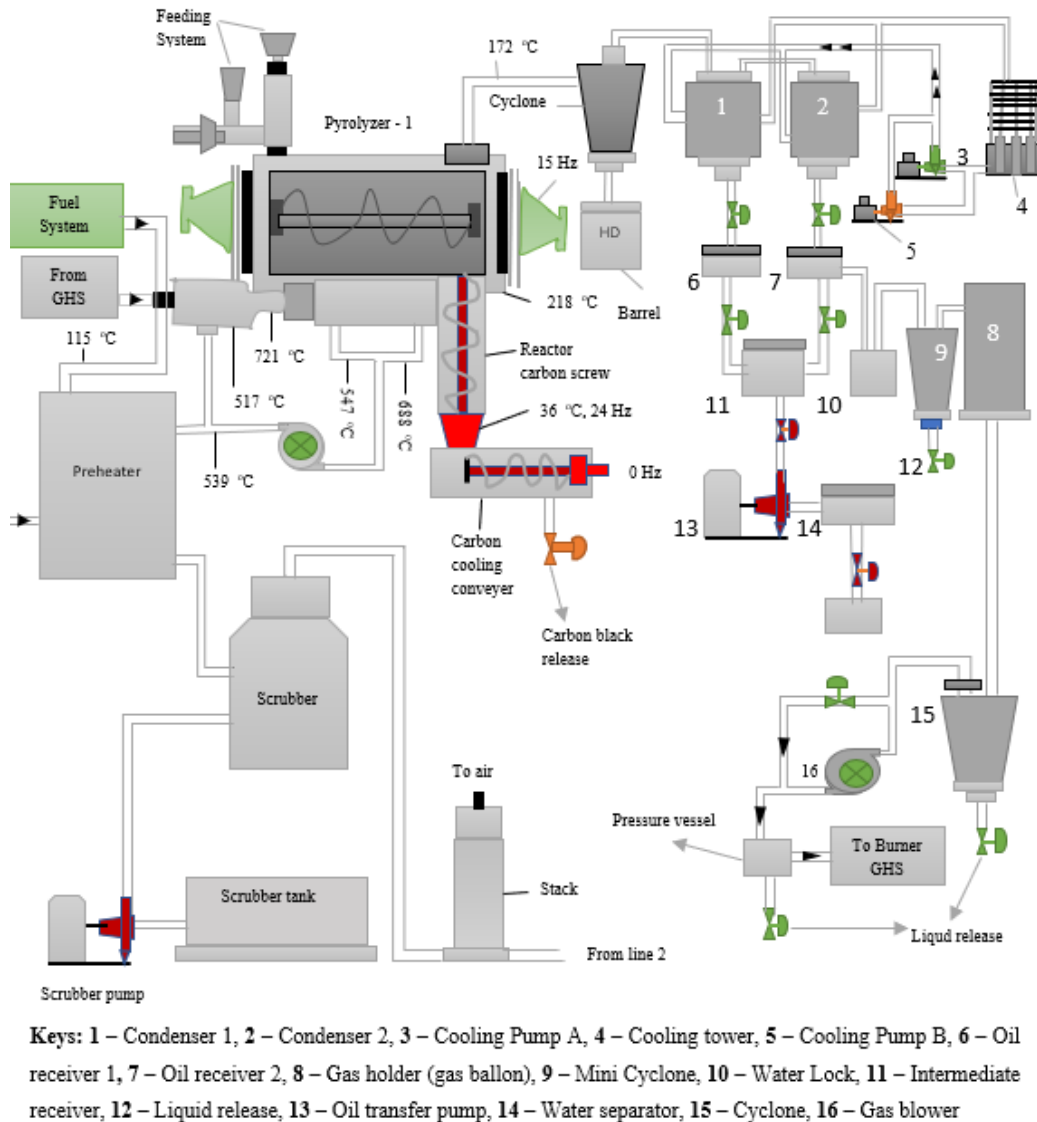


**Figure 2.1: Flow Chart showing production of HD from plastic pyrolysis**  
(Source: AESL)

## 2.5 Upgrade of Heavy Oil

Several literatures have shown the potential of upgrading heavy oil into light fuel to increase its market value. Demirbas *et al.* examined heavy oil pyrolysis into gasoline

and diesel-like products using sodium carbonate as a catalyst (Ayhan, Demirbas et al., 2017). The study employed a pyrolysis reactor with a process reaction temperature of 230-350 °C; the catalyst to heavy oil ratio of 2, 5, 7, and 10 %; heating rate of 20, 40, 60, and 80 °C/min and a constant heating time of 45 min for all experiments. Their findings showed that gasoline and diesel-like product amounts increase as temperature and catalyst ratio increase. The study employed a homogenous catalyst use in heavy oil upgrading, however, their uses are associated with long reaction times, and in addition, they cannot remove some impurities and unwanted compounds from the products. There was insufficient cracking ability by use of the catalyst ( $\text{Na}_2\text{CO}_3$ ) as nearly 17% of heavy oil remains in the product. The study highlighted that all kinds of heavy oils are highly viscous and contain asphaltenes making them denser which thus requires upgrading to obtain competitive economic value.

Kar *et al.* investigated characterization of light diesel fractions generated from upgraded heavy oil (Yakup Kar et al., 2018). The study pyrolyzed heavy oil in a pyrolysis reactor placed inside an electrical heating mantle with both thermal and catalytic pyrolysis. Thermal degradation/pyrolysis is important as a control process and acts as a basis for understanding catalytic degradation effects on product quality and yields (Yakup Kar et al., 2018). In the study, the product oil yields of catalytic upgrading are found to be higher than those of thermal pyrolysis as there is a strong cracking effect on the use of catalyst over the latter with the formation of more light fractions. The diesel fuels produced from both thermal upgrading and catalytic upgrading in the study showed n-alkanes with maximum concentration happened in the carbon number range of  $\text{C}_{15}$ – $\text{C}_{18}$  which are in the diesel range of  $\text{C}_7$ – $\text{C}_{23}$ . Amongst present hydrocarbons, hexadecane ( $\text{C}_{16}\text{H}_{34}$ , 4.17%) is stated for thermal upgrading whereas heptadecane ( $\text{C}_{17}\text{H}_{36}$ , 4.04%) is for the catalytic upgrading of light diesel fuel. However, there is a slight difference

obtained by activated molasses soil usage as a pyrolysis catalyst for production of diesel-like fuels compared to thermal upgrading. Furthermore, the catalyst requires further improvements by employing chemical activation methods for upgrading heavy oil and its derivatives to attain lighter fuels which thus increase the economics of pyrolysis process. Thus, the selection of catalyst can impact the product yield during heavy oil up-gradation and it is important for economic reasons.

## **2.6 Heavy Distillate Degradation**

The degradation of heavy distillate is complex and varies from one source to another. The pathways by which polymers degrade can be considered using the six main mechanisms i.e., main chain scission, side group scission, elimination, depolymerization, cyclization, and cross-linking (Duncan et al., 2000). In main chain scission, the bonds are broken in the main polymer chain leading into low molecular weight and volatile formation. This may happen at the chain end or random positions in the chain. For end chain scission, here individual monomer units are sequentially detached at the chain end which results in the monomer generation, and this process is referred to as unzipping. Meanwhile, in random chain scission, here chain scission occurs at seemingly arbitrary positions in the polymer chain which leads to production of both monomers and oligomers (polymer units with 10 or fewer monomer units) and variety of other chemical species. Side group scission encompasses elimination and cyclization reactions. In the elimination reaction, the bonds linking side groups of the polymer chain to the chain itself are broken, and the side groups reacts often with other eliminated side groups. In cyclization reactions, two adjacent side groups react to form a bond between them, leading to cyclic structure production. Cross-linking happens after some chain stripping (in which atoms or groups not part of the polymer chain or backbone are cleaved) and entails bonds creation between two adjacent polymer chains.



The cross-linking process just like cyclization ones is very significant in the chars formation (Bernardo, 2011), and it also produces a higher molecular weight structure that volatilized easily (Ng et al., 2018). Cyclization and cross-linking rarely result in any change of sample mass until it happens in combination with other mechanisms mentioned earlier, and they cannot be detected by thermogravimetry. Except for cyclization and cross-linking, all the other pathways lead to formation of volatile products with an associated mass change. In an inert environment, some polymers give nearly quantifiable yield of their parent monomers. In the air, the sample oxidized completely to oxides of its constituent elements (Ng et al., 2018). Nitrogen-containing polymers generate some ammonia or hydrogen cyanide whereas Halogen-containing polymers produce respective hydrogen halides (Matthews & Minard, 2006).

## **2.7 Chemistry of Heavy Distillate**

Heavy oils normally contain complex compounds with large molecular weights. The components contained in heavy crude oils are shown in Figure 2.2 which are synonymous with heavy distillate. It comprises asphaltenes, which is the heavy hydrocarbons, and maltenes which are commonly known as petrolenes. Maltenes are sub-divided into resins, aromatics, and saturates (Aske et al., 2002). During pyrolysis, both asphaltenes and maltenes are broken down into their respective monomers which are light in weight hence forming light oil fractions (Adebiyi, 2021). The complexity of SARA (saturates, aromatics, resins, and asphaltenes) compounds makes it hard to precisely identify their chemical structures as shown in Figure 2.3, hence heavy fractions characterization is usually based on species identification with certain properties unique from each other (Mansoori et al., 2013).

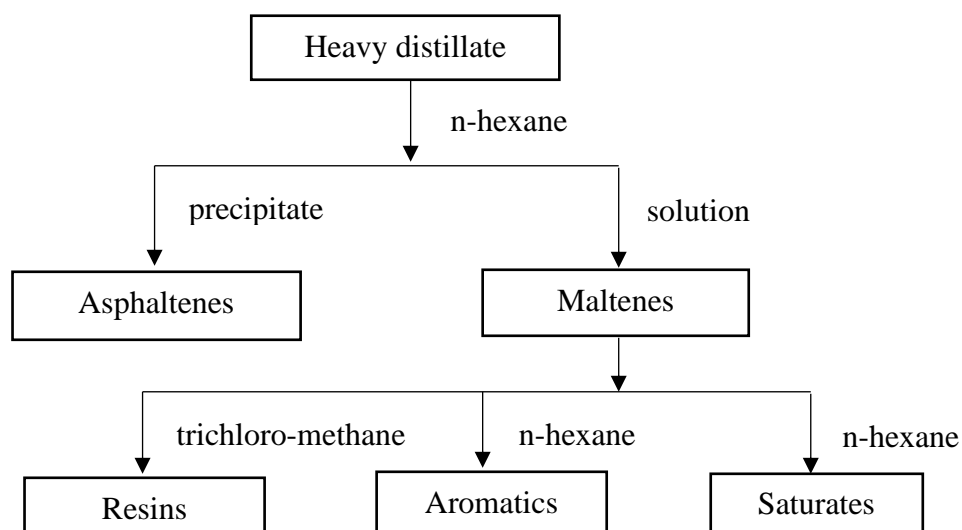


**Figure 2.2: The Components of Heavy Distillate**

*Source:* (Aske et al., 2002)

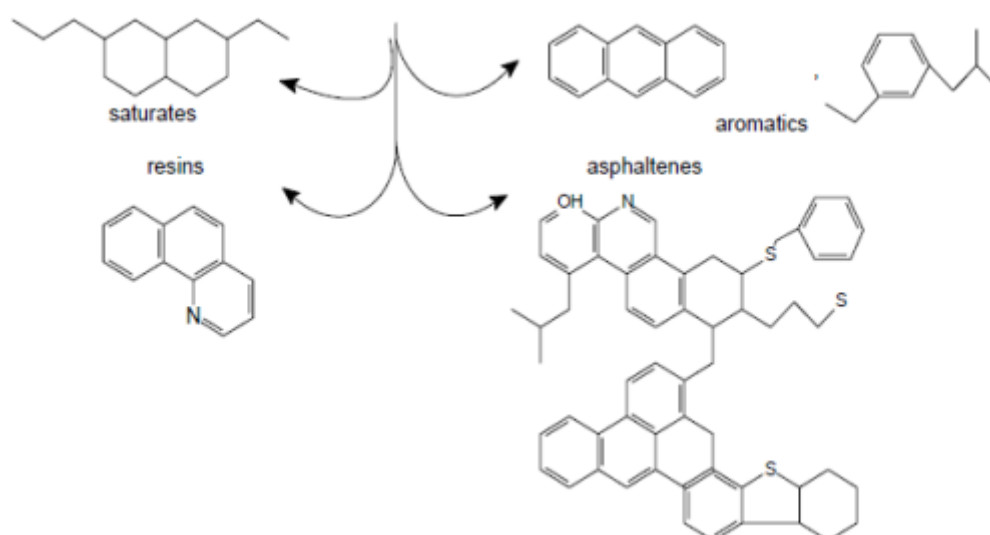


**Figure 2.3: Structure depiction for resins, saturates, asphaltenes and aromatics**

*Source:* (Lucena et al., 2004)

## 2.8 Thermal Decomposition of Heavy Distillate

Weight loss of heavy distillate happens in one or a mixture of three ways. One of these is through random chain scission and consequent pyrolysis of the heavy distillate or due to loss of volatiles and low molecular weight fragments such as saturates and aromatics. Secondly, through decomposition of light hydrocarbons (aromatics and resins) and

finally, due to decomposition of high molecular weight fractions and heavy hydrocarbons (asphaltenes) (Lucena et al., 2004). Some authors like Farhan and his team (Farhan et al., 2017) studied silica and alumina layer combinations as a catalyst to separate maltenes into their basic components. Their findings show that the proportion of saturated (paraffin) is higher in the resulting oil product followed by the proportion of aromatics with a small value of resins noticed in the final product which gives the oil its desired preference. Resins have large molecular weights which increase the viscosity of the fuel (Soliman, 2019) thus its increase is unwanted in desirable fuels.

### **2.8.1 Saturates**

Muhammad and coauthors defined saturates (aliphatics) as non-polar hydrocarbons, without double bonds, but those that include straight-chain, branched alkanes, and cycloalkanes (naphthenes) (Muhammad et al., 2013). Cycloalkanes contain rings (one or more), and can have numerous alkyl side chains. The saturates proportion in heavy oil commonly decreases as molecular weight portions increase which makes it the lightest part of the heavy oil. Wax is a sub-class of saturates which includes straight-chain alkanes ( $C_{20}$  -  $C_{30}$ ). Wax usually precipitates as a solid particulate at low temperatures which affects the emulsion stability properties of heavy oil systems (Kok et al., 2018).

### **2.8.2 Aromatics**

Aromatics refer to benzene and its structural derivatives (Muhammad et al., 2013). They are common to all petroleum with majority comprising alkyl chains and cycloalkane rings, and extra aromatic rings. They are classified as mono/di/tri-aromatics as per number of aromatic rings existing in the molecule. Polar, higher molecular weight aromatics may fall in the resin or asphaltene fraction. Heavy oil

contains numerous aromatic hydrocarbons such as mono aromatic hydrocarbons (benzene), and poly aromatic hydrocarbons (PAHs) with fused aromatic rings. At least 85% of the aromatic hydrocarbons in heavy oil encompass one or more alkyl substituents on their aromatic rings (Muhammad et al., 2013). The aromatic compounds containing sulfur and nitrogen atoms in the ring e.g. (thiophenes) are commonly available (Z. Wang et al., 1994).

### **2.8.3 Resins**

The resin fraction comprises of polar molecules having heteroatoms (nitrogen, oxygen, or sulfur containing compounds) (Demirbas & Taylan, 2016). It is basically a soluble fraction in light alkanes like pentane and heptane, yet insoluble in liquid propane. Resins contain a higher hydrogen to carbon ratio (1.2-1.7) than asphaltenes (0.9-1.2), with its structure analogous to asphaltenes, but lower in molecular weight i.e. less than 1000 g/mole (Farhan et al., 2017). Naphthenic acids (NA) are typically regarded as a fragment of the resin. NA are composed of a functional group with carboxylic acid attached to a hydrocarbon molecule i.e. alicyclic carboxylic acid and saturated aliphatic acid mixture (Feyisayo et al., 2019). NA causes corrosion thus reducing the lifespan of equipment used, with it being accountable for heavy oil acidity. The deletion of NA compounds from heavy oil is central in upgrading heavy oil (Feyisayo et al., 2019). Blending can be done to remove NA from heavy distillate; however, this technique has low efficiency with ability to remove 2-3% only (Simanzhenkov & Idem, 2003). Deacidification removal techniques have also been used which included catalytic destructive, non-catalytic destructive, and non-catalytic non-destructive methods (Feyisayo et al., 2019). One of the examples for non-catalytic destructive methods is thermal decomposition but it is ineffective in reducing acidity in heavy oils. This method requires higher temperature which is usually greater than 400 °C for successful

thermal cracking, which then results in coke formation. The catalytic decarboxylation process provides alternative to the non-catalytic destructive methods for removing naphthenic acids (NAs) from heavy oil. The catalytic-based methods offer effective solution but their effect depend on catalyst surface area and calcined temperature (Feyisayo et al., 2019).

#### **2.8.4 Asphaltenes**

This refers to solubility class which is a fraction of crude oil precipitating in light alkanes like pentane, hexane, or heptane (Soleymanzadeh et al., 2019). It is a soluble precipitate in aromatic solvents such as benzene and toluene. The determination of the actual structures of the constituents for asphaltene fraction is problematic. The complexity of asphaltene fraction hinders formulation of the individual molecular structures. Asphaltenes entail condensed aromatic nuclei that carry alkyl and alicyclic systems with heteroelements (nitrogen, oxygen, and sulphur) and organometallic constituents (nickel, vanadium, iron) dispersed throughout various locations. Based on solvent used and surrounding environment, molecular weights of asphaltenes ranges from 750 to 30,000 g/mol (Hassan, 2014; Lordeiro et al., 2021). The lighter parts of the asphaltenes easily volatilize followed by the heavier fractions (Chakma, 2000). This is associated with the lower initial activation energies which represents lighter parts and it increases as the heavier ones are cracked. Chakma reviewed asphaltene cracking mechanisms during heavy crude oil processing (Chakma, 2000). The study shows that the reaction kinetics of asphaltene degradation is a first-order type which obeys Arrhenius relationship. The catalyst such as sand affects products distribution and results in lowering activation energies of the reactions as a result of the catalytic role played by the sand matrix. The asphaltenes has been separated from heavy crude oil through precipitation with 40 volume of n-heptane at temperatures (350-565 °C) in

batch reactors to study asphaltene reaction mechanisms (Savage et al., 1985). Hydrocarbon gases, cycloalkanes, and paraffin are usually the primary products for high temperature conditions resulting from the fission of carbon-to-carbon bonds. The study disclosed that coke, maltenes and gas are fashioned from the primary reactions.

### **2.9 Chemistry of Catalytic Cracking of Heavy Distillate**

The kinetics, chemical reactions and mechanism of the catalytic degradation process of vacuum gas oil have been widely studied (Gao & Xu, 1999). A qualitative elucidation of catalytic cracking reactions can be understood from the carbonium ion theory. In carbonium ions, the intermediate active particles come from breaking of the hydrocarbon chain resulting from external force or the adduction of hydrocarbon with acid radicals short of electrons. The various reactions that occur in catalytic cracking process of vacuum gas oil is summarized in Figure 2.4.

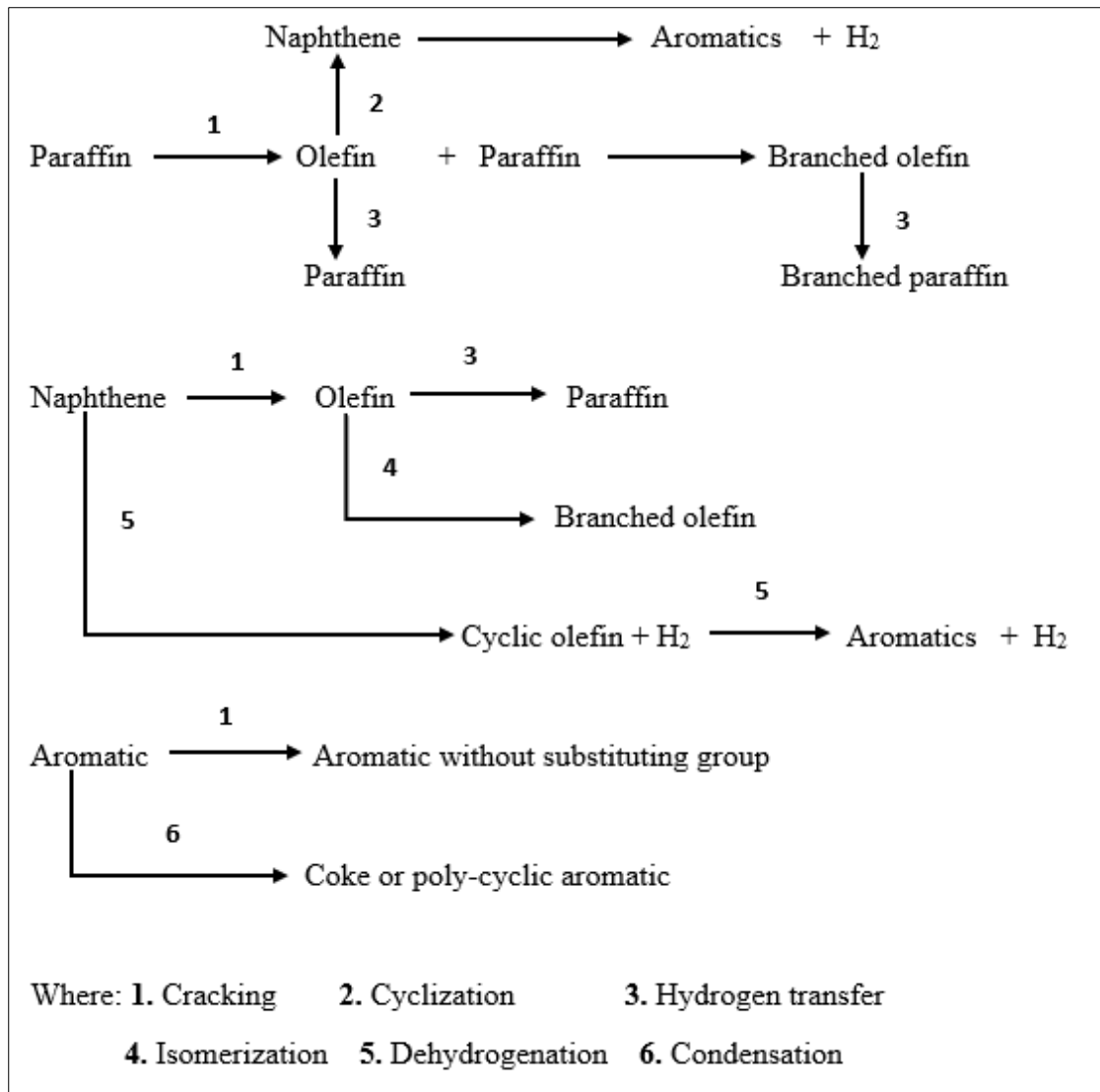


**Figure 2.4: The Chemistry of Catalytic Cracking of Heavy Distillate**

*Source:* (Gao & Xu, 1999)

## 2.10 Kinetics of Polymer Substance

Most earlier work on heavy oil reaction mechanisms overlooked the kinetic and thermodynamic characteristics hence difficult to understand energy variation of the pyrolysis process (Khelkhal et al., 2022). The kinetic and thermodynamic parameters such as enthalpy, entropy, activation and gibbs free energies are key parameters that allow assessing the efficiency of the pyrolysis process. The kinetics of heavy distillate decomposition is heterogenous. By heterogeneity, it means the reactants or products can exist in gas and solid states and this ascends nearly in every solid-state reacting

system (Hatakeyama & Quinn, 1999). It increases in polymer blends such as mixing of two different forms of polymers to obtain plastic owing to extra components added to the system. The disintegration of polymers like heavy distillate is accompanied by a decrease in their mass which generally takes the reaction equation in Equation 2.1 (Matheka, 2012).

$$S(s) = P_1(s) + P_2(s) \quad (2.1)$$

The rate of disappearance of species (S) can be computed using Equation 2.2:

$$\frac{dx}{dt} = kf(x) \quad (2.2)$$

where S(s) is the reactant, P<sub>1</sub>(s) and P<sub>2</sub>(s) are the residue and gaseous product, k is the rate constant following Arrhenius equation for the early stage of the reaction, x is the conversion factor of the decomposed substance at time, t. The conversion factor, x can be calculated using Equation 2.3 (Akhyar et al., 2019a). The Arrhenius model assumed the oxidation rate of the total sample relied entirely on the rate constant, mass of remaining sample and temperature (Li et al., 2013).

$$x = \frac{W_o - W_t}{W_o - W_f} \quad (2.3)$$

Where  $W_o$  is original weight of the substance (before decomposition starts),  $W_t$  denotes the weight of the substance at a particular temperature,  $W_f$  stands for final weight of the substance after reaction is completed.

The general kinetic equation in relations to conversion factor, x is given by Equation 2.4 (Matheka, 2012).

$$\frac{dx}{dt} = A(x)^n \exp\left(\frac{-E_a}{RT}\right) \quad (2.4)$$

$E_a$  denotes activation energy, A denotes frequency factor, R denotes the universal gas constant, T denotes the temperature in degree kelvin and n denotes reaction order.



When the sample temperature changes by a constant heating rate,  $\beta = \frac{dT}{dt}$  the conversion factor variation can be estimated as a function of temperature, this temperature depends on the heating time. Matheka (2012) defined the rate of reaction as in Equation 2.5:

$$\frac{dx}{dt} = \frac{A}{\beta} (x)^n \exp\left(\frac{-E_a}{RT}\right) \quad (2.5)$$

Equation 2.4 can be integrated mathematically using different assumption to derive a non-integral Equation 2.6 which is valid only for the first-order reaction (Broido, 1969).

$$\ln\left(\ln\frac{1}{x}\right) = \frac{-E}{RT} + \frac{\ln RZT_m^2}{E_a\beta} \quad (2.6)$$

where  $x$ ,  $Z$  and  $E_a$  denote “residual mass”, “frequency factor” and “activation energy”, respectively. Whereas  $R$ ,  $T$ ,  $T_m$ , and  $\beta$  denote the universal gas constant, absolute temperature, maximum reaction temperature, and heating rate, respectively. The Figure 2.5 displays plot of natural logarithm of the residual mass verses reciprocal temperature indicating linear dependency, which agrees with Broido Equation 2.6.  $E_a$  is evaluated directly from the slope (Matheka, 2012).

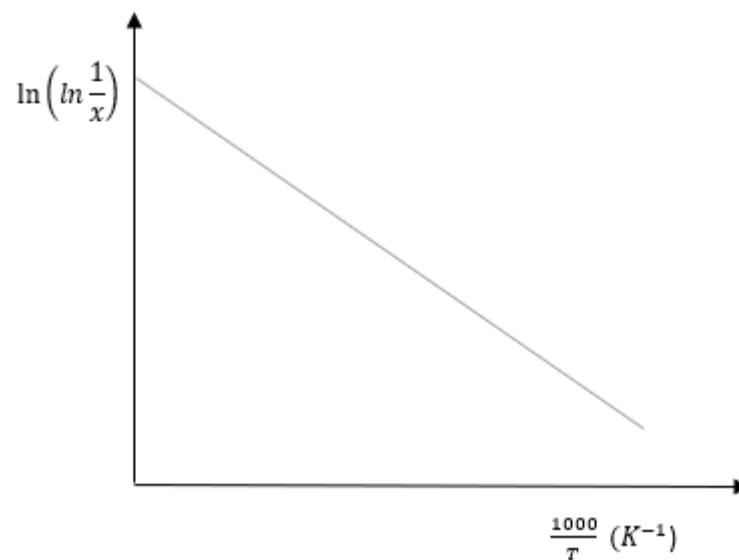


**Figure 2.5: Natural logarithm of residual mass against reciprocal Temperature**

*Source:* (Matheka, 2012)

### 2.10.1 Estimation of Activation Energy from thermal analysis

Several methods for evaluation of activation energy of polymer samples from thermogravimetric analysis (TGA) have been employed. These methods are classified into two: differential and integral methods in which both methods obey the Arrhenius relationship. In differential methods, it includes Borchardt and Daniels method (Borchardt & Borchardt, 1999), Freeman and Carroll's method (Freeman & Carroll, 1975), Coats and Redfern method (Coats & Redfern, 1964), Friedman method (Friedman, 1964), and Kissinger method (Kissinger, 1957). Additionally, isocoverisional/differential methods such as the deactivated activation energy model (DAEM) method (Fan et al., 2013), Flynn Wall Ozawa (FWO) method (Thomas et al., 2020), Kissinger-Akahira-Sunose (KAS) method (Lim et al., 2016), and modified Coats Redfern method (Akhyar et al., 2019a) are currently employed to study kinetic parameters of polymer materials. For integral methods, it is assumed that a single non-isothermal TGA curve is equal to a large number of similar isothermal curves, but the assumption might be incorrect (Akhyar et al., 2019a). This is because the analysis of kinetic parameters from a single integral TGA curve encompasses unwieldy curve fitting approaches which might yield equivocal result. Hence, the differential methods are much preferred over integral methods for estimating kinetic parameters. The modified Coats and Redfern method which is one of the differential methods in Equation 2.7 has been used for this study since it is the most suitable reaction mechanism which obeys the first order for pyrolysis of polymer substance as stated in previous work (Akhyar et al., 2019a; Dubdub & Al-Yaari, 2020).

$$\ln [-\ln(1 - x)] = \ln \frac{ART^2}{\beta E_a} - \frac{E_a}{RT} \quad (2.7)$$

Where A denotes “frequency factor” which can be obtained using Equation 2.11,  $\beta$  denotes “linear heating rate”, R denotes “general gas constant (8.3143 kJ kmol<sup>-1</sup> K<sup>-1</sup>)”,

$E_a$  denotes “activation energy”,  $T$  denotes “absolute temperature (K)” and  $x$  denotes “conversion factor” at time,  $t$  given by Equation 2.3.

Using Equation 2.7, the graph of  $\ln[-\ln(1-x)]$  against  $1000/T$  for each phase can be plotted to determine the slope, and using Equation 2.8, activation energy is evaluated from the slope of the linear fit:

$$-\frac{E_a}{R} = \text{Slope} \quad (2.8)$$

Although different kinetic investigations of heavy oils have been studied, most are inaccurate and inconsistent due to their simple assumption of reaction mechanisms of using a single heating rate. Kinetics parameters derived from the assumed model of a single heating rate give erratic and sometimes senseless results (Burnham & Dinh, 2007). Thus, it is necessary to employ different heating rates to exclusively understand the reaction mechanisms of heavy distillate from plastic waste.

### **2.10.2 Thermodynamics parameters analysis of Polymer Sample**

Besides activation energy, several other thermodynamic (kinetics) properties also influence the thermal decomposition of polymer (heavy distillate) sample which include rate constant, half-life, frequency factor, change in enthalpy, change in entropy and change in Gibbs free energy. The rate constant and half-life of the polymer substance at various heating rates are usually determined from the slope by plotting a graph of  $\ln(1-x)$  against time at various stages (Akhyar et al., 2019a). The slope of the graph equals to the rate constant of the substance at any particular phase. The half-life ( $t_{1/2}$ ) of the polymer sample can be determined using Equation 2.9 (Akhyar et al., 2019a).

$$t_{1/2} = \frac{0.693}{k} \quad (2.9)$$

Where  $k$  denotes “rate constant” of a substance, and  $t_{1/2}$  denotes “half life”

The entropy changes ( $\Delta S$ ) of the polymer sample reaction process can be determined using Equation 2.10.

$$\Delta S = R \times \ln\left(\frac{Ah}{KT}\right) \quad (2.10)$$

Where, A is the Frequency factor of reaction substance given by Equation 2.11 (Akhyar et al., 2019b; Khelkhal et al., 2022), R is the universal gas constant, h is Planck's constant, K denotes Boltzmann's constant, and T denotes temperature in Kelvins (K).

$$A = \frac{\beta E_a}{RT^2} \times \exp^{intercept} \quad (2.11)$$

The enthalpy changes ( $\Delta H$ ) can be determined using Equation 2.12 (Khelkhal et al., 2022).

$$\Delta H = E_a - RT \quad (2.12)$$

And Gibbs free energy ( $\Delta G$ ) changes can be determined using Equation 2.13 (Graciani et al., 2005; Khelkhal et al., 2022).

$$\Delta G = \Delta H - T\Delta S \quad (2.13)$$

### **2.11 Kaolin clay catalyst for Heavy distillate Pyrolysis**

Kaolin contains a high proportion of silica-alumina components which makes it desirable as a catalyst for upgrading heavy oil (Luo et al., 2021), it favours formation of aromatic compounds (Gandidi et al., 2018b). Fadhillah *et al.* (2021) reviewed different clay-based catalysts for pyrolysis processes. The findings showed that catalytic reactions of polymer pyrolysis process with kaolin clay depends on solid acid mechanisms which include cracking, isomerization, oligomerization, cyclization, and aromatization reactions. The vital role of the solid acid mechanism is to accelerate the reaction process which results to linear reduction in the activation energy of the reaction process. Such mechanisms are ruled by density, porous size, acidity, and porous structure of the catalyst surface. The study revealed that both Lewis and Bronsted acid

sites of a clay catalyst play parts in the cracking mechanism as initiated by hydride ion abstraction from the polymer structure by Lewis acid sites of the catalyst, or proton addition to the carbon - carbon bonds by Bronsted acid sites of the catalyst. The Bronsted acid sites having high amount on the surface of the catalyst gives more hydrogen ions for double bond cleavage and more propagation steps. The surface acidity and high specific surface area of the catalyst also play key role in generating liquid products rather than gas products (Fadillah et al., 2021). This mechanism augmented the liquid yield as a considerable improvement over thermal cracking which tends to yield gas as an outcome of the radical (random scission) mechanism. The existence of micropores in the clay structure has the influence to act as a heat sink and tolerates a greater residence time for feed molecules to engross the heat and partake contacts that result in hydrogen transfer (Luo et al., 2021). The core role of a solid catalyst in the liquid product is to enhance the capacity to degrade the polymer structure to form an intermediate in the mechanism (Fadillah et al., 2021). Kaolin clay has lower surface acidity compared to zeolites due to its lower Bronsted acidity thus minimizing the possibility of secondary reactions for instance over-cracking mechanism which favours liquid products yield (Gandidi et al., 2018b).

## **2.12 Heavy oil properties**

### **2.12.1 Density**

This refers to mass to volume ratio of a substance. The density of heavy oil is usually over  $900 \text{ kg/m}^3$ . The density of liquid fuels can be measured using a pycnometer bottle. The bottle is purely glass-made having ground glass stopper with a capillary tube to escape air bubbles. It uses a balance to measure specific gravity or density of a substance (water or mercury). Kumar *et al.* used specific gravity bottle with 10 mL capacity to determine the specific gravity of the samples (Senthil Kumar et al., 2017).

Here 10 mL sample is pipetted into a pre-weighed bottle until it reaches its brim. The sample weight is divided by 10 mL volume to obtain its density. Specific gravity is determined by Equation 2.14.

$$\text{Specific Gravity} = \frac{\text{Density of Sample}}{\text{Density of Water}} \quad (2.14)$$

### **2.12.2 Kinematic viscosity**

Viscosity is a measure of flow resistance of the liquid fuels (Ahmad et al., 2015). Its value increases with decreasing temperatures and contrarywise. The viscosity value includes temperature at which the viscosity is measured. A DAIHAN Scientific digital constant temperature viscosity bath can be used to measure the viscosity of liquid oils following ASTM D445 standard procedure. A digital viscometer is also used to determine oil's viscosity. Heavy oil has viscosity higher than 100 MPas (Zhao et al., 2021). The viscosity of heavy oil based on API gravity scale is less than 22.3° (Demirbas et al., 2016).

### **2.12.3 Pour and cloud points**

Pour point can be defined as the temperature at which the oil solidifies and it gives information on fuel behaviour at several sea temperatures. The oil solidifies when the pour point is 10–15 °C above the sea temperature which relates to the oil's wax content (anne Fritt-Rasmussen, Susse Wegeberg, Kim Gustavson, Kristin Rist Sørheim et al., 2018). As temperature decreases, the oil waxes crystallize, and this prevents flow. Cloud point is defined as a temperature where waxes commence precipitation. Fuel oils from waxy and paraffinic crude oils mostly have a high pour point with values ranging from -2 to 24 °C depending on weather conditions (anne Fritt-Rasmussen, Susse Wegeberg, Kim Gustavson, Kristin Rist Sørheim et al., 2018). The cloud and pour

points of the liquid fuels are determined following ASTM D2500 and ASTM D97 standards.

#### **2.12.4 Flash Point**

Flash point can be defined as the lowest temperatures at which the atomized vapor can ignite itself. This point is particularly concerned with fuel safety in terms of handling and storage and the amount of low boiling fraction present in the liquid fuel (Senthil Kumar et al., 2017). It is correlated with fuel volatility to help the engine to start and warm. Kumar *et al.* (2017) used Pensky Martens closed cup flash point test to determine the flash point of the fuel sample. Here, a 30 mL sample is heated and stirred for every 1 °C temperature rise. An ignition source is then directed into the cup at constant intervals with unbalanced stirring until a flash that spreads inside a cup is observed. The flash point of heavy oil is usually greater than 60 °C (Huth & Heilos, 2013).

#### **2.12.5 Calorific value**

Calorific value is a measure of energy emitted when a unit mass of fuel is burned with sufficient air. The higher heating value (HHV) of the liquid fuels can be measured using a bomb calorimeter following ASTM D711. In this, the calorimeter crucible is filled with a known mass of fuel and then ignited. This heats surrounding water, then initial and final temperatures are recorded using a thermometer. The calorific value is then determined using the heat balance i.e., heat given by the fuel is equal to the heat gained by the water as illustrated in Equation 2.15. The calorific value of heavy oil ranges from 39.5 to 40.9 MJ/kg (Huth & Heilos, 2013).

$$M_f \times CV = M_w \times c \times \Delta T \quad (2.15)$$

Where  $M_f$  – mass of fuel used,  $CV$  - Calorific value,  $M_w$  - mass of water,  $c$  - specific heat capacity and  $\Delta T$  - temperature change

## **2.13 Types of Pyrolysis**

Pyrolysis can be defined simply as thermal cracking of polymers under relatively mild conditions of atmospheric pressure, temperature range of 200-750 °C, and inert atmosphere to generate solid, liquid, and gaseous fuels (Sankaran et al., 2018). It encompasses thermal decomposition of the substance without oxygen (Santhoshkumar & Anand, 2019). Pyrolysis still fashions tremendous interest due to its economics and environmental prospects (Khelkhal et al., 2022), and involves two probable steps that is primary pyrolysis followed with secondary pyrolysis (Fernandez et al., 2011). In the context of primary pyrolysis, it encompasses the devolatilization of the substance where various reaction zones appear with respect to thermal decomposition of the main constituents. In secondary pyrolysis, secondary decomposition reactions in the solid form and secondary reactions between the volatiles release (homogeneous reactions) or between carbonaceous residue and volatiles (heterogeneous reactions) are involved. In first stage; dehydration, dehydrogenation, decarboxylation, or decarbonization reactions take place. The second stage includes thermal or catalytic cracking processes, where heavy compounds further break into gases, or char is converted into gases such as CO, CO<sub>2</sub>, CH<sub>4</sub>, and H<sub>2</sub> by reactions with gasifying agents, as well as partial oxidation, polymerization and condensation reactions. Pyrolysis is further categorized into different forms which include thermal pyrolysis, catalytic pyrolysis and microwave pyrolysis as discussed in the proceeding subsections.

### **2.13.1 Thermal Pyrolysis**

This process requires a setup with some equipment which includes metal container, condenser, and fuel receiver (Anthony et al., 2019). The metal container used needs to resist high temperatures above 300 °C (Hartulistiyoso et al., 2015). A heat source is provided on a metal container and this heat source should be satisfactory to attain high



temperatures within a short time when the above conditions are satisfied. As the HD is transferred into the container for pyrolysis, the container is then heated by desired heat source in the absence of oxygen. When polymer substance like heavy distillate is burnt with no oxygen it will not catch fire but rather burn and forms a gaseous state. The gaseous fuel formed is pressurized to condenser which cools down the temperature and changes into liquid state (liquid fuel). This light fuel is then collected using a suitable container such as a beaker.

### **2.13.2 Catalytic Pyrolysis**

This is used to advance polymer thermal pyrolysis results, by broadly utilizing stimuli (catalytic effect) to enhance pyrolysis process. Some catalysts help to decrease unsaturated hydrocarbons, promote aromatics and naphthenes yield, and increase stability, cetane, and octane numbers in the oil product (Pujro et al., 2012). Catalytic pyrolysis via in-situ process approach happens in a single reactor where catalyst and polymer substance are mixed thoroughly. The vapors from primary pyrolysis often diffuse into catalyst pores where they are catalytically cracked (Pujro et al., 2012). Kaolin is one of the catalysts used for enhancing pyrolysis of polymer substance into quality fuel. Hadi *et al.* (2017) studied a batch reactor with kaolin as a catalyst to analyze the effect of neat kaolin on product yield and composition during pyrolysis of polystyrene plastic waste at 400 and 450 °C. The study generally showed that Kaolin-based catalysts act as a green process for converting waste plastic materials into useful fuels. A high product yield of 85-99% was obtained with the use of kaolin as a catalyst and many aromatic compounds were contained in the oils (Hadi et al., 2017). There was low impurities and unwanted compounds in the final composition of the products with ability to remove toxin and heavy metals. Catalytic pyrolysis can lead to a decrease in entropy and enthalpy during activation of pyrolysis (Khelkhal et al., 2022). It offers

encouraging results on the optimization, process control and energy consumption which makes it vital for improving pyrolysis process (Rafey et al., 2023).

### **2.13.3 Microwave pyrolysis**

This involves microwave dielectric heating of the polymer material (Bartoli et al., 2019). Microwaves lie between radio waves and infrared radiation in the electromagnetic spectrum region; it involved those waves between 0.001 and 1 m wavelengths corresponding between 300 and 0.3 GHz frequencies (Fernandez et al., 2011; Zhi et al., 2017). It favours solid and gas yields with lower liquid yield compared to conventional pyrolysis (Huang et al., 2016), but has an increased rate of thermal transfer with reduced energy consumption (Fernandez et al., 2011). Microwave pyrolysis technology is gaining popularity in waste management as a tool to recover energy from waste plastics, biomass, and heavy oils among others.

## **2.14 Common Factors affecting process reactors**

The process pyrolysis reactors are usually affected by factors such as reactor types, temperatures, catalysts used, residence/ retention times, heating rate, and catalyst ratio (Budsareechai et al., 2019a; Kumar & Singh, 2011; Omol et al., 2020; Panda et al., 2016).

### **2.14.1 Types of pyrolysis reactors**

Typically, the reactor systems include batch and semi-batch; fixed bed; fluidized bed; spouted bed; and screw kiln reactors. Their potential and limitations are briefly discussed.

#### **2.14.1.1 Batch and semi-batch reactors**

Batch and semi-batch reactors are widely adopted for research for the catalytic cracking of polymer material due to their ease of design and operation (Budsareechai et al.,

2019a; Demirbas et al., 2017). There is a substantial variation between batch and semi-batch reactors. The semi-batch reactor is usually swept by unremitting flow of an inert gas (such as nitrogen) that eliminates the volatile products from the medium at the reacting temperature. The elimination of the volatile compounds leads to secondary reactions of the main cracking products (e.g., oligomerization, cyclization, and aromatization) to take place only to a little extent (Budsareechai et al., 2019; Ayhan. Demirbas et al., 2017). This does not happen in a batch reactor in which secondary reactions are encouraged.

#### **2.14.1.2 Fixed bed reactors**

Fixed bed reactors could possibly be the most classical catalytic reactor (Augado et al., 2006). However, its usage with some polymers as feed is not direct due to high viscosity and low thermal conductivity which are problematic during loading of reactor. In some systems, the molten polymer is introduced inside the reactor with a capillary tube from a pressurized tank. This could require carrying out thermal cracking of the polymer and its derivatives using the batch as a technical solution. After which, the gaseous or liquid products resulting from thermal process are fed easily into the fixed bed.

#### **2.14.1.3 Fluidized-bed reactors**

Fluidized bed reactors present temperature and composition uniformity of the polymer degradation during pyrolysis (Augado et al., 2006). This is a notable benefit for polymers cracking due to their high viscosity and low thermal conductivity which often leads to the appearance of temperature gradients in some reaction systems where heat is not well shifted. Kaminsky developed the Hamburg process of fluidized bed type for pyrolysis of polymer materials (Kaminsky, 2006). It has inside diameter (450 mm), height (900 mm), long freeboard zone with no sand fluidizing (1075 mm) and height of

the fluidized sand bed (650 mm). Kaminsky also developed another fluidized bed reactor consisting with diameter (154 mm, height tube of stainless steel (670 mm) filled with sand (9 kg) and a gas distributor at the bottom shaped by 108 tubes of steel plate (Augado et al., 2006). A 5-kW filament is used as a heat source to heat the reactor and the polymer material is then fed into reactor with two screw conveyors. The obtained products are divided into numerous stages having cyclones, coolers, and electrostatic separators. Originally, this system has been used solely for polymer thermal cracking by preheated steam or nitrogen fluidizing agent. This process however had waxy components in its final liquid products but costly to run an experiment in the reactor due to additional components (Augado et al., 2006; Mertinkat et al., 1999).

#### **2.14.1.4 Spouted bed reactors**

Spouted bed reactor has an internal recycle reactor that work at low contact times (1-10 s) and appropriate catalyst to oil ratio (De La Puente & Sedran, 1998). In this reactor, the catalyst is placed in a basket then gases are incited by a turbine situated in the upper part which circulates through the basket (Elordi et al., 2011). The feed is injected at zero time and a valve is opened when the reaction is done, which then releases product into a vacuum chamber for analysis. This reactor can optimize gasoline yield and reduce gas components and coke formation. However, this reactor has a more complicated design compared to fixed and batch reactors with many pumps which must be installed. This thus increases the capital cost of the process. Some challenges arise as reactor functions during catalyst feeding, catalyst entrainment, and product collection.

#### **2.14.1.5 Screw kiln reactors**

Screw kiln reactors are of recent development for thermal and catalytic degradation of polymer substance. The start of the art of the reactor, advantages and limitations of this

reactor are well elaborated by Serrao *et al.* (2002). In this reactor, temperature is always controlled by series of integral thermocouples to avoid the presence of cold spots and plastic solidification (Serrano *et al.*, 2002). Screw speed usually varies from 0.5–25 rpm, thus altering the residence time of the polymer substance. The small diameter of the screw guarantees that the radial temperature profiles are practically insignificant. The catalyst is mixed together with polymer at the hopper to achieve a consistent reacting mixture and it follows polymer movement through the whole system, then later recovered by filtration. As compared to batch reactor, the screw kiln reactor results to lower formation of gaseous products and reduction of the over-cracking of the heavier fractions (Serrano *et al.*, 2003). There are also partly cracked polymers as there is no selective elimination of the volatile hydrocarbons that happen within the reactor.

#### **2.14.2 Catalysts used**

The catalysts used for polymers pyrolysis are mainly homogenous and heterogeneous. The majority of challenges associated with the use of catalysts can be addressed with an effective catalyst loading methodology. Catalysts can either be applied in a vapor contact phase or a direct contact (liquid) phase (Oyeleke *et al.*, 2021). The direct contact phase or sometimes referred to as the liquid phase involves the application of the catalyst and feedstock jointly inside reactor for the thermal degradation process. It has certain benefits for the pyrolysis decomposition process by improving energy efficiency and decreasing the overall process temperature as well as the residence time (Oyeleke *et al.*, 2021). However, the disadvantages associated with this method involve the inability of catalyst recovery, and deposition of impurities on the catalyst surface such as chlorine, nitrogen, and sulfur which ends up blocking the pores of the catalyst, and this, in turn, limits its economic value and application (Syamsiro *et al.*, 2014). Meanwhile, the indirect contact phase which is sometimes referred to as the vapor phase

involves the indirect contact of catalyst with the vapor formed after the pyrolysis process. This is characterized by a two-stage process involving a furnace unit for initial feedstock thermal degradation and then a separate reactor unit for catalytic cracking (Budsareechai et al., 2019b; Oyeleke et al., 2021). After pyrolysis vapors evolved from the furnace, it is then fed through the second stage of the reactor unit containing the catalyst, this ensures there is no direct contact of catalyst and feedstock, efficient catalyst recovery, and no coke formation and reduction in catalyst deactivation (Al-Salem et al., 2017). However, some of the said authors argue that this can lead to the additional cost of energy, equipment, and complexity of the setup.

#### **2.14.2.1 Homogeneous catalysts**

Homogeneous catalysts involve degradation of polyolefins with classical Lewis acids like aluminum chloride ( $\text{AlCl}_3$ ), metal tetrachloroaluminates, and catalytic systems based on organic ionic liquids. Ivanova *et al.* (1990) degraded polyethylene catalytically with  $\text{AlCl}_3$  at 370 °C which resulted to higher yields of gaseous compounds (88.2 wt%) than thermal cracking (40 wt% of gases at 400 °C) (Ivanova et al., 1990). Catalytic systems over ionic liquids are used as solvents for green chemistry processes due to their low volatility and ease of product separation with light alkenes ( $\text{C}_3\text{-C}_5$ ), such as isobutene, and branched and cyclic alkanes as the major product components (Adams et al., 2000).

#### **2.14.2.2 Heterogenous catalysts**

Current research has drawn attention on the application of heterogeneous catalysts during catalytic cracking of polymer substances. The common acid solids catalysts successfully applied for catalytic cracking of hydrocarbon feedstocks which are heterogenous include: silica-alumina and aluminas (Ivanova et al., 2002), zeolites

(Serrano et al., 2002), fresh and spent fluid catalytic cracking (Cardona & Corma, 2000); aluminum pillared clays and mesostructured (Aguado et al., 1996); nanocrystalline zeolites (Editor John Scheirs & Polyesters, 2006); superacid solids (Lin et al., 1997), expanded perlites (Kar, 2011), external surface (nano-zeolites) (Serrano et al., 2002), activated carbon and activated carbon-supported catalysts (Mark et al., 2020; Uemichi et al., 1989), and clay-based catalysts (Fadillah et al., 2021). The design of catalysts proficient for overcoming steric distractions by using available acid sites placed either into larger pores for the cracking of polyolefins is desirable which has attracted current research on clay-based catalysts such as kaolin. This clay is of low-cost, naturally available and desirable for pyrolysis process due to presence of silica ( $\text{SiO}_2$ ) and alumina ( $\text{Al}_2\text{O}_3$ ) contents (Hakeem et al., 2018; Rahman et al., 2020). Hakeem *et al.* (2018) revealed that pyrolysis of polymer substance with kaolin as a catalyst generated liquid products whose properties are similar to conventional fuels. The use of kaolin in pyrolysis process also results in reaction time decrease and an increase in liquid fraction (Eltohami & Mustafa, 2019).

### **2.14.3 Operating temperatures**

Temperature is essential variables affecting catalytic cracking of polymer substance (Hartulistiyoso et al., 2015). The rate of pyrolysis increases with temperature. The optimum reaction temperature for catalytic pyrolysis of polymers lie between 300-500 °C and that for production of diesel products from plastic waste pyrolysis lie between 300-450 °C (Editor John Scheirs & Polyesters, 2006). The temperature increase leads to a parallel action for enhancement of the catalysts (Pan et al., 2021). Temperature largely affects the pyrolysis process as reported on the catalytic cracking of heavy crude oils (Demirbas et al., 2017; Khelkhal et al., 2022). At high temperatures, the instantaneous occurrence of reactions from thermal cracking is favored, which modifies

product selectivity. The reactions required in the carbocationic chain pathway like initiation, propagation and termination are affected differently by temperature which include selectivity change, and mono or bimolecular formations.

#### **2.14.4 Residence and heating times**

Pyrolysis of heavy oil depends on residence and heating times. Different researchers employed several retention times during pyrolysis ranging from 0 min to more than 1 hour (R. Miandad et al., 2016). Lopez and coauthors conducted plastic waste pyrolysis at retention times of 0-15, 15-30, and 120 min (López et al., 2011). Improving the catalyst' surface area has been shown to reduce residence time of the pyrolytic processes (Budsareechai et al., 2019b). Kumar and Singh (2011) investigated HDPE pyrolysis at different temperature ranges of 400-550°C, and found as temperature increases retention time decreases as 760 min (400 °C), 290 min (450 °C), 68 min (500 °C), and 54 min (550 °C) (Kumar & Singh, 2011). High residence times coupled with high temperature increase cracking rate leading to an increase in the fraction of gaseous products, and light olefins (Pan et al., 2021). Optimum residence time is dependent on the intended products and the feedstock being pyrolyzed (D. Wang et al., 2013). It is hard to control residence time directly with exception of batch pyrolysis, but can be achieved by varying feeding rate, carrier gas flow rate and product discharge rate (Pan et al., 2021). Pan et al. (2021) varied residence time between 20 to 60 mins and found that an increase in residence time increases gas production. The longer residence time can enhance  $\beta$  cleavage likelihood for gas formation (Cai et al., 2021). The heating time is of immense importance to complete the carbonization at the selected temperature. At very low heating time, incomplete carbonization of the material will result.



## **2.15 Common Analytical techniques for heavy distillate and oil product analysis**

Several analytical techniques have been employed on heavy oil and oil product analysis and some have experienced more improvements as briefly described in the proceeding sections.

### **2.15.1 Gas chromatography-mass spectroscopy technique**

*Column chromatography* is used to separate, identify and purify components of a solid-liquid mixture for qualitative and quantitative analysis (Coskun, 2016). In this technique, the mobile (normally liquid) phase with a mixture of compounds is triggered to move together with a packed absorbent solid stationary phase. The liquid chromatography (LC) and gas chromatography (GC) are two major types of column chromatography with several chromatographic forms used which include partition, adsorption, gel, and ion exchange (Coskun, 2016). The high-performance liquid chromatography (HPLC) and ultra high-performance liquid chromatography (UHPLC) have been used for characterization of polymer material. The technique does not permit solvent to drip through a column under gravity but forced under high pressures of up to 400 atmospheres. A standard HPLC typically has column particles with 3  $\mu\text{m}$  to 5  $\mu\text{m}$  sizes, whereas UHPLC uses columns with particles size of 1.7  $\mu\text{m}$ , and pressures above 1000 bars.

*Mass spectrometry (MS)* is powerful analytical tool based on the measurement of the mass to charge ratio of ions from ionization and disintegration of sample molecules in the gas phase (Grabarics et al., 2022). The ensuing ion disintegration pattern identifies and quantifies known or unknown compounds in the sample, and explicate the structures and chemical properties of such molecules. In this technique, the mass spectrometer is mostly attached with GC or LC systems for detection purposes (Tsizin

et al., 2020). The LC or GC is applied to realize separation of sample compounds which can then be directed to the mass spectrometer successively to ionize, separate, and detect generated ions.

### **2.15.2 Infrared spectroscopy**

This is a quick and non-destructive method appropriate for structural analysis (Hong et al., 2021). It is versatile technique for crystal lattice determination and producing empirical qualitative relationships between specimens. In this technique, the infrared (IR) absorption spectrum is measured to study the vibrational energy levels of a molecule. This spectrum acts as a fingerprint for mineral identification which includes providing inimitable information about the mineral structure, family of minerals to which the sample belongs, degree of consistency within the structure, nature of isomorphic substituents, distinction of molecular water from constitutional hydroxyl, and hint for crystalline and non-crystalline impurities. Dry, ground clay powder is mixed with potassium bromide (KBr) in a polystyrene mortar and assorted evenly with a pestle (Olori et al., 2021). The assortment is then pressed into a disc with a hand press in preparation for Infrared spectrophotometer (IRS) analysis. The device is attached to a computer program that generates spectra and records wave numbers. The recorded wave numbers identify corresponding substances.

*Fourier Transform Infrared (FTIR) spectroscopy* is used to obtain the infrared spectrum of emission, absorption, and photoconductivity of liquids, solids and gases (Abdul Jameel et al., 2017). It can also be used to identify functional groups and chemical bonds of a substance through interpreting wavelengths from the spectrum (Balan et al., 2019). The mid infrared spectrum is separated into four regions i.e., single bond region (2500-4000  $\text{cm}^{-1}$ ), triple bond region (2000-2500  $\text{cm}^{-1}$ ), double bond region (1500-2000

cm<sup>-1</sup>), and fingerprint region (600-1500 cm<sup>-1</sup>) (Nandiyanto et al., 2019). The fingerprint region of a substance is used to differentiate between compounds, but has no real practical application as it contains numerous peaks which makes it hard to identify individual peaks (Balan et al., 2019).

### **2.15.3 Nuclear magnetic resonance spectroscopy**

This is modern technique which involves energy absorption as the nucleus of an atom is excited from the lower energy spin state to the highest ones (Tampieri et al., 2021). Many compounds are not easily elucidated by nuclear magnetic resonance (NMR) spectroscopy, while others cannot be studied completely. In natural products chemistry, carbon and hydrogen elements in organic molecules have isotopes (<sup>1</sup>H and <sup>13</sup>C, respectively) which generates NMR spectra rich in structural form. A proton NMR (<sup>1</sup>H NMR) spectrum provides detail about the chemical environments for hydrogen atoms in an organic molecule while carbon-13 NMR (<sup>13</sup>C NMR) spectrum gives for carbon atoms. Altogether, <sup>1</sup>H and <sup>13</sup>C NMR determine the exact molecular structure of a compound. It is used after preliminary studies with spectrometric techniques such as FTIR, ultra violet visible spectroscopy (UV-Vis), and mass spectrometry.

### **2.15.4 Scanning Electron Microscopy and Energy Dispersive X-ray**

Energy Dispersive X-ray (EDX) is used for elemental identification and quantitative composition (Shirley & Jarochovska, 2022). In this, the electron beam hits the inner shell of an atom and then knockouts an electron from the shell which leave a positively charged electron from an outer shell to fill the vacancy. It works on the principle that allows high-energy electromagnetic radiation to release core electrons from an atom. Scanning Electron Microscopy (SEM) is used for structural morphology and can be coupled with EDX for elemental identification and compositional analysis.

## **2.16 Thermal Analysis of Polymer Substance**

Thermal analysis is used to study structural changes in polymer substances through measuring changes in the heat capacity, and exothermic and endothermic heat flows occurring during degradation process (Cebe, 2005). The thermal properties of the polymer (heavy distillate) characterization are necessary to understand the operating conditions of the pyrolysis processes. The common techniques employed for the analysis of polymer substance include thermogravimetric analysis (TGA), differential scanning calorimetry (DSC), differential thermal analyzer (DTA), and simultaneous thermal analyzer (STA). Thermal analysis is widely used in various applications as it preferably offers benefits over other techniques such as simple in operation, more likely adaptable to characterization and kinetic analysis (Kök et al., 2017). The determination of thermal properties using various techniques requires certain atmospheres such as air, oxygen, carbon dioxide, and nitrogen. The nitrogen atmosphere has been widely used for several characterizations of various substances due to its low cost and abundance.

### **2.16.1 Thermogravimetric Analysis (TGA)**

Thermogravimetry refers to change in sample mass in relation to temperature (Feist, 2015). Thermogram provides information about the thermal stability and composition of the initial sample, intermediates, and residue which helps to study thermal decomposition kinetics of the organic substance (Gul et al., 2013). The TGA is divided into three various types that are dynamic, isothermal or static, and quasi-static (Loganathan et al., 2017). In dynamic TGA, the sample is heated at a constant heating rate which has a normal linear increase with time. In isothermal or static, the sample is kept at a constant temperature for a specified time and the difference in sample weight or mass is monitored. And meanwhile, for quasi-static TGA, the method involves the

sample being heated to a constant weight at every pace of the sequences of increasing temperatures.

### **2.16.2 Differential Thermal Analysis (DTA)**

This technique include dynamic relationship between temperature and change in physical property such as mass change or enthalpy change (Klancnik et al., 2010). Here the investigated material and an inert reference material such as aluminas, silicon carbide among others are exposed to similar heating method while the temperature is linearly increased. The temperature difference between the sample and reference material is recorded (Klancnik et al., 2010). The sample can undergo a physical or chemical change during experiment which can either be exothermic or endothermic thus making the process to develop a difference in temperature. For the endothermic process, the specimen exhibits a lower temperature compared to the reference which is accompanied by a minimum DTA shape whereas in exothermic the specimen shows a higher temperature compared to reference as seen by maximum DTA shape.

### **2.16.3 Differential Scanning Calorimetry**

The International Confederation for Thermal Analysis and Calorimetry (ICTAC) has defined differential scanning calorimetry (DSC) as measure of heat flow difference between sample and reference material (Klancnik et al., 2010). The concept of DSC initiated from past DTA instruments (Gill et al., 2010). The difference in temperature is measured by DTA whereas DSC grants for modified measurement in the enthalpy of a substance. The DSC tools are divided into two forms i.e., power compensation and heat flux (Gill et al., 2010). All the types are extremely versatile and very comparable and can be purposely employed to measure heat flow.

#### **2.16.4 Simultaneous Thermal Analyzer (STA)**

The use of STA can be viewed as a recent advance in analysis of thermal properties that eliminates uncertainties of separate TGA and DTA/DSC instruments such as sample geometry, temperature inaccuracies, and sample inhomogeneities. The application of TG and DTA/DSC allows an almost complete sample characterization, particularly for complex reactions. Thermal analysis techniques (TGA, DTA, and DSC) can also be linked to different analytical techniques such as FTIR and MS to identify the functional and chemical composition of the substance respectively. Kok *et al.* employed a multipurpose approach of thermal analysis on crude oil, the study investigated thermogravimetry (TGA) connected with Fourier transform infrared (FTIR), differential thermal analysis (DTA) and mass spectrophotometry (MS) instruments respectively to identify functional groups, thermal properties and chemical composition of the crude oils (Kök et al., 2017).

### **2.17 Analytical Techniques Suitable for Kaolin Characterization**

#### **2.17.1 Atomic Absorption Spectrometry (AAS) Analysis**

This is used to determine specific metal element concentration in a sample, with ability to analyze concentrations of more than 70 different elements in a solution (Helaluddin et al., 2016). It involves absorption of radiant energy by atoms of a sample (Jaiswal et al., 2010). The specimen is atomized by spraying a sample into a flame and the absorption radiation are studied from an electric lamp producing the spectrum of the element to be generated (Helaluddin et al., 2016). A dry powder of 1g is weighed in an electronic balance and transferred into a clean bottle. 100 mL of 1M Nitric acid is then added to the powder. The bottle is corked and its mixture digested. The mixture is then put in a centrifuge to allow for solid separation. The supernatant liquid can be kept in a volumetric flask in readiness for AAS analysis.

### **2.17.2 X-Ray Fluorescence Spectrophotometer (XRFS) Analysis**

This is used to give the mineral composition of the sample (Oyedotun, 2018). Here 20g of oven-dried clay powder is weighed using electronic balance and shifted into a clean dry porcelain crucible. The sample is added with 2g starch powder. The mixture is grinded into fine powder using pulverizer and then shifted into the pellet binder. The mixture of clay-starch is put in a compressor and compressed 175 KN to produce clay pellets (Owino et al., 2016). The pellets are labeled and analyzed for mineral composition. The obtained clay pellets sample is placed into the sample holders in the XRF spectrometer. The clay analysis mode setting is selected from the default program in the XRF software. The software has default calibrations for a particular element to be analyzed which then proceed automatically after button press. The element in oxide form is then displayed on the screen with its percentage composition.

### **2.17.3 X-Ray Diffraction (XRD) Analysis**

XRD is a multipurpose non-destructive technique that provide facts about the crystallographic structure and chemical composition of a substance. It is used to identify phase of crystalline materials and provide information on unit cell dimensions (Tun & Onn, 2020), such as identification and characterization of clay minerals (Zhou et al., 2018). The cavity of the glass-walled sample holder of the spectrometer is fed with dried clay powder sample for analysis. The holding capacity for each sample holder is around 0.35 g of clay powdered sample. Flattening and compression of sample surface maybe done. The remaining sample on the glass plate is usually wiped off with a clean paper soaked with alcohol. The XRD front side door can be opened and a standard sample holder is mounted on the selected position of the glass sample plate. The door knob is turned in the clockwise direction to lock the door. The sample holder is rotated by setting x-ray diffractometer with angle  $\theta$  and detector by  $2\theta$  (Zhou et al., 2018). X-

rays of Cu  $\alpha$ k wavelength  $1.54056 \times 10^{-10}$  m can be carefully chosen to scan the samples at  $2\theta$  between  $10^\circ$  and  $45^\circ$  which produces signals on a screen with printed names and formulae of the minerals.

### 2.18 Design of Experiment (DOE)

A response surface methodology (RSM) has attracted recent attention in the optimization of pyrolysis process. It is used to map out a design space using a relatively small number of experiments (Bhattacharya, 2021). Singh *et al.* examined process optimization using RSM with a central composite design (CCD) to achieve maximum oil yield (Singh et al., 2020). The study showed that pyrolysis process vastly depends on temperature followed by retention time, and gas flow rate. Bett *et al.* (2022) used RSM-CCD to study effect of reaction temperature, reaction time, and particle size on response yields from used tyres pyrolysis and this helps to identify optimal yield points (Bett et al., 2022). RSM consists of mainly Box Behnken Design (BBD) and CCD (Bhattacharya, 2021; Borkowski et al., 2021). The limitations of BBD are that it does not consider axial points or alpha values and two factors cannot be analyzed with it as compared to CCD where axial points and two factors are possible (You et al., 2022). Alpha ( $\alpha$ ) value means calculated distance of each axial/star point from the center (Asghar et al., 2014; Bhattacharya, 2021). For alpha ( $\alpha$ ) less than 1, shows the axial point must be a cube, and that greater than 1 shows it is outside the cube (Bhattacharya, 2021). There are five levels in each factor during a CCD which includes: extreme low star point, low point, center point, higher point, and extreme high star point,. The Alpha ( $\alpha$ ) and uncoded values can be evaluated using Equation 2.16 and Equation 2.17, respectively (Bhattacharya, 2021):

$$\alpha = (\text{Number of factorial runs})^{1/4} = (2^k \text{ or } 2^{k-r})^{1/4} \quad (2.16)$$



Where  $k$  is the number of factors.

$$\text{Uncoded Value} = (\text{Coded value} \times L) + C \quad (2.17)$$

Where,  $L$  = Length expressed in real units between center points and + 1 value of factor, and  $C$  = Centre point value expressed in real units.

The RSM-CCD are inbuilt in Design Expert and Minitab software which provides screening, comparative tests, optimization, characterization, mixture designs, robust parameter design, and combined designs (Jankovic et al., 2021). The software determines the main factor effects and factor interactions through varying all factor values in parallel which helps to understand multi-dimensional surface with non-linear profiles, and provide a feature which helps to analyze the optimum process (Bhattacharya, 2021).

### **2.19 Literature Summary**

A summary of selected literatures with its findings and limitations is presented in Table 2.2.

**Table 2.2: The Summary of Selected Literatures**

Research Aim	Findings	Limitations/Gaps
Produce gasoline and diesel like products from heavy oil via catalytic pyrolysis (Demirbas et al., 2017)	<ul style="list-style-type: none"> <li>• The oil product yields increase as temperature and catalyst ratios increase by use of Na<sub>2</sub>CO<sub>3</sub> as catalyst.</li> </ul>	<ul style="list-style-type: none"> <li>• High concentration of aromatic hydrocarbons in the oil products with use of this catalyst.</li> <li>• Insufficient cracking ability by catalyst due to high heavy oil contents (17%) remaining in product.</li> </ul>
Catalytic hydrocracking of heavy wax from pyrolysis of plastic wastes using Pd/H $\beta$ for naphtha-ranged hydrocarbon production (Choi et al., 2022)	<ul style="list-style-type: none"> <li>• Excessive cracking with Pd/H<math>\beta</math> catalyst, leads to the liquid yield reduction.</li> <li>• Low catalyst ratio (0.2%) yielded low naphtha production</li> </ul>	<ul style="list-style-type: none"> <li>• Low liquid yield with Pd/H<math>\beta</math> catalyst.</li> <li>• Very low catalyst ratio affect naphtha yield.</li> <li>• Excessive aromatics (83.2% in the naphtha fraction).</li> </ul>
Compare natural zeolite and kaolin as a catalyst in the isothermal-catalytic cracking of municipal solid waste (MSW) for bio-oil production. (Gandidi et al., 2018)	<ul style="list-style-type: none"> <li>• Kaolin showed higher oil yield of 23.6% compared to zeolite 21.4% due to its higher active site and lower surface acidity.</li> <li>• Oil product from kaolin had relatively lower viscosity (2.0 cSt)</li> <li>• Kaolin has good cracking ability than natural zeolite (2.5 cSt).</li> </ul>	<ul style="list-style-type: none"> <li>• High viscosity with natural zeolites.</li> <li>• Lower cracking ability of zeolites toward liquid fraction.</li> <li>• The study shows that Kaolin can provide a better alternative as a catalyst necessitating its choice for this research.</li> </ul>

## **CHAPTER THREE**

### **MATERIALS AND METHODS**

#### **3.1 Introduction**

This chapter includes materials and methods that were used to achieve study objectives.

#### **3.2 Materials Used**

The materials collected were heavy distillate and kaolin clay.

##### **3.2.1 Collection and preparation of HD sample**

The heavy distillate sample of 5L was collected from Alternative Energy Systems Limited (AESL), Thika, Kenya. The collected sample (heavy distillate) shown in Plate B.1 (Appendix B) was used for this study at Chemical and Process Engineering Laboratory of Moi University (Kenya) to produce diesel-like products via catalytic and thermal pyrolysis. The distillate sample was used “as received” for the pyrolysis experiment without any prior chemical or physical processing. The company was chosen since they are producing heavy distillate as a byproduct from pyrolysis of plastic waste and also due to the study relevance for improving its operational and market value.

##### **3.2.2 Kaolin collection, preparation and characterization**

Kaolin clay was obtained from Eburru Hill, Nakuru county - Kenya where the deposit is located for use as a catalyst. The obtained kaolin was sundried for 7 days. The sundried kaolin was pulverized with a mortar and pestle to produce a fine powder and then sieved using a laboratory test sieve before use to achieve a uniform size by using a sieve mesh size of 400  $\mu\text{m}$  as in literature (Dewi et al., 2018; Luo et al., 2020) and was prepared and sieved as shown in Plates A.1-3 (Appendix A). The sieved kaolin was put in an electric oven (model: LDO-150F LabTech, DAIHAN LABTECH CO. Ltd, South

Korea) and dried for 3 hours to obtain uniform sample moisture content and was stored at room temperature for pyrolysis experiment.

### 3.2.2.1 Moisture content of fresh Kaolin

The kaolin moisture content (MC) was determined with oven drying method using Daihan LabTech Oven (Model: LDO -150F). Three samples of fresh kaolin clay were prepared and weighed together with a crucible before it is put for normal oven drying at 105 °C. The weights of the porcelain crucibles were first taken before samples were put in and then put in the oven for 24 hours. The oven was then allowed to cool for one hour after which the crucible and dried samples together were reweighed using an analytical balance (Model: HZT - A200 with 0.001g accuracies). The MC (dry basis) was then determined using Equation 3.1. The obtained values of MC of kaolin clay are presented in Table A.1 in Appendix A.

$$M. C_{dry\ basis} = \frac{m_2 - m_3}{m_2 - m_1} \times 100 \quad (3.1)$$

Where,

$m_3 = \text{Weight of Crucible and sample after drying (g)}$

$m_1 = \text{Weight of Crucible (g)}$

$m_2 = \text{Weight of crucible and sample before drying (g)}$

$M. C_{dry\ basis} = \text{Moisture Content on dry basis (\%)}$

### 3.2.2.2 XRF Analysis of Kaolin Clay

A 4 g sample of oven-dried sieved 400 µm clay powder was analyzed with a Bruker S1 Titan 600 handheld XRF Analyzer (Bruker Nano Analytics, Berlin, Germany) for chemical compositions and suitability for pyrolysis process. The sample was transferred into a clean dry 32 mm polyethylene sample cup with film. The sample cup was then positioned in the XRF detector, scanned, and analyzed using Bruker XRF

software, the desktop was jointly connected to the analyzer with USB cable connectivity and the results were manipulated, displayed, and printed.

### 3.3 Equipment Used

A locally made modified brick electric furnace (MBEF) located at Chemical and Process Engineering laboratory, Moi University (Kenya) was utilized as a heating source for the pyrolysis of heavy distillate with and without kaolin into diesel-like oils. The flowchart of the furnace was as shown in Figure 3.1 and its specifications in Table 3.1. The resistance heating element of the MBEF was purchased, sized and installed as a heating source for pyrolysis. The kanthal spiral heating resistance wire of 530 mm unstretched length, 8.3 mm in diameter, and 0.8 mm in thickness with a rated power of 3,000 W and 65  $\Omega$  resistance was bought from a local electrical shop in Nairobi [Kenya] for use as furnace heating element wire and was first sized. The sizing of the minimum and maximum resistances of the heating wire required was obtained using Equation 3.2 and Equation 3.3 respectively. The standard values of current,  $I$  (10 A), and voltage,  $V$  (220 V) were taken directly from a single-phase electronic kWh meter specification to determine the minimum resistance of the heating wire required for a brick furnace as 22  $\Omega$  using Equation 3.2. The heating resistance coil (wire) had a standard design capacity to dissipate 3000 W of power and with the current of 10 A flowing through the circuit from the kWh meter the maximum resistance of 30  $\Omega$  was obtained using Equation 3.3. The required resistance of the resistance heating element for the furnace was established to lie within 22-30  $\Omega$ . Based on this range, a 25  $\Omega$  resistance was selected for use as a heating resistance wire for a brick electric furnace. The original 65  $\Omega$  spiral resistance heating wire was manually stretched by holding it from either side until there was no contact between them. Stretching of the resistance heating wire is important to avoid short-circuiting during operation and to obtain accurate resistance

measurements. The DT-830D digital multimeter with 0.01  $\Omega$  accuracy was used to measure the required 25.00  $\Omega$  resistance heating wire from the standard 65.00  $\Omega$  stretched resistance heating wire and the wire was then wound inside the created sinusoidal grooves of two fire bricks spaced apart within the heating chamber in a modified brick furnace and connected through the connector.

$$R_{min} = \frac{V}{I} \quad (3.2)$$

$$R_{max} = \frac{P}{I^2} \quad (3.3)$$

Where  $R_{min}$  is minimum resistance ( $\Omega$ ),  $I$  is current (A),  $V$  is voltage (V),  $R_{max}$  is maximum resistance ( $\Omega$ ),  $P$  is power (W).

The insulating refractory bricks of 235 x 114 x 77 mm standard size were laid in the basement in rectangular form. Three grooves spaced at equal intervals were made in each of the two oppositely fire bricks (230 x 113 x 35 mm) standard size spaced 235 mm apart on top of the basement refractory bricks and laid between the heat resistance refractory bricks to form a rectangular heating chamber with length x breadth x height (235 x 235 x 77 mm). The 25  $\Omega$  kanthal spiral heating resistance wire with 3000 W capacity to dissipate power was carefully wound inside the grooves. The surrounding portions were covered with refractory bricks as an insulation material. A 31 mm diameter hole which is equivalent to the neck outer diameter of 250 mL borosilicate round-bottomed flask with arm (outer neck diameter – 30 mm) was created mid-way of the fire brick covering the top of the heating chamber for easy covering of the flask. The glassware flask (250 mL borosilicate round-bottomed flask) was employed as a batch reactor for pyrolysis of heavy distillate. A sheathed K-thermocouple (OKAZAKI AEROPAK) was inserted within the pyrolysis chamber to monitor temperature inside

the heating (pyrolysis) chamber. The other end of the thermocouple was connected to a digital PID temperature controller with 1 °C accuracy connected to the main source. A single-phase electronic kWh meter with 0.1 W (watt) degree accuracy (model: DDS2811, LINIER Electric Co. Ltd, Germany) with voltage - 220V and current - 10(60)A was connected to the main source (250 V, 13 A) to monitor power consumption during the pyrolysis process.

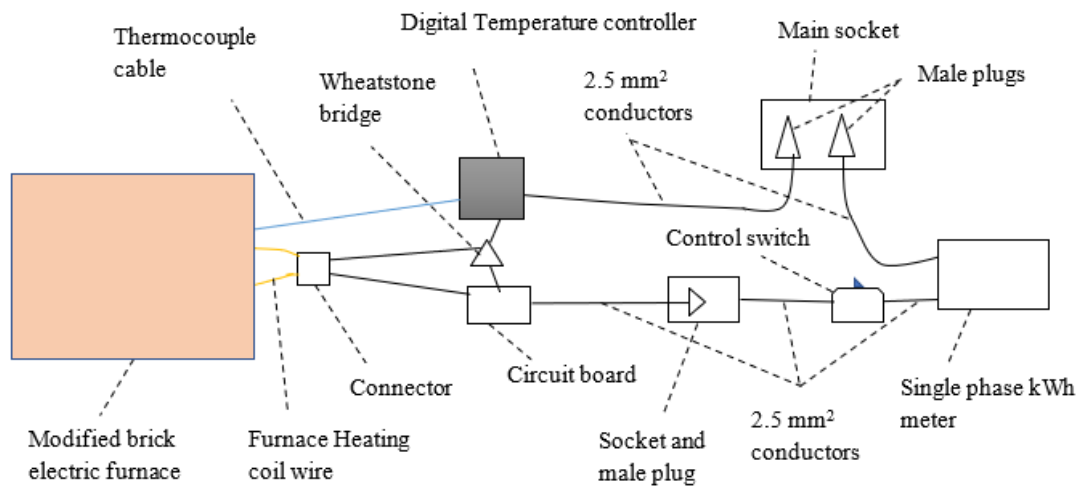


**Figure 3.1: Flowchart showing description of modified brick electric furnace**

**Table 3.1: Specifications of Modified Brick Electric Furnace**

S/N	Quantity	Description	Specification	Model	Manufacturer
1	3	Male plug	250V, 13A	Elite FAB	Elite FAB
2	1	Single phase electronic kWh meter	IEC 61036, 220V, 10(60)A	DDS28II	Linier Electric Co. Ltd
3	1	Control Switch	230/400V, GB/T 10963.1	DZ47.63 ANDELI	ANDELI
4	1	Socket	-	Goldlite	Goldlite
5	1	Conductor	2.5 mm <sup>2</sup> , 3 m	-	-
6	1	Circuit Board	30A, 250VAC/30VDC	SLA-12VDC-SL-C	SONGLE
7	1	Wheatstone bridge	-	-	-
8	1	Sensor transformer	AC 110V/220V AC 12Vx1 500 MA	AMIR	AMIR, China
9	1	Temperature Controller	Lot No.: 01Y3MR	E5CN-R2T OMRON	OMRON, China
10	1	Connector	15A, 250V	15A,250V	China made
11	1	Thermocouple	Element K Class:1, Sheath Mt 1:H2300, No.: KPM61633	K type	OKAZAKI AEROPAK
12	1	Resistance Heating Element Wire	Thickness: 0.8 mm, Spiral	STAR SUNLITE 26 SWG Nichrome Wire	Star Sunlite
13	3	Fire bricks	230 x 113 x 35 mm size	Standard size	-
14	13	Refractory Bricks	235 x 114 x 77 mm size	Standard size	-

### 3.4 Experimental Procedure

A batch reactor was used for the study since it is the most widely used laboratory reactor and also it is simple and easy to set up (Hashimoto & Al, 1994; Varma & Mondal, 2017). The process setup was as shown in Figure 3.2 and Plates B.2-3 (Appendix B). The whole setup of this reactor consisted of a modified brick furnace, 250 mL round-bottomed flask with arm, 300 mm Liebig condenser, heating assembly, digital PID temperature controller (connected to a thermocouple), temperature sensor (thermocouple), a heating chamber (for housing glassware – borosilicate round-



bottomed flask with arm), storage/collection flask with gas exit line. After feeding heavy distillate into the round-bottomed flask with an arm, the flask was then put inside the heating chamber and sealed with refractory bricks. The operating temperature was set by manually adjusting the temperature controller knob until it reaches the desired value and the process was started by turning on the power and control switch for the electric furnace. The sample inside the round-bottomed flask with an arm was heated by a modified brick electric furnace as an external heat source at a constant temperature. During operation, the vapor from the reactor process moves upward and goes through the round-bottomed flask's arm and then condensed in a Liebig condenser. The condensed oil is collected on the beaker which is coupled to the Liebig condenser through plastic tubing. The weight of oil formed with time was monitored every 2.5 mins using SCALTEC electronic weighing balance with 0.01g degree accuracy.

Thermocouple connected  
to temperature controller

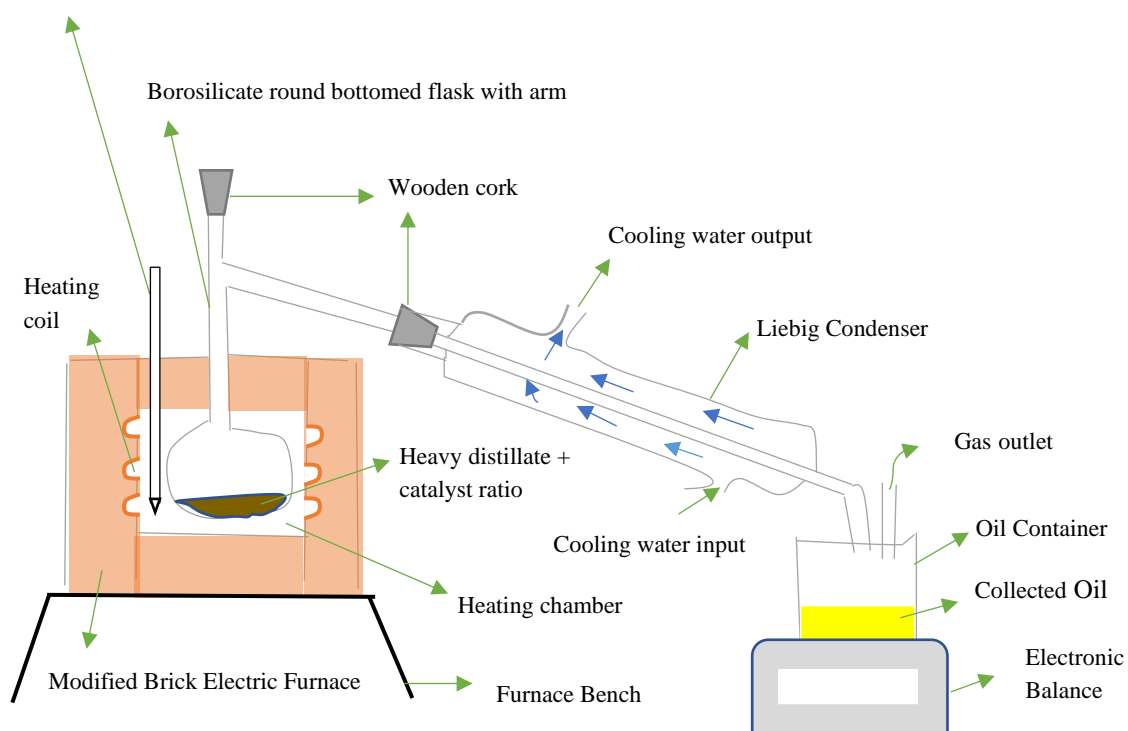


**Figure 3.2: Pyrolysis setup showing cross-section of a Batch Reactor**

During thermal pyrolysis (TP), reaction temperature and heating time were used as pyrolysis process parameters and a response surface methodology central composite design (RSM-CCD) was used as the design matrix for the two process variables. Thirteen (13) runs were performed by following the RSM-CCD matrix for TP as shown in Table 3.4. The TP was done as a control method to comprehend the effect of the catalyst on product yield. The weight of heavy distillate (HD) used in each experimental run was 80 g. The empty borosilicate round-bottomed flask with an arm was first weighed using an electronic weighing scale (SCALTEC model) then tared and 80 g of heavy distillate was weighed inside the tared flask. The weighed HD inside the flask was put in the heating chamber of the modified brick electric furnace and then carefully sealed with two refractory bricks for the experiment. During Catalytic Pyrolysis (CP); reaction temperature, heating time, and catalyst ratio were used as pyrolysis process parameters with CCD-RSM used as a design matrix for the three process variables. Twenty (20) runs for CP were carried out following the design matrix shown in Table 3.5. The catalyst (kaolin) ratio in heavy distillate was varied at 5, 10 and 15% of HD amount whereas reaction temperatures (350, 375, 400 °C) and heating times (90, 120, 150 mins) were used. The 80 g heavy distillate was maintained during CP and mixed with kaolin catalyst at varying ratios and then put into the reactor (round-bottomed flask with an arm inside the modified brick electric furnace) for CP experimental runs. The prepared sample of feedstock (heavy distillate and kaolin mixture) was weighed into the round-bottomed flask with an arm. The weighed mixture inside the flask was then put inside the heating chamber of the modified brick electric furnace and the experiment was done as that for thermal pyrolysis. The sample of diesel like oils obtained during experiments are presented in Plate B.4 (Appendix B). Uncondensed gases produced during each experimental run were obtained by the difference in the oil amount and

residue from the heavy distillate used. The obtained yield was calculated by measuring the fractions of liquids, gases, and remaining residues on a weight basis for thermal and catalytic pyrolysis experiments. The liquid oil, solid residue and gas yields from each test-run of catalytic and thermal pyrolysis were calculated in terms of the percentage by using Equation 3.4, Equation 3.5 and Equation 3.6, respectively (Ahmad et al., 2015; Choi et al., 2022).

$$\text{Liquid oil yield (\%)} = \frac{\text{Weight of liquid (diesel) oil produced (g)}}{\text{Weight of the Heavy distillate Used (g)}} \times 100 \quad (3.4)$$

$$\text{Solid Residue yield (\%)} = \frac{\text{Weight of solid residue left (g)}}{\text{Weight of heavy distillate used (g)}} \times 100 \quad (3.5)$$

$$\text{Gas yield (\%)} = 100 - \text{Liquid oil yield} - \text{Solid residue yield} \quad (3.6)$$

### 3.5 Experimental Design

A response surface methodology central composite design (RSM-CCD) was employed for thermal and catalytic pyrolysis experiment. The CCD matrix involved determining alpha values and uncoded values for the design matrix. The alpha and uncoded values for thermal and catalytic pyrolysis experiments were determined using Equation 2.16 and Equation 2.17, respectively as done in previous work (Bhattacharya, 2021). To determine the alpha values for thermal pyrolysis (TP) two factors i.e., temperature and heating time; and for catalytic pyrolysis (CP) three factors i.e., temperature, heating time and catalyst ratio were considered which gives Alpha ( $\alpha$ ) =  $(2^2)^{1/4} = 1.41421$  and Alpha ( $\alpha$ ) =  $(2^3)^{1/4} = 1.68179$ , respectively. The reaction temperatures of 350, 375, and 400 °C; heating times of 90, 120, 150 mins were used for thermal pyrolysis, and a catalyst ratio of 5, 10, and 15% added during catalytic pyrolysis experiment. The uncoded values of reaction temperature and heating time for TP were determined as:

$$\begin{aligned} \text{Uncoded value of } -\alpha &= (\text{Coded value} \times L) + C = (-1.414 \times 25) + 375 \\ &= 339.65 \text{ } ^\circ\text{C} \end{aligned}$$

$$\begin{aligned} \text{Uncoded value of } +\alpha &= (\text{Coded value} \times L) + C = (1.414 \times 25) + 375 \\ &= 410.35 \text{ } ^\circ\text{C} \end{aligned}$$

$$\begin{aligned} \text{Uncoded value of } -\alpha &= (\text{Coded value} \times L) + C = (-1.414 \times 15) + 60 \\ &= 38.79 \text{ min} \end{aligned}$$

$$\begin{aligned} \text{Uncoded value of } +\alpha &= (\text{Coded value} \times L) + C = (1.414 \times 15) + 60 \\ &= 81.21 \text{ min} \end{aligned}$$

The uncoded values for TP are thus summarized in Table 3.2. Similarly, for the catalytic pyrolysis experiment, the uncoded values (for corresponding alpha values) for temperature, heating time, and catalyst ratio evaluated are summarized in Table 3.3. The Design Expert 13 version software was used to create matrix design of the experiments for thermal and catalytic pyrolysis as shown in Table 3.4 and Table 3.5. The software is inbuilt with CCD-RSM and automatically creates a design matrix that incorporates alpha values.

**Table 3.2: Number of Factors and  $\alpha$  Value for TP experiment**

Level of Factor	$-\alpha$ (-1.414) (Lowest)	-1 (Lower)	0 (Center Point)	+1 (High)	$+\alpha$ (+1.414) (Highest)
Temperature (°C)	340	350	375	400	410
Heating Time	77.58	90	120	150	162.42

**Table 3.3: Number of Factors and  $\alpha$  Value for CP experiment**

	$-\alpha$ (-1.68179)	-1	0	+1	$+\alpha$ (+1.68179)
Temperature (oC)	333	350	375	400	417
Catalyst Ratio (%)	1.59	5	10	15	18.41
Heating Time (min)	69.55	90	120	150	170.45

**Table 3.4: Design Matrix for DOE for Thermal pyrolysis**

StdOrder	RunOrder	PtType	Blocks	Temperature (°C)	Heating Time (min)	Product Yield (%)
8	1	-1	1	375.000	162.426	-
9	2	0	1	375.000	120.000	-
10	3	0	1	375.000	120.000	-
11	4	0	1	375.000	120.000	-
2	5	1	1	400.000	90.000	-
7	6	-1	1	375.000	77.574	-
12	7	0	1	375.000	120.000	-
1	8	1	1	350.000	90.000	-
13	9	0	1	375.000	120.000	-
6	10	-1	1	410.355	120.000	-
4	11	1	1	400.000	150.000	-
5	12	-1	1	339.645	120.000	-
3	13	1	1	350.000	150.000	-

**Table 3.5: Design Matrix for DOE for Catalytic Pyrolysis**

StdOrder	RunOrder	PtType	Blocks	Temperature (oC)	Heating Time (min)	Catalyst Ratio (%)	Product Yield (%)
12	1	-1	1	375.000	120.000	18.4090	-
10	2	-1	1	417.045	120.000	10.0000	-
13	3	-1	1	375.000	69.546	10.0000	-
18	4	0	1	375.000	120.000	10.0000	-
1	5	1	1	350.000	90.000	5.0000	-
2	6	1	1	400.000	90.000	5.0000	-
17	7	0	1	375.000	120.000	10.0000	-
4	8	1	1	400.000	90.000	15.0000	-
9	9	-1	1	332.955	120.000	10.0000	-
14	10	-1	1	375.000	170.454	10.0000	-
8	11	1	1	400.000	150.000	15.0000	-
6	12	1	1	400.000	150.000	5.0000	-
3	13	1	1	350.000	90.000	15.0000	-
20	14	0	1	375.000	120.000	10.0000	-
16	15	0	1	375.000	120.000	10.0000	-
11	16	-1	1	375.000	120.000	1.5910	-
19	17	0	1	375.000	120.000	10.0000	-
15	18	0	1	375.000	120.000	10.0000	-
7	19	1	1	350.000	150.000	15.0000	-
5	20	1	1	350.000	150.000	5.0000	-

### **3.5.1 Statistical Analysis of Selected Process Parameters**

The study analyzed the effects of catalyst to heavy distillate ratio, heating time, and reaction temperatures on product oil yield using desktop statistical analysis techniques. Design Expert 13 and Minitab 18 version software were used to analyze oil yield. The software were used to evaluate the effect of reaction temperatures and heating times on oil yield for the thermal pyrolysis experiment as well as the effect of catalyst ratio, operating temperature, and heating time for catalytic pyrolysis ones. A three-dimensional (3D) Surface, Pareto, Contour, and Normal plots were generated using the software to show the effects of selected parameters on oil yield. A contour and surface plots were generated with the Design Expert 13 software for each experiment to analyze the effect of independent variables on response oil yield. The Pareto and Normal plots were generated using Minitab 18 version statistical software to show different interaction effects on oil yield. Regression response models were obtained using the coefficients of the models obtained after ANOVA of the oil yield with the statistical software. Predicted oil yields were also generated using the software.

### **3.6 Characterization of heavy distillate from plastic waste**

This was done to understand heavy distillate properties and its pyrolysis products and to provide the basis for comparison and optimum conditions of pyrolysis processes. Different characterization techniques were employed for determining physical properties, elemental analysis, and thermal properties of the heavy distillate.

#### **3.6.1 Physical properties**

The physical properties (density, calorific value, viscosity) of heavy distillate were determined following ASTM method standard guidelines. Similarly, these properties

were also determined for pyrolytic liquid oils (PLOs) produced with and without catalyst.

### **3.6.1.1 Determination of density of heavy distillate**

The density of the heavy distillate (HD) sample was determined by the displacement method at room temperature following Archimedes' principle (Quesada et al., 2022). The calibrated measuring cylinder was first weighed, and a certain amount of HD sample was carefully dropped inside the cylinder and weighed together, the HD sample weight was obtained through subtracting cylinder weight, and a 40 mL water was then added inside the cylinder with HD and the displaced water was taken as its volume. The weight of the HD was divided by volume to obtain density of the HD sample. The procedures were repeated three times and average values were taken as the density of the HD sample as shown in Table B.1 (Appendix B).

### **3.6.1.2 Determination of Calorific (Heating) Value**

The calorific value of heavy distillate and pyrolytic liquid oils (HD & PLOs) fuels was determined using a Bomb Calorimeter (model: 1013-J, Yoshida Seisakusyo Co., Ltd, Japan) following ASTM D2015 and ASTM D240 method, respectively. For comparison purposes, the higher heating values of the HD & PLOs were also determined according to Dulong's Formula in Equation. 3.7 as in previous work (Quesada et al., 2022).

$$HHV = 8080C + 34460 \left[ H - \frac{O}{8} \right] + 2250S \quad (3.7)$$

Where C, H, S, and O represent mass fractions of carbon, hydrogen, sulphur, and oxygen respectively. The units for Equation 3.1 are calculated in kcal/kg and hence was converted in this study to MJ/kg (1 kcal = 0.004184 MJ).

### 3.6.1.3 Determination of kinematic and dynamic viscosities

The kinematic viscosities of the heavy distillate and PLOs were determined at 40 °C using CT 500 constant temperature viscosity bath (CANNON Instrument Co., 2139 High Tech Road, State College, PA, 16803, USA) following standard guidelines by the ASTM D445 method and in accordance to ISO 3104/3105. The dynamic viscosity of the samples was evaluated by multiplying the measured kinematic viscosity (cSt) with sample density as specified in ISO 3104:2020 using Equation 3.8 (International Organization for Standardization [ISO], 2020).

$$\eta = \nu \times \rho \quad (3.8)$$

Where  $\nu$  is kinematic viscosity (cSt),  $\eta$  is dynamic viscosity (cP), and  $\rho$  is density

### 3.6.2 Elemental Analysis

This involves an accurate chemical analysis by mass of the important elements in the fuel. It is also referred to as ultimate analysis. The sulphur, carbon, and hydrogen contents of the heavy distillate and pyrolytic liquid oils (HD & PLOs) were determined using ELTRA HELIOS CHS 580A analyzer (ETRA GmbH, Germany) following the standard test methods on ASTM D5291 for hydrogen, nitrogen and carbon in petroleum products and ASTM 2622 for sulfur. The Ultraviolet-Visible (UV-Vis) spectrophotometer (Spectro-UV-11 model, mrc laboratory instruments, Hagavish 3 Holon, Israel) was employed to determine the composition of nitrogen content in the heavy distillate and pyrolytic liquid oils. Oxygen content was calculated by taking the difference from total CHNS content from 100 using Equation 3.9 (Omar et al., 2019).

$$\text{Oxygen (\%)} = 100 - (\%C + \%H + \%N + \%S) \quad (3.9)$$



### 3.6.3 Thermal Properties

The thermal properties of heavy distillate were studied using simultaneous thermal analysis (STA). The STA simultaneously produce both thermogravimetry and differential scanning calorimetry (TGA-DSC) results comprising time, weight, program temperature, sample temperature, heat flow, microvolt, and R25 diagnostic signal.

#### 3.6.3.1 Thermogravimetric Analysis (TGA)

Thermal analysis of heavy distillate (HD) samples was carried out in PerkinElmer STA 6000 Simultaneous Thermal Analyzer (made in the Netherlands) in an alumina crucible (6 mm diameter). The thermogravimetry (TG) experiments were conducted under a nitrogen atmosphere of 20 mL/min flow rate, temperature range of 25 to 800 °C, heating rates of 5, 10, 15, and 20 °C/min and approximately 20 mg mass sample.

TGA analysis based on time, weight and sample temperature from the STA data was conducted to comprehend the volatilization characteristics of the HD for the pyrolysis process. Weight loss over time or temperature were taken under non-isothermal conditions. The STA data was used to analyze HD Sample kinetics at each heating rate using Modified Coats Redfern Model (MCRM). A thermogram was plotted as shown in Figure 4.2 for a graph of  $\ln(-\ln(1-X))$  verses  $1000/T$  at every heating rate, and their slopes were evaluated at three-phase transformations (1, 2, and 3) from the thermogram curve as shown in Figures E.1-3 in Appendix E to determine various thermodynamic parameters. The obtained slope was used to compute the activation energy of the heavy distillate at each phase and heating rate. The modified Coats Redfern method (MCRM) was used to determine activation energy values as described in Equation 2.7. The intercept of the graph in Figures E.1-3 were used to compute frequency factor and frequency factor was used to compute entropy, enthalpy and Gibbs free energy of HD

at respective phases. The rate constant and half-life of the heavy distillate at various heating rates were determined from the slope through plotting a graph of  $\ln(1-x)$  against time at different stages as shown in Figure 4.3 and in Figures F.1-3 (Appendix F). The slope of this graph gives the rate constant of the substance at any particular phase. The half-life of HD sample was determined using Equation 2.9. The frequency factor (A) for the sample was determined using Equation, 2.11. The entropy changes ( $\Delta S$ ) of the HD reaction process were determined using Equation 2.10 and enthalpy changes ( $\Delta H$ ) of HD were determined using Equation 2.12. And the changes in Gibbs free energy ( $\Delta G$ ) were determined using Equation 2.13.

### **3.6.3.2 Heat flow profiles**

The heat flow curves for heavy distillate sample were determined by plotting STA data based on temperature ( $^{\circ}\text{C}$ ) and heat flow (mW) as in previous work (Khelkhal et al., 2022). The results give the decomposition temperature of the sample where optimum values were ascertained.

### **3.6.4 FTIR Analysis**

The functional group composition of heavy distillate and its pyrolytic liquid (diesel) oil products samples was identified using a Fourier Transform Infrared (FTIR) Spectroscopy (Model: FT/IR -6600 Type A, JASCO Corporation, Japan). The absorption of infrared radiation was measured between  $4000\text{-}400\text{ cm}^{-1}$ . The sample was positioned over the attenuated total reflectance (ATR) crystal and maximum pressure was applied by the slip-clutch mechanism of the clamp. All spectra were collected at  $4\text{ cm}^{-1}$  spectral resolution. The obtained spectra were searched using the accessory JASCO Technologies ATR PRO ONE Spectral Database and detected using a triglycine sulfate (TGS) detector with a standard light source. The automatic scanning

speed of the spectra was 2 mm/sec. The data points recorded were 3,736 with a data interval of approximately  $0.964\text{ cm}^{-1}$  wave number. An excel sheet csv-file was then exported for data analysis and interpretation.

### 3.6.5 GC-MS Analysis

The organic chemical composition presence in heavy distillate and pyrolytic liquid oils (HD & PLOs) was characterized using Gas Chromatograph-Mass Spectrometer (GCMS-QP2010 SE, SHIMADZU Corporation) as per ASTM D6420 method. A capillary gas chromatograph 30 m long and 0.25 mm wide column coated with a 0.25  $\mu\text{m}$  thick film of 5% acetone (2-Pentanone, 4-hydroxy-4-methyl-) was used for separation. The column oven temperature was set at 35.0 °C for 3 min and then augmented up to 250 °C using a 5 °C/min heating rate. The ion source and transfer line temperatures were kept at 200 and 250 °C, respectively and splitless injection was then applied at 250 °C. Acetone (1 mL) was used as the solvent and about 20  $\mu\text{L}$  sample was injected, and the solvent cut time was 1.50 min. The carrier gas, helium was used for GC with a 5.7 psi pressure, and purge flow of 3.0 mL/min under linear velocity flow control mode with a velocity of 30.0 cm/sec. The mass spectrometer start time was 2.10 min and the end time was 78.00 min. The start charge to mass (m/z) ratio was 35.00 and the end m/z ratio was 500.00. The chromatographic peaks were identified using mass spectral data library (National Institute of Standards and Technology - NIST) (NIST14.lib), and the peak percentages were assessed for their total ion chromatogram (TIC) peak area. The name of the molecular compound, its molecular weight, and the molecular formula were obtained from the NIST14.lib and were separated according to hydrocarbon groupings and the total area percentages for each grouping were then obtained.

### **3.7 Characterization of Fuel Properties**

The oil products from thermal and catalytic pyrolysis experiments were characterized based on physical properties, elemental, FTIR, and GC-MS analyses. The determination method of physical properties such as viscosity, calorific values; elemental analysis, functional groups analysis, and GC-MS analysis of pyrolytic liquid oils (PLOs) were done as earlier explained with that of heavy distillate. The density, pH, pour point, flash point, and freezing point of PLOs were determined as follows in proceeding sections.

#### **3.7.1 Determination of Density**

The density of oil samples was determined with a specific gravity bottle following guidelines by the ASTM D1298 method.

#### **3.7.2 Flash point Determination**

The flash point of liquid oil product was determined in accordance to guidelines by ASTM D93 method using Seta Semi-Automatic Cleveland Open Cup Flash Point Tester (Model: 13811-3p, Stanhope-Seta, London Street, Chertsey, Surrey KT16 8AP, England, UK).

#### **3.7.3 Freezing and Pour points Determination**

The freezing and pour points of the liquid product were determined using Azmayesh Abzar cloud and pour point tester (Azmayesh Abzar, Iran) as per guidelines by ASTM D97 method.

#### **3.7.4 Determination of pH**

A digital pH meter with 0.01 high accuracy was used to determine the pH value of the pyrolytic liquid oils.

### **3.8 Data Analysis**

The OriginPro software (version 2021b, Origin Lab Corporation Northampton, MA, USA) was used to plot thermogravimetric analysis and heat flow curves from STA data, and FTIR spectra from FTIR data. The weight of oil formed with time during pyrolysis processes was also plotted using Origin software. The data collected during the STA and FTIR experiments were stored in one folder on a computer installed with data analysis software for easy accessibility and analysis. All the collected STA data were stored in an Excel csv file. This data is compatible with the Origin 2021b software and was imported and then analyzed. The software provides a platform to obtain derivative thermogravimetric curves which aid interpretation of the data quickly. The STA data were first analyzed in Spreadsheet using the modified Coats Redfern method of kinetic analysis and the results were then imported into origin software to generate thermograms and heat flow curves.

### 3.9 Methodology Summary

This section summarizes methods and materials that were used to achieve the objectives of the study as shown in Figure 3.3.

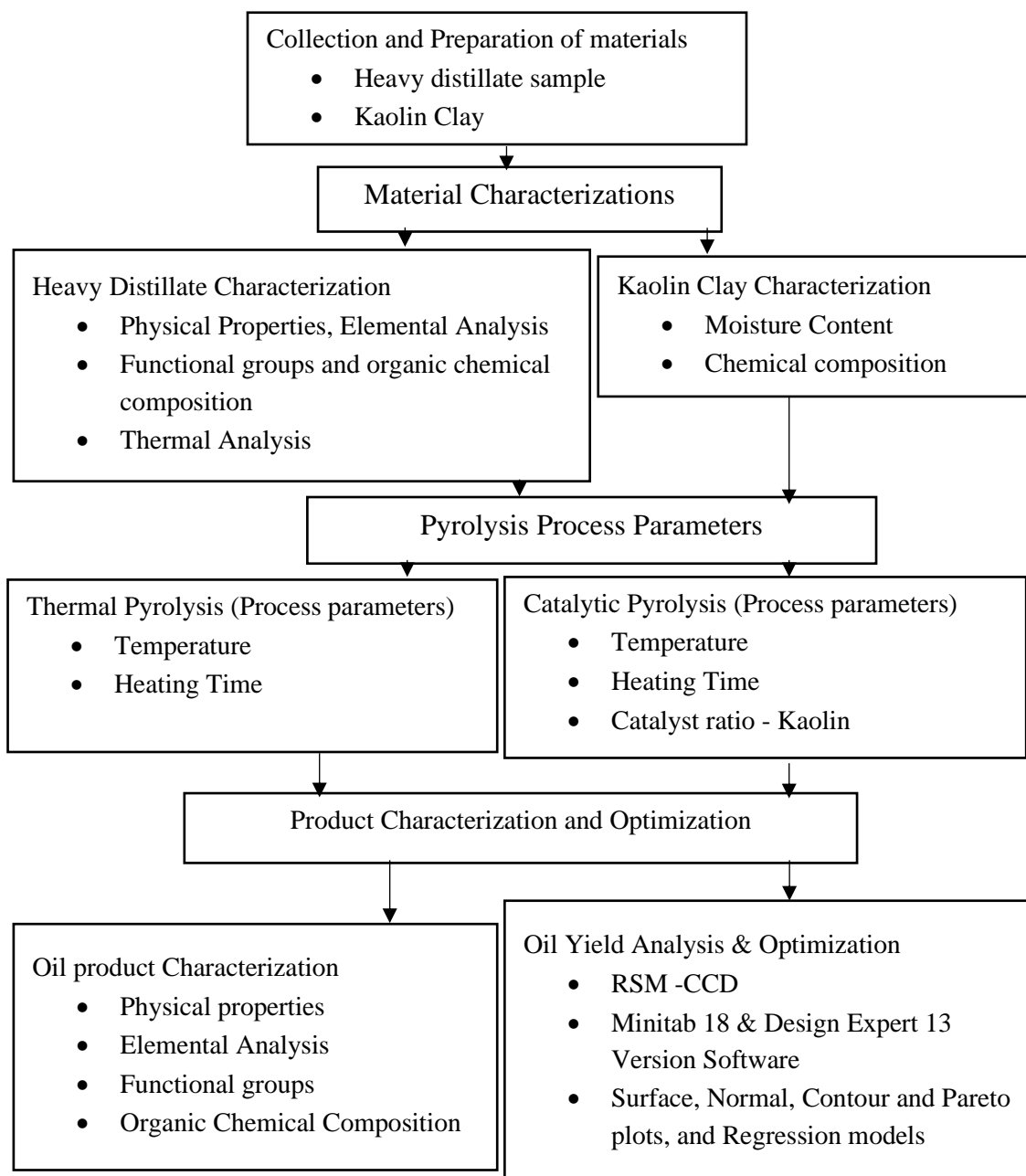


**Figure 3.3: Flow Chart showing methodology overview**

## **CHAPTER FOUR**

### **RESULTS AND DISCUSSION**

#### **4.1 Introduction**

This chapter presents the various findings from the study. The findings are presented mainly in tables, figures, and graphs, The discussion of various results obtained for heavy distillate and its pyrolytic liquid oils investigation are done where the results were analyzed, interpreted, and reported.

#### **4.2 Kaolin Clay Characterization**

The characterization studies on kaolin clay based on moisture content and XRF analysis are presented and discussed.

##### **4.2.1 Moisture Content of Kaolin Clay**

The result for moisture content (MC) of kaolin clay is presented in Table A.1 (Appendix A). The optimum moisture content of kaolin was  $29.931 \pm 1.867\%$ . Water content is one of those volatile constituents present in kaolin. The determination of the kaolin moisture content has been one of the most crucial steps as its presence affects the pyrolysis process which requires drying before application. The moisture content of kaolin clay is the maximum amount of water that a kaolin clay body can hold or is simply defined as the weight of water in a particular sample to solids weight (Ojo et al., 2017). The moisture content of different clays varies depending on their particle size (Hubadillah et al., 2016). The small particle size in the clay body offers a large surface area for voids which increases moisture trapping as compared to those that have a large percentage of crystalline particles. Most clays have an optimum moisture content ranging from 15-40% (Dafalla, 2013) which is true for the result obtained for kaolin obtained from Eburru – Nakuru. When originally mined, China kaolin clay has MC range of 15-22%

and 33-35% for kaolin lump or cake. Ojo *et al.* from Nigeria analyzed dry season samples of kaolin based on its natural moisture content and the percentage of MC results ranges from 15-20.82% (Ojo et al., 2017). Moisture content in kaolin does affect the pyrolysis process as it would require more heat to evaporate it hence this would reduce the catalytic effect of pyrolysis process. The moisture content of about 1% in kaolin is the target for a commercial product hence further drying is required. This necessitated kaolin drying for 3 hours at 105 °C in an oven before use in the pyrolysis process for the aforementioned reasons. Uniform MC is necessary to achieve accurate pyrolysis optimization results.

#### **4.2.2 XRF Analysis Results of Kaolin from Eburru Hill**

The XRF analysis results of the elemental composition of Kaolin clay from Eburru Hill (Nakuru county, Kenya) are presented in Table 4.1 and it revealed the presence of SiO<sub>2</sub>(54.800%), Al<sub>2</sub>O<sub>3</sub> (41.153%), MgO (0.483%), K<sub>2</sub>O (0.255%) and P<sub>2</sub>O<sub>5</sub> (0.089%) as the major elements and 3.22% trace elements. The results showed that silica-alumina are the major compounds present in Kaolin from Eburru Hill with a silica-alumina ratio (SiO<sub>2</sub>/ Al<sub>2</sub>O<sub>3</sub>) of 1.33. Kaolin is a hydrated aluminum silicate (Fang, 2015). The silica-aluminas (SiO<sub>2</sub>-Al<sub>2</sub>O<sub>3</sub>) component is a valuable chemical in the catalysis and adsorption field (Pal & Tiwari, 2020) and thus uniquely necessary for the pyrolysis process. The ratio determines the acidity of the catalysts, and silica-aluminas is amorphous with Bronsted acid sites as ionizable hydrogen atoms and Lewis-acid sites as electron acceptors, it also possesses good selectivity and makes product change according to temperature (Tan et al., 2018). A high composition of silica-alumina is most desirable and good for pyrolysis. Hakeem et al. characterized Ahoko kaolin from Nigeria and reported SiO<sub>2</sub> (72.26%), Al<sub>2</sub>O<sub>3</sub> (18.96%), TiO<sub>2</sub> (1.485%), Fe<sub>2</sub>O<sub>3</sub> (1.05%), K<sub>2</sub>O (0.431%), MgO (0.13%), Na<sub>2</sub>O (0.021%), and MnO (0.004%) as the major



elements with silica-alumina ratio of 3.81 (Hakeem et al., 2018). Panda and Singh characterized commercial kaolin procured from Chemtex Corporation located in Kolkata, India and the results showed SiO<sub>2</sub> (43.12%), Al<sub>2</sub>O<sub>3</sub> (46.07%), TiO<sub>2</sub> (0.74%), CaO (0.030%), MgO (0.027%), ZnO (0.0064%), K<sub>2</sub>O (0.001%), and Fe<sub>2</sub>O<sub>3</sub> (nil) as the main elements which give a silica-alumina ratio of 0.94 (Panda & Singh, 2013). Pal and Tiwari characterized commercial silica-alumina and found a silica-alumina ratio of 1.2 (Pal & Tiwari, 2020). The silica-alumina ratio of 1.33 obtained from this study is within the reported range of 0.94-3.81. The low silica-alumina ratio indicates the high acidity of kaolin from Eburru Hill which is most desirable properties of the catalysts. The high composition of silica and alumina obtained in kaolin from Eburru Hill is anticipated since the main clay constituent are silica and alumina. The disparity in silica-alumina ratio is common in different types of clay as reported in literature (Hakeem et al., 2018; Panda et al., 2010). Treatment and modification processes of kaolin used can lead to observed differences in the silica-alumina ratio. The presence of other trace elements is unwanted during the pyrolysis process, for instance, chlorine in the gas phase may enhance the volatilization of several elements (Zevenhoven et al., 2006). The other metal oxides maybe present in kaolin which increase its acceptability as a catalyst (Hakeem et al., 2018). The metal oxides (Na, Mg, K, Ca, Fe) if present in clay may have catalytic effect as they can act as a based catalyst during the polymer pyrolysis. Kumagai and coauthors studied the use of calcium oxide as a catalyst in the thermal decomposition of plastic wastes, and the study showed that there is enhanced steam cracking, increased gas, and liquid yield, and a decrease in wax content (Kumagai et al., 2015). The increase in Na, Ca, and Mg contents may lead to a gradual increase of the apparent activation energy of the pyrolysis process (Liu et al., 2020) thus small values of them are desirable. The high silica-alumina component in kaolin has a greater

catalytic effect and its use as a catalyst is paramount for maximum oil yield (Yamada et al., 2022).

**Table 4.1: XRF analysis result of Kaolin from Eburru Hill**

Element Name	Chemical Formula	Elemental Composition (wt.%)
<i>Major Elements</i>		
Silicon dioxide (silica)	SiO <sub>2</sub>	54.800
Aluminum oxide (alumina)	Al <sub>2</sub> O <sub>3</sub>	41.153
Magnesium oxide	MgO	0.483
Potassium oxide	K <sub>2</sub> O	0.255
Phosphorous pentoxide	P <sub>2</sub> O <sub>5</sub>	0.089
Calcium oxide	CaO	0.000
<i>Trace Elements</i>		
Titanium	Ti	1.028
Iron	Fe	0.894
Sulphur	S	0.507
Zirconium	Zr	0.349
Cerium	Ce	0.158
Niobium	Nb	0.098
Yttrium	Y	0.053
Tin	Sn	0.026
Chlorine	Cl	0.026
Manganese	Mn	0.016
Hafnium	Hf	0.015
Thorium	Th	0.011
Lead	Pb	0.009
Thallium	Tl	0.008
Platinum	Pt	0.005
Tantalum	Ta	0.005
Bismuth	Bi	0.004
Zinc	Zn	0.003
Strontium	Sr	0.002
Copper	Cu	0.002

### 4.3 Heavy Distillate Characterization

The characterization results of HD sample based on functional groups, thermal properties are presented and discussed. Meanwhile, the physical properties, elemental and chemical compositions are presented and discussed in section 4.7.

### 4.3.1 FT-IR Analysis results

The FT-IR analysis was done to identify the functional groups of the HD and PLOs with and without catalyst from HD pyrolysis process and its stabilization, and the results are presented in Figure 4.1. The band was assigned according to the wave numbers and regions of the infrared spectra occurrence as shown in Table 4.2. There was a linear relationship in the broadband for HD and PLOs as observed from the spectrum of Figure 4.1.

The spectrum revealed a similar broad band in the range of 2800-3000  $\text{cm}^{-1}$  characteristic of the C-H stretch of hydrocarbon compounds for all oil samples. The presence of main peaks corresponding to HD and PLOs in the FT-IR spectra indicates the presence of hydrocarbon ions on the samples as previously reported by other studies on polymer samples (Coates, 2000, 2006; Sánchez-Lemus et al., 2016). The strong transmittance peaks observed at 2954.4114, 2915.842, and 2848.3457  $\text{cm}^{-1}$  correspond to symmetric and asymmetric stretching modes for methyl ( $\text{CH}_3$ ), methylene ( $\text{CH}_2$ ), methyldyne ( $\text{CH}$ ) which are typical of the aliphatic hydrocarbons as reported on polymers (Coates, 2006). This shows the presence of alkene (for instance polypropylene, and polyethylene) related compounds as it was predominantly the main feedstock for the pyrolysis process of the plastic industry where the heavy distillate sample was obtained from. The small peak observed at 3075  $\text{cm}^{-1}$  matches to small aromatic C-H stretching. The peak at 2954  $\text{cm}^{-1}$  represents the asymmetric stretching vibration of bond C-H in methyl.

At the finger print region (400-1400  $\text{cm}^{-1}$ ), the aromatic C-H in-plane bend was observed at 1168 and 1159  $\text{cm}^{-1}$ , and aromatic C-H out of the plane bend at 887  $\text{cm}^{-1}$ . The alkenyl C=C stretch and C=C-C Aromatic ring stretch were observed at 1649 and

1459  $\text{cm}^{-1}$  respectively. This possibly indicates the presence of alkylene-related compounds in HD and its PLOs samples.

Another characteristic transmittance band of the PLO is observed at 1649  $\text{cm}^{-1}$ , this transmittance is attributed to the stretching of the C=O double bond of the carbonyl compound. The two distinct transmittance peaks at 1457 and 1376  $\text{cm}^{-1}$  were identified and attributed to the flexion or deformation experienced by the C-H bond which was in agreement with other work done by Coronado *et al.* (Coronado et al., 2017). Some of the transmittance peaks that constitute methyl esters were observed within the fingerprint region at 1157, 969, 887, and 719  $\text{cm}^{-1}$  for HD and PLOs samples. The peaks at 1457, 1376 and 887  $\text{cm}^{-1}$  were more stretched for PLOs (with and without catalyst) compared to HD whereas between 2800-3000  $\text{cm}^{-1}$  (with the exception at 2954  $\text{cm}^{-1}$ ) HD had more stretching than PLOs which could have resulted due to large molecular weights of aliphatic compounds present in the HD compared to the PLOs. The decrease in stretching of the PLOs accompanied with high percentage transmittance proved successful thermal decomposition of the HD into PLOs.

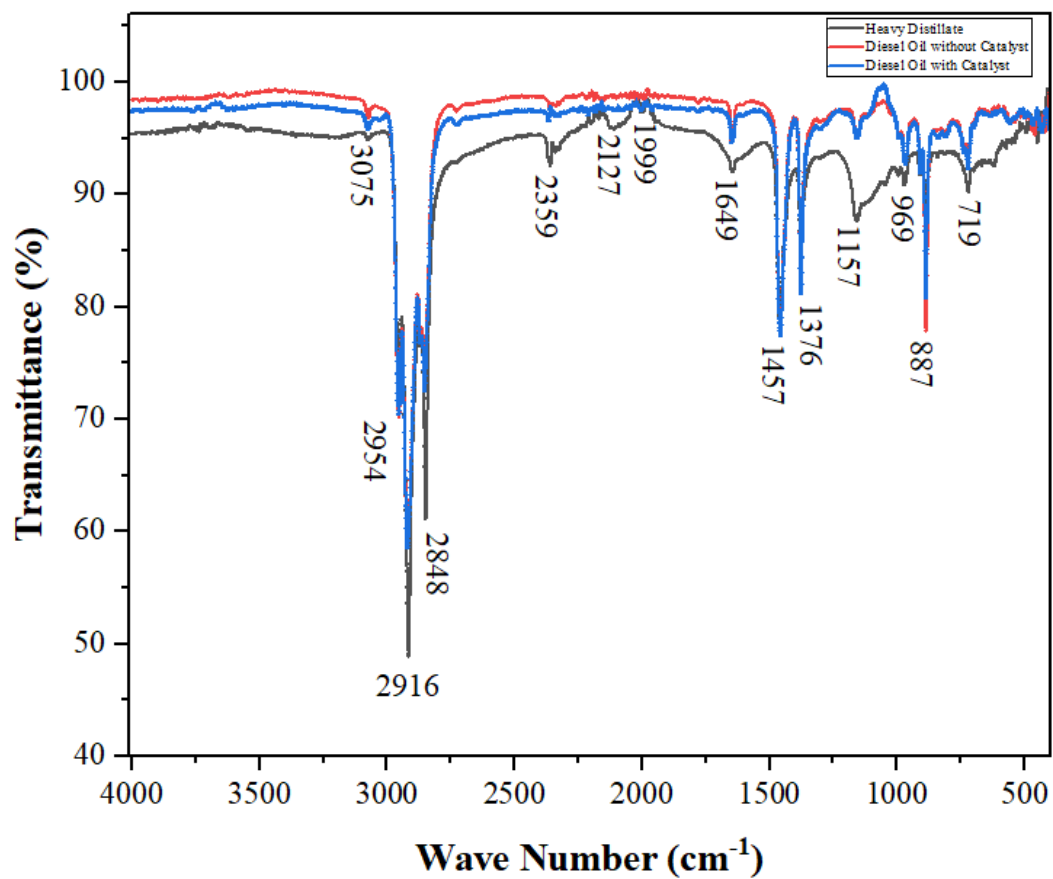


Figure 4.1: FTIR Spectra of Heavy Distillate and pyrolytic liquid (Diesel) Oils

**Table 4.2: Band Assignment for Infrared Spectra of HD and PLOs**

<b>Wave Number (cm-1) – This study</b>	<b>Band Assignment</b>	<b>Wave Number (cm-1) from Literature</b>	<b>References</b>
3075	Aromatic C-H stretching vibration	3130-3070	(Coates, 2000; Nandiyanto et al., 2019)
	Terminal (vinyl)C-H stretch	3095-3075	(Coates, 2000, 2006)
	Pendant (vinylidene C-H stretch		
2954	Asymmetric stretching vibration of C-H in methyl (CH <sub>3</sub> )	2970-2950	(Coates, 2000; Sánchez-Lemus et al., 2016)
2916	Asymmetric stretching vibration of bond C-H methylene (CH <sub>2</sub> )	2935-2915	(Coates, 2000, 2006)
2848	Symmetric stretching vibration of bond C-H in methylene (CH <sub>2</sub> )	2865-2845	(Coates, 2006)
2360	NH Component (Amino-related component)	2330-2360	(Nandiyanto et al., 2019)
	C≡C Terminal alkyne (monosubstituted)	2140-2100	(Coates, 2000)
2127	Isothiocyanate (-NCS)	2150-1990	(Coates, 2000, 2006)
1999	Aromatic combination band; Isothiocyanate (-NCS)	2000-1660 (several)	(Coates, 2000, 2006)
1648	Alkenyl C=C stretch	1680-1620	(Coates, 2000, 2006)
1461	C=C-C Aromatic ring stretch	1510-1450	(Coates, 2000, 2006)
1377	Symmetric bend/vibration of C-H in methyl (CH <sub>3</sub> )	1380-1370	(Coates, 2000, 2006)
1159	Symmetric bend/vibration of C-H in methyl (CH <sub>3</sub> )	1225-950 (several)	(Coates, 2000, 2006)
887	Aromatic C-H out-of-plane bend	900-670 (several)	(Coates, 2000, 2006)

### 4.3.2 Kinetic analysis results for heavy distillate

The kinetic analysis results of the heavy distillate sample were based on STA data. The Weight loss, derivative weight loss, and heat flow curves were generated.

Thermodynamic properties obtained from kinetic analysis such as rate constant, activation energy, change in enthalpy, change in entropy and change in Gibbs free energy are presented and discussed.

### **4.3.3 Activation Energy and other thermodynamic behaviors of HD**

The activation energies results of HD at different heating rates determined from the slope of the curve in Figure 4.2 and other various thermodynamic parameters evaluated are presented in Table 4.3 and in Tables G.1-16 (Appendix G). From Figure 4.2, three stages (phases) correspond to the TG curve. The phases from this curve show the dehydration, decomposition, and condensation of the heavy distillate during the experimental process. In stage I, the apparent activation energy is around 36.86 kJ/mol followed by an increase to 63.037 kJ/mol in stage II and a further rapid decrease to 7.45 kJ/mol in the final stage III at 5 °K/min heating rate. Similar trends for activation energy changes were observed at other heating rates of 10, 15, and 20 °K/min. The similarity of activation energies of HD at different heating rates and stages shows the similar kinds of reaction processes. There is a positive correlation for all the values of activation energy obtained for the HD sample which closely meets the exponential relationship as described in the literature (Dubdub & Al-Yaari, 2020). The activation energies were highest in the second phase which clearly shows the decomposition process of the substance at that phase and the very low activation energies in the third stage confirm the condensation process. The dehydration process normally dominates the first stage. The values of activation energy were slightly lower than that of heavy crude oil reported in previous work (Kök et al., 2017), and much lower than that of plastic wastes (Ding et al., 2021). The activation energy values of heavy crude oil ranged from 10-22 kJ/mol for low-temperature oxidation (LTO) and 50.0-177 kJ/mol in high-temperature oxidation (HTO) as compared to 7.45-11.11 kJ/mol for LTO and 61.52-70.16 kJ/mol

for HTO in this study. The activation energy is linked to the energy difference between transition state and reactants, and the frequency factor is connected to the change in order degree (Khelkhal et al., 2022), and it is necessary to analyze each phase separately for accurate results since their reaction schemes are not the same (Karimian et al., 2016).

Fan et al. examined heavy oil oxidation using TGA and the study obtained three distinct phases of the oxidation process i.e., low-temperature oxidation (LTO), plateau region and high-temperature oxidation (HTO) (Fan et al., 2013) which is similar in comparison to phases (dehydration, decomposition, and condensation). The decomposition of the HD sample occurred mostly in the plateau region. In this study, the oxidation of HD from plastic waste can similarly be unglued into three main stages, that is, low temperature oxidation -LTO (105-268, 146-289, 142-331, and 164-341 °C), plateau section (268-352, 289-378, 331-406, and 341-442 °C), and high temperature oxidation - HTO (352-489, 378-517, 406-555 and 442-601 °C), at heating rates of 5, 10, 15 and 20 °K/min respectively as observed from TG and rate constant profiles and Table 4.3. More thermal hysteresis at a higher heating rate boosts the disappearance of platform and uncontrollability of sample temperature for heavy distillate. The oxidation behavior of the distillate predicted from kinetic parameters suggests a good approach to the experimental data. This investigation offers new acumens on the type of reactions occurring, an accurate reaction kinetics model of HD oxidation to understand the reactivity of HD from plastic waste and gain a novel efficient pyrolysis process.

In phase 2 as shown in Table 4.3, the sample exhibited the highest values of enthalpy for all the heating rates of around 56-64 kJ/mol which shows the sample needs the utmost heat to decompose. At lower and higher temperatures, the entropy contribution



with values ranging from -184 to -302 J/mol/K are much smaller for HD at various heating rates compared to one of heavy crude oil reported in literature with values ranging between 14-53 J/mol/K (Khelkhal et al., 2022). Under same circumstances, this shows the process will proceed much faster in HD pyrolysis than that of heavy crude oils. At higher temperatures, the valuable decrease in enthalpy will be mainly repressed by entropy contribution which is consistent to previous work (Khelkhal et al., 2022). All the phases are non-spontaneous endothermic reactions as observed by positive values of change of Gibbs free energy obtained for each phase in Table 4.3 and Figure 4.2. This confirmed all phase transformations were first-order reactions similar to previous work (Akhyar et al., 2019a). The use of low heating rates (5, 10, 15 and 20 °K/min) was chosen to lessen the effect of thermal analysis and heat accumulation and acquire reliable kinetic parameters as reported in earlier work (Fan et al., 2013).

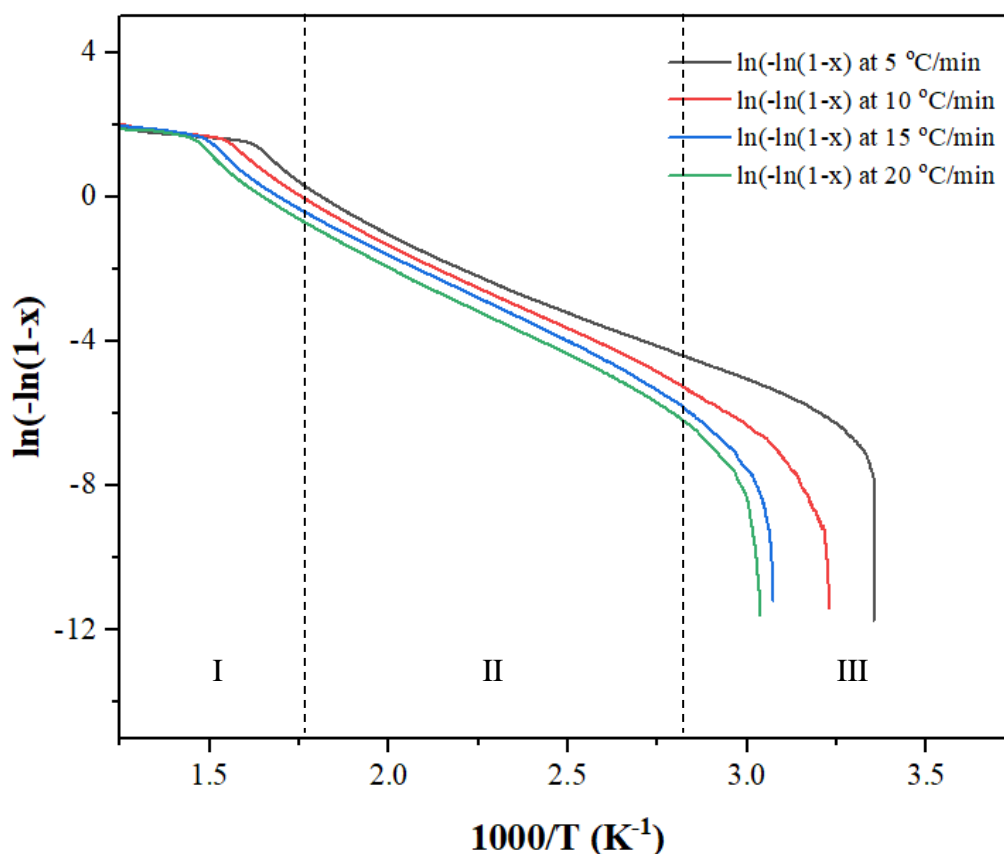


**Figure 4.2: MCRM curve of heavy distillate at different heating rates**

#### 4.3.4 Rate constant and Half-life of Heavy distillate

The rate constant curve is shown in Figure 4.3. The slope of the curve gives a rate constant,  $k$  ( $\text{min}^{-1}$ ), and the half-life was obtained using Equation 2.9 and the results of rate constants and half-life of HD at different heating rates are presented in Table 4.3. Rate constant of the HD sample increases with decreasing half-life during decomposition stage. The half-life of the pyrolysis processes is useful to predict the associated reaction rates (Khelkhal et al., 2022). This (half-life) directly gives the temperature range at which pyrolysis befalls. The obtained half life was lowest at stage 2 ranging between 0.62-2.86 min which indicate highest pyrolysis reaction rates of HD and this is believed to be most intense zone where HD pyrolysis occurs as reported in literature (Khelkhal et al., 2022). Previous work on pyrolysis of heavy oils at large scales observed this zone to occur at temperature less than 300°C under

aquathermolysis (Vakhin et al., 2020). In the zone, there is transformation of complex parts into light fractions which enhances oil quality and decreases oil viscosity.

**Table 4.3: Activation Energy and other thermodynamic Properties of HD**

HR (K/min)	Ph	T (K)	K (min <sup>-1</sup> )	t <sub>1/2</sub> (min)	E <sub>a</sub> (kJ/mol)	ΔH (kJ/mol)	ΔS (J/mol/K)	ΔG (kJ/mol)
5	1	541	0.0193	35.91	36.863	32.365	-240	162.290
	2	625	0.2424	2.86	63.037	57.840	-190	176.790
	3	763	0.0503	13.78	7.453	1.109	-302	231.776
10	1	562	0.05	13.86	40.904	36.231	-229	164.787
	2	651	0.4641	1.49	61.519	56.106	-192	181.127
	3	790	0.142	4.88	10.042	3.474	-291	233.238
15	1	604	0.0819	8.46	41.101	36.079	-229	174.338
	2	679	0.8822	0.79	70.159	64.514	-179	185.899
	3	828	0.235	2.95	11.111	4.227	-286	241.236
20	1	614	0.108	6.435	43.829	40.994	-219	115.647
	2	715	1.111	0.62	65.571	61.896	-184	143.216
	3	874	0.208	3.33	8.031	3.034	-290	176.955

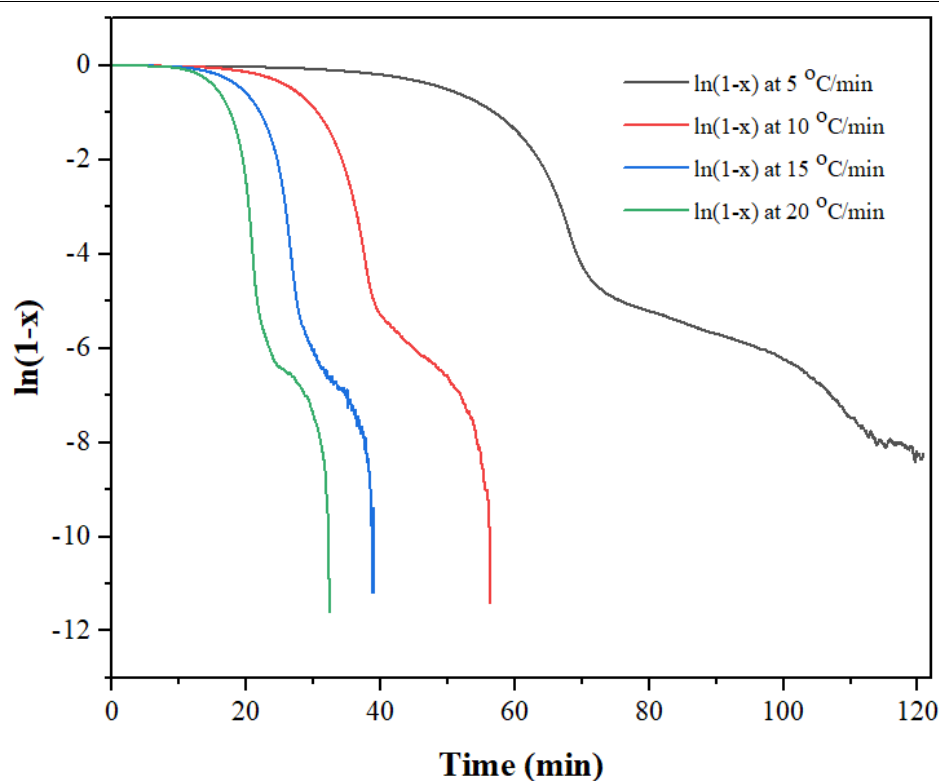


**Figure 4.3: Plot for Determination of Rate Constant and Half-Life of HD**

#### 4.3.5 Weight Loss of HD at the various Heating rates

The weight loss curves of heavy distillate at different heating rates are presented in Figure 4.4. The mass loss at 5% can be seen in Figure 4.4, and immediately past 100

°C, there was a tremendous change in the curve showing surface water has been removed at that state. This proves weight change for heavy distillate with the temperature at various heating rates. It can be speckled from Figure 4.4 that the weight loss of heavy distillate increases as temperatures and heating rates increase. The thermograms were similarly observed which confirm a single degradation step of heavy distillate at each heating rate with complete degradation. The TG characteristics temperatures ( $T_{peak}$ ) of the heavy distillate sample at different heating rates were in the following order: 20>15>10>5 °C/min with decomposition of heavy distillate observed to happen with a hasty weight loss. Previous work has shown at heating rate of above 25 °K/min, there is no appreciable change in weight loss curves and the decomposition temperature remains almost constant (Karimian et al., 2016). The weight loss is basically as a result of hydrocarbons release and it shows a rapid release of hydrocarbons from the pyrolysis process which is termed devolatilization. The pyrolysis of heavy distillate occurs in a single step which is similar to plastic thermal degradation behavior as reported in the literature (Dubdub & Al-Yaari, 2020). At peak temperatures as shown in Table 4.4, the remaining weight percentages were 0.32, 1.11, 1.22, 0.84% at respective heating rates which shows maximum decomposition of the sample.

**Table 4.4: Thermogravimetric Analysis of HD showing remaining weight percent**

Test Number	Heating Rates (°C/min)	Peak Temperatures ( $T_{peak}$ ) (°C)	Weight Sample (mg)	Weight left (At $T_{peak}$ ) - mg	Weight Percent (%)
1	5	340.67	26.77413	0.08587	0.32
2	10	372.82	19.47870	0.21609	1.11
3	15	393.68	15.58739	0.18935	1.22
4	20	411.82	23.43935	0.19717	0.84

Li *et al.* (2013) observed that 0.34% of the light crude oil sample remained at around 600 °C from the thermogravimetric profile which shows higher temperature needed compared to this research where 0.84% remained in the sample at heating rates of 20 °C/min with lower temperature of 411.82 °C. This shows that due to distillation, complex oxidation and pyrolysis reaction of the heavy distillate; the HD sample mass kept decreasing in a comparatively quick rate as temperature increases and it also confirms the ease of breaking heavy distillate compared to crude oils.

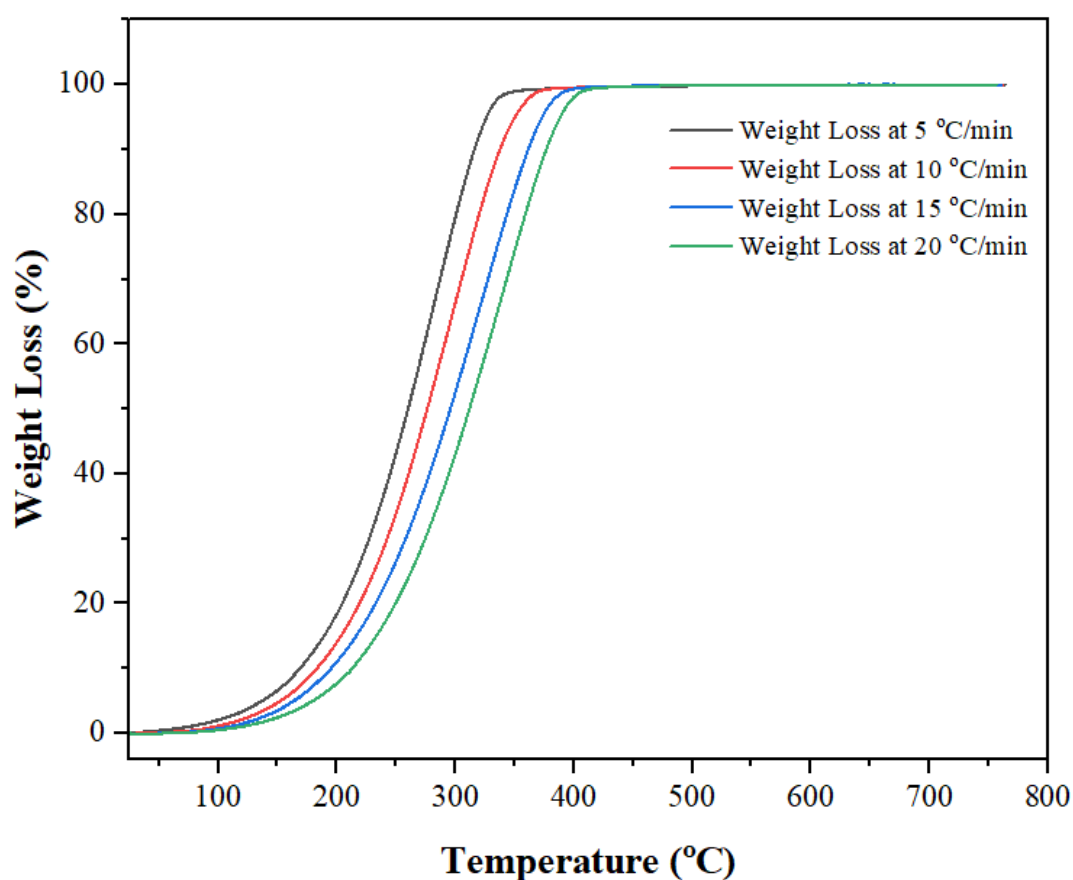


**Figure 4.4: Thermogram of HD sample at different heating rates**

#### 4.3.6 Decomposition of Heavy Distillate at different Heating Rates

The decomposition of heavy distillate at different heating rates was extracted from the STA data and the result was tabulated as shown in Table 4.5. From the table, the decomposition temperature range shows lowest and higher temperatures which the

sample degrades at 1 and 99.9% respectively. The temperature range for thermal decomposition of heavy distillate which degrades during TGA is affected by the selected heating rate. At higher heating rates, there is an increase in the temperature range at which degradation happens as reported in literature (X. C. Wang et al., 2015). There is little distinction in the temperature interval at which heavy distillate decomposition transpires at different heating rates. Other similar studies have also reported that the temperature interval where decomposition befalls is independent of the heating rates (Burnham & Dinh, 2007).

**Table 4.5: Decomposition of HD at different heating rates**

S/N	Heating Rate	HD sample (mg)	T <sub>max</sub> (°C)	Remaining Weight (%) at T <sub>max</sub>	(dw/dt) <sub>max</sub> (%/min)	Time when (dw/dt) <sub>max</sub> (min)	Decomposition temperature range (°C) (1% wt loss – 99.9% wt loss)
1	5	26.77413	340.67	1.62	8.98	69.61	74.35-521.85
2	10	19.47870	372.82	0.89	6.58	38.48	96.74-502.37
3	15	15.58739	393.68	0.92	7.86	27.20	108.56-505.65
4	20	23.43935	411.82	0.76	5.22	21.51	118.94-550.03

#### 4.3.7 Derivative Thermogravimetric (DTG) Curves of HD

The derivative weight loss curves for the heavy distillate sample are given in Figure 4.5. The curve gives the precise temperature value in the form of an endothermic peak for every scenario (crystallization, phase transformation) that happens. The peak in Figure 4.5 denotes the maximum point for the weight loss rate. From the DTG curve, the small peak was seen between 100 and 150 °C, which shows a first thermal event for HD sample, and corresponds to a mass loss of about 5% as a result of residual/bound water removal. As shown in Figure 4.5, the sample breaks at 285.77, 290.63, 327.02 and 343.46 and fully decomposes at 365.83, 391.38, 412.42 and 424.40 °C at different heating rates of 5, 10, 15 and 20 °C/min, respectively, and this acted as a basis for the

selection criterion for the experimental temperatures of the pyrolysis process for the study.

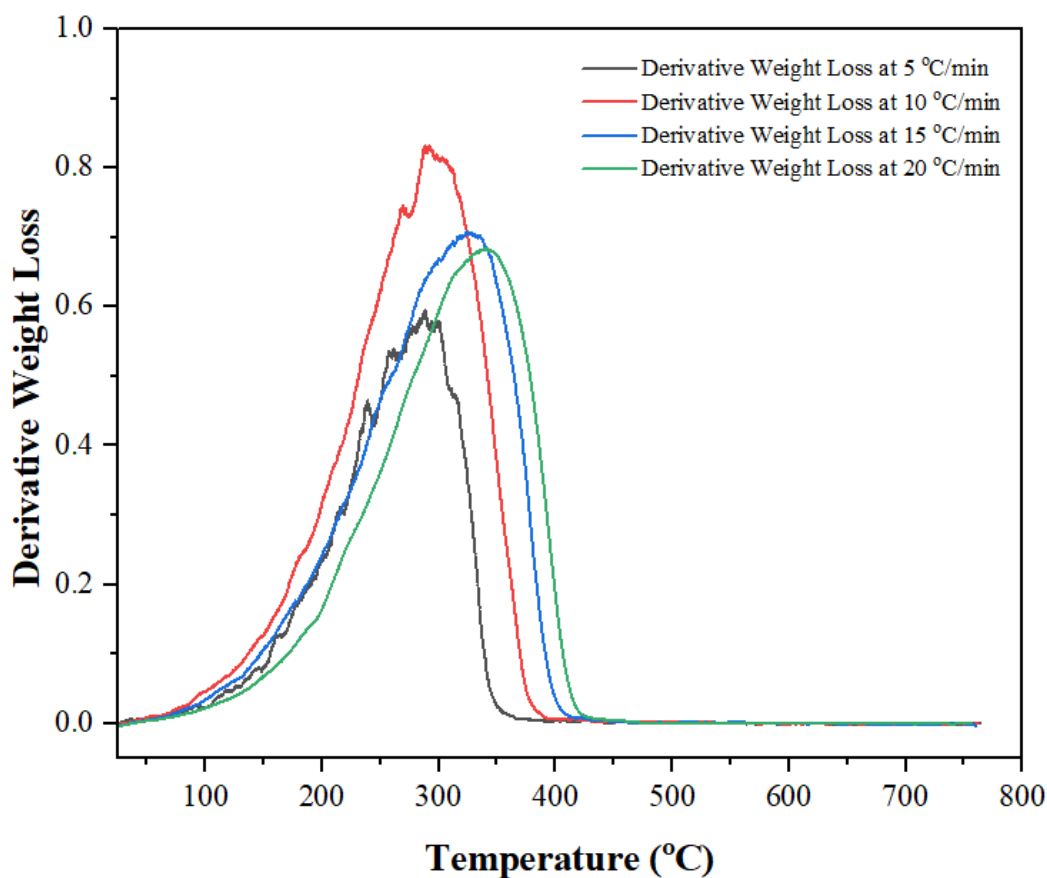


**Figure 4.5: Derivative Thermogram of HD sample at different heating rates**

#### 4.3.8 Heat Flow of HD at various heating rates

The heat flow curve of HD sample at different heating rates are presented in Figure 4.6. The curve shows that the sample exhibited an endothermic event between 400 -450 °C for all the heating rates which relates to the decomposition of the hydrocarbon with medium molecular weight existing in heavy oils (Mothé et al., 2016). Mothe et al. investigated the thermal analysis of heavy oils using DSC and found the endothermic event at 462 °C (Mothé et al., 2016), which is higher than that of heavy distillate. This shows that endothermic reactions of HD are lower than the ones of heavy crude oil hence it would require less energy for the thermal decomposition process. The

endothermic peaks ranging from 350 to 500 °C show zone for pyrolysis for extra heavy oils as reported in previous study (Khelkhal et al., 2022). This peak is in agreement with this study which ranges from 370 to 450 °C. As observed in Figure 4.5 and Figure 4.6, as the heating rate increase, the oxidation reactions onset is shifted to higher temperatures which instigate further heat flow and mass loss, and the same was reported in previous work (Karimian et al., 2016). It leads to narrower peaks in heat flow and DTG curves which shows that the reaction proceeds faster with increase in heating rate.

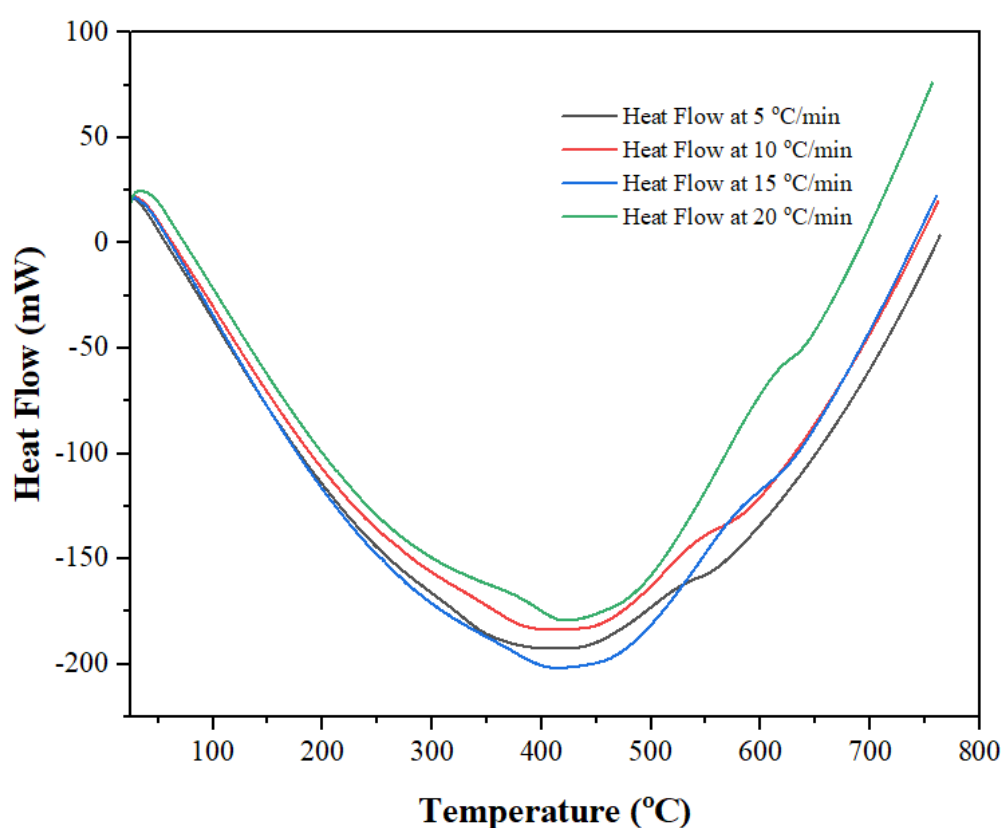


**Figure 4.6: Heat Flow Curve of HD Sample at various heating rates**

#### **4.4 Thermal and catalytic pyrolysis experimental results**

The results of oil yields generated from thermal and catalytic pyrolysis of heavy distillate are presented in Table 4.6 and Table 4.7 respectively. During thermal pyrolysis (TP), the reaction temperatures varied from 340 to 410 °C and the heating



time varied from 78 to 162 min as process parameters. From Table 4.6 for thermal pyrolysis, the highest total conversion occurred at temperature (410 °C) and heating time (120 min) with oil yield (74.88 wt.%) and the lowest yield (11.88 wt.%) was at 340 °C for 120 min. At process combinations (400 °C, 150 min; 400 °C, 90 min; 350 °C, 150 min; 350 °C, 90 min), oil yields obtained were 65.63, 61.63, 18.88, 15.25 wt.%, respectively. During catalytic pyrolysis with process combinations (400 °C, 5%, 150 min; 400 °C, 5%, 90 min; 350 °C, 5%, 150 min; 350 °C, 5%, 90 min), oil yields (73.28, 66.80, 20.5, 17.88 wt.%) were obtained; and using 15% catalyst, obtained oil yields were 70.13, 64.21, 28.50, 24.75 wt.%. This shows increased yield with catalyst than thermal pyrolysis. There was slightly less yield obtained when the catalyst ratio was increased to 15% at high temperature (400 °C) and yet this appreciably favoured formation of more yields at low temperature (350 °C). Pan *et al.* showed that too much catalyst amount is not necessary as this affects oil yields (Pan *et al.*, 2021). This means the maximum catalyst ratio necessary for pyrolysis had been exceeded hence causing low yield. Previous studies has showed catalyst ratio of 10% generates high oil yields (Eltohami & Mustafa, 2019) and this was also reported by other work (Budsareechai *et al.*, 2019a). The catalytic effect on oil yields is highly dependent on operating temperatures as observed in this study, catalyst at low temperature produces low yields and high yields at high temperature as reported by (Pan *et al.*, 2021; Panda & Singh, 2013). Thus, increase in temperature increase oil yields and increase in catalyst at high temperature had little impact.

Heavy distillate contains long chain molecules which follow the mechanism of random chain scission while being thermally degraded, which needs higher temperature. At temperatures below 350 °C, there was minimum degradation of heavy distillate into liquid oil fuel which is further accompanied by long heating time to produce the oil

yield due to its difficulty to break the strong bonds. High yields were obtained during high temperatures. According to Rivas-Perez *et al.* preheating furnaces usually heat heavy oil at 390 to 400 °C after which the liquid and gas fractions having different boiling points are separated off (Rivas-perez et al., 2014). This range of temperature was found to agree with the HDP process where a temperature of 400 °C gave a stable oil yield and unstable at above 410 °C.

The stability of pyrolytic liquid oils was directly observed as shown in Table 4.6 and Table 4.7 for the thermal and catalytic pyrolysis, respectively. At a reaction temperature of 410 °C, the liquid oil product from thermal pyrolysis was moderately unstable with the formation of waxy substances which formed at the bottom of the collected oil container. This was exacerbated further during catalytic pyrolysis at a temperature of 417 °C, where the oil produced was only waxy substances. Literature has shown that the unstable oils which result during the pyrolysis process are a result of short residence time (Pan et al., 2021; Panda et al., 2020). The existence of a waxy substance in oil products is an indication of partial cracking of the polymers. Higher temperatures would yield more liquid oils; however, a point is reached beyond which reaction temperature favors more gas formation coupled with increased viscosity and this leads to unstable oils. For instance, Diaz *et al.* investigated the simulation of chemical reactions occurring during the thermal recovery processes of heavy crude oil and observed that at higher temperatures (500 °C) the oxidation of organic matter is not enough to stop recombination reactions, as kinematic viscosity and Conradson carbon (CCR) increased considerably (Diaz et al., 2015).

During TP, the non-condensable gases were 2.12 and 6.37% at 340 and 410 °C and for CP at 333, 417 °C were 2.63, 9.33 wt.%, respectively. Temperature increase leads to an

increase in both oil yield and non-condensable gases during pyrolysis but further increased with use of catalyst. Wang *et al.* studied temperature effects on product yield from oil shales and found that as temperature increased above 430 to 520 °C both oil and gas yields improved as oil and gas yield ratio reduced (Sha Wang et al., 2014). High temperatures promote secondary cracking for liquid fuels so as to produce shorter chain pyrolysis gas (Wei et al., 2017). Standlick and coauthors found that thermal cracking to non-condensable gases is favoured by longer residence time of the vapours thus causing a reduction in liquid yield (Stanlick et al., 2017). At 400 °C and 15% catalyst for heating time of 90 and 150 mins, the non-condensable gas obtained were 4.55 and 5.87 wt% and meanwhile at 5% catalyst, the gas yields were 5.13 and 5.87 wt% for 90 and 150 mins, respectively. As observed, more gases were produced at the longer heating time and high temperatures. Catalytic pyrolysis had more diesel oil yield compared to thermal ones and it was observed that the non-condensable gas drastically increased during catalytic pyrolysis process.

The conversion rate increases with an increase with heating time for a certain limit, yet more increase in the heating time does not give any meaningful increase in the conversion rate. This effect of reaction time on oil yield has also been studied by Pan *et al.* and observed the same (Pan et al., 2021).

Energy usage (power consumption) during pyrolysis process was monitored and the results are presented in Table 4.6 (column 8) for TP and Table 4.7 (column 9) for CP. At process combinations (400 °C, 150 min; 400 °C, 90 min; 350 °C, 150 min; 350 °C, 90 min), energy utilized were 2.4, 1.4, 1.7, 1.3 kWh, respectively. The energy utilized during catalytic pyrolysis with process combinations (400 °C, 5%, 150 min; 400 °C, 5%, 90 min; 350 °C, 5%, 150 min; 350 °C, 5%, 90 min) were 2.3, 1.8, 1.7, 1.1 kWh;

and using 15% catalyst, energy utilized were 2.2, 1.5, 1.7, 1.7 kWh. Energy usage increases with an increase in temperature and heating time as expected in both TP and CP but decreases by use of catalyst during CP. Catalyst pyrolysis played a key role in reduction of energy usage which is in line with previous work (R.-X. Yang et al., 2022). However, the high increase in energy consumption from 1.4 kWh during TP (400 °C, 90 min) to 1.8 kWh at 5% catalyst ratio (400 °C, 5%, 90 min) and from 1.3 kWh during TP (350 °C, 90 min) to 1.7 kWh during CP at 15% catalyst ratio (350 °C, 15%, 90 min) could be attributed to weather condition (cold weather) and time of experiment (night) which leads to unusual energy consumption.

**Table 4.6: TP experimental results**

Run	Temp (oC)	Heating Time (min)	Actual Yield (wt.%)	Predicted Yield (wt.%)	Unreacted Residue (wt.%)	Gas Yield (wt.%)	Energy Usage (kWh)	Oil Stab.
1	375	162	42.25	41.35	53.88	3.87	2.0	S
2	350	150	18.88	20.09	77.75	3.37	1.7	S
3	410	120	74.88	75.38	18.75	6.37	2.2	NS
4	375	120	40.25	40.25	56.50	3.25	1.9	S
5	350	90	15.25	15.49	82.00	2.75	1.3	S
6	375	120	40.13	40.25	56.50	3.37	1.7	S
7	375	120	40.38	40.25	56.25	3.38	1.6	S
8	375	120	40.38	40.25	56.25	3.38	1.6	S
9	375	78	34.13	34.59	63.13	2.75	1.1	S
10	375	120	40.13	40.25	56.50	3.38	1.6	S
11	400	90	61.63	60.86	35.13	3.25	1.4	S
12	400	150	65.63	65.83	30.38	4.00	2.4	S
13	340	120	11.88	10.95	86.00	2.12	1.4	S

**Key:** S - Stable, NS - Not Stable, stab. – stability

**Table 4.7: CP experimental results**

Run	Tem p (°C)	Catalyst Ratio (%)	Heating Time (min)	Oil Yield (wt.%)	Predicted Yield (wt.%)	Solid Residue (wt.%)	Gas yield (wt.%)	Energy Usage (kWh)	Oil Stab .
1	375	10	120	46.25	46.27	49.50	4.25	1.7	S
2	350	15	150	28.5	29.26	67.38	4.13	1.7	S
3	375	10	120	46.28	46.27	49.35	4.37	1.6	S
4	400	15	150	70.13	69.79	24.00	5.87	2.2	S
5	375	10	70	42.13	42.50	54.38	3.50	1.1	S
6	333	10	120	12.13	10.29	85.25	2.63	1.7	S
7	375	10	120	46.3	46.27	49.40	4.31	1.8	S
8	350	15	90	24.75	25.61	71.63	3.63	1.7	S
9	400	15	90	64.21	63.12	31.24	4.55	1.5	S
10	375	10	120	46.25	46.27	49.50	4.25	1.7	S
11	350	5	150	20.5	21.62	75.63	3.87	1.7	S
12	375	10	120	46.27	46.27	49.39	4.34	1.9	S
13	375	10	170	51.36	50.94	43.89	4.75	2.2	S
14	375	10	120	46.29	46.27	49.38	4.34	1.8	S
15	400	5	90	66.80	66.07	28.08	5.13	1.8	S
16	350	5	90	17.88	18.25	78.75	3.37	1.1	S
17	400	5	150	73.28	72.46	20.85	5.87	2.3	S
18	375	18	120	45.32	45.22	50.14	4.55	1.6	S
19	417	10	120	82.80	84.59	7.88	9.33	2.3	NS
20	375	2	120	41.23	41.28	54.65	4.13	1.6	S

**Key:** *S* - Stable, *NS* - Not Stable, *Stab.* – Stability

#### 4.5 Length of pyrolysis time effect on oil yield

The formation of diesel oil with length of pyrolysis time during thermal and catalytic pyrolysis observed were as shown in Figures 4.7 and 4.8, respectively. The fastest diesel oil yield rate happened during thermal pyrolysis within the first 30 min from the initial drop and during catalytic pyrolysis in the first 20 min. The oil yield gradually augmented in the next 30 min, and then sharply decreased. There was no appreciable increase in oil yield while the length of pyrolysis process was prolonged after hundred minutes which showed that the pyrolysis process ended. More of the diesel oils were formed faster within 60 min, and this is mainly because the simple molecular weights are easy to break in the shortest time while the complex ones require more time and higher temperatures. The oil yield increases with an increase in temperature and were

formed faster when temperature increases with a sharp increase compared to when low temperatures were used. At high temperatures, oil yield reaches its peak at a faster rate during pyrolysis and this increases further with the use of a catalyst. At lower temperatures, lower yields were attained and this could be due to large molecular weights of heavy distillate which are complex to degrade at lower temperatures and hence would require high temperatures to break and achieve high yields. As observed, production was generally less during thermal pyrolysis than catalytic pyrolysis and this could be due to catalytic effect which facilitates more production as more heat would be retained on the surface of the catalyst. There was no effect of pyrolysis time above 90 min, which shows the production was complete since there was a gradual change in the amount of oil yield and this could possibly mean the thermal decomposition of the polymer substance into light ones was complete for that particular process. The length of pyrolysis time is not certainly an economical ones (Hariadi et al., 2021), and this is simply because as pyrolysis time increases more yields may still be achieved. There is however little amount which could still be achieved after 90 min, in the extension of pyrolysis time by 180 min (i.e. from 90 to 270 min) until the pyrolysis process is complete, only 9.94% increase in oil yield was achieved in their study. The pyrolysis time can be reduced through blending of different polymers (Hariadi et al., 2021), and use of catalyst (Miandad, Rashid; Mohammad et al., 2019) which thus helps to complete decomposition of the polymer substance. The time of pyrolysis of heavy distillate at all operating parameters affected the percentage of diesel oil yielded.

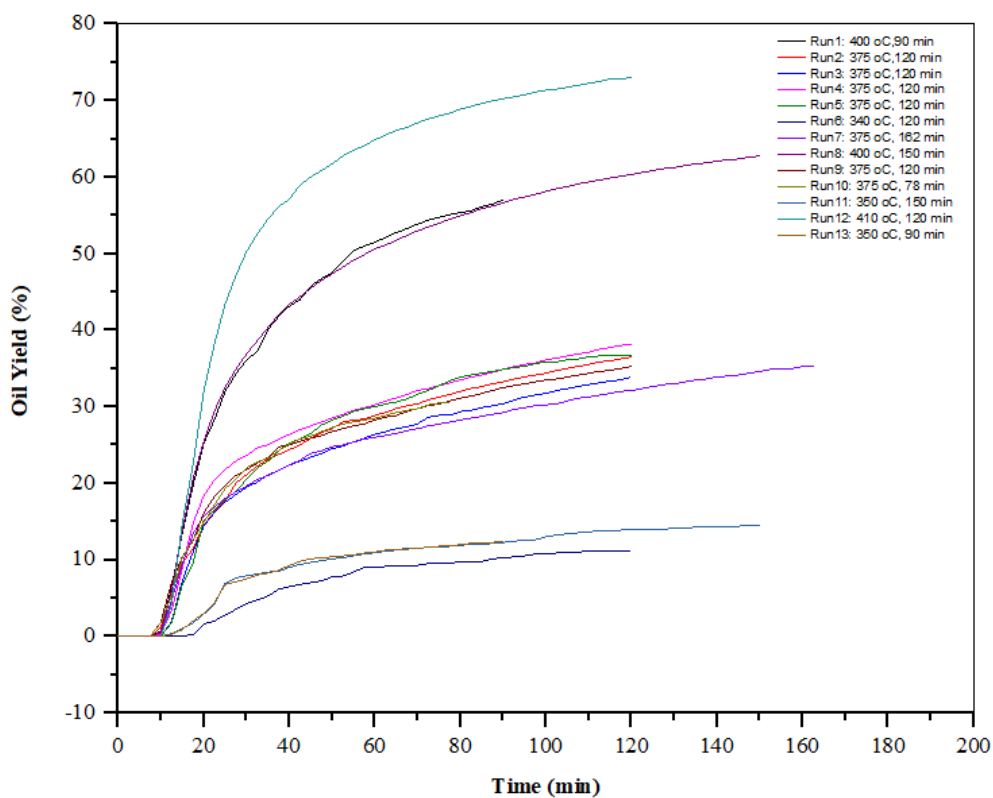


**Figure 4.7: Formation of diesel-like oil with time during TP**

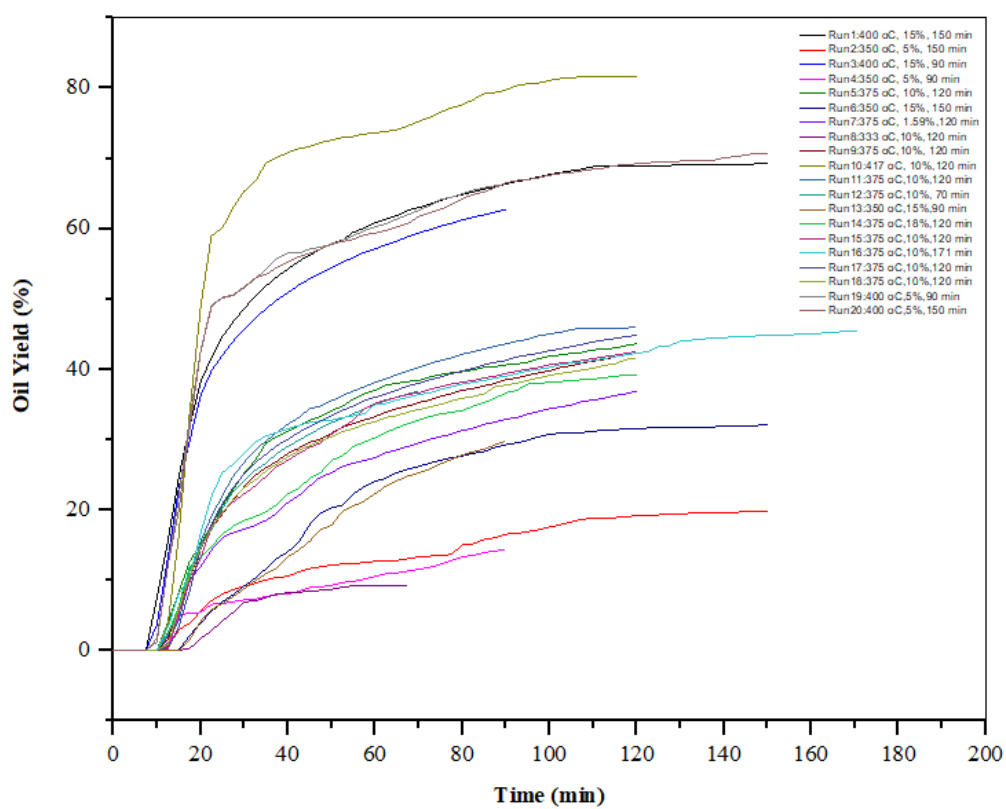


**Figure 4.8: Formation of diesel-like oil with time during CP**

## **4.6 Analyzing the effects of process parameters on Oil yield**

The effect of process variables on oil yields were analyzed during both thermal and catalytic pyrolysis processes. The variables such as the catalyst ratio, reaction temperature, and heating time were analyzed to understand their effects on PLO yield produced from heavy distillate pyrolysis. Experimental data were fitted into the correlation, which was then plotted in surface, Pareto, normal and contour plots that depict operating conditions.

### **4.6.1 Analysis of variance for PLO yield**

The PLO yield from the thermal and catalytic pyrolysis process presented in Table 4.6 and Table 4.7, respectively was tested for fit for a linear, two-factor interaction (2FI), quadratic and cubic polynomials at 5% significance level. Tables 4.8 and 4.9 show the sequential model sum of squares for oil yield produced from the thermal and catalytic pyrolysis, respectively. From Table 4.8, based on the F-value (21.84) and p-value (0.0010), Cubic was aliased while the quadratic model was suggested for oil yield from thermal pyrolysis. During catalytic pyrolysis in Table 4.9, based on the F-value (5.80) and p-value (0.0146), and Adjusted  $R^2$  (0.9966), a quadratic model was suggested for predicting oil yield.

Table 4.10 gives the Analysis of Variance (ANOVA) of PLO yield generated from TP with the significant model F-value of 1363.70 and also based on p-values ( $< 0.05$ ), the model terms temperature (A), heating time (B), temperature-temperature ( $A^2$ ), and heating time – heating time ( $B^2$ ) were significant. The Predicted  $R^2$  of 0.9929 was in reasonable agreement with the Adjusted  $R^2$  of 0.9982 as their difference is less than 0.2 which shows the model was good for predicting PLO yield. The Adequate Precision measures the signal-to-noise ratio with a ratio greater than 4 said to be desirable thus



adequate precision of 120.4920 indicates an adequate signal of the model. Hence the model could be used to predict the oil yield using the values of coefficients for the model presented in Table 4.12. The coefficient estimate represents the expected change in response (oil yield) per unit change in factor value when all remaining factors are held constant. The intercept in an orthogonal design is the overall average response of all the runs. The observed variance inflation factor (VIF) was approximately 1.0 hence this shows the factors are orthogonal. VIFs greater than 1 indicate multi-collinearity, the higher the VIF the more severe the correlation of factors. As a rough rule, VIFs less than 10 are tolerable. Thus, the model for coded and uncoded coefficients during TP are shown in Equation 4.1 and Equation 4.2, respectively.

Table 4.11 gives the Analysis of Variance (ANOVA) for the quadratic model of diesel oil yield produced from catalytic pyrolysis. Based on the F-value of 628.22, the model was significant with significance model terms (p-value < 0.05) being temperature (A), heating time (B), catalyst ratio (C), temperature – catalyst ratio (AC), and catalyst ratio – catalyst ratio ( $C^2$ ). The most significant factor in the PLO yield from catalytic pyrolysis is the temperature (A), followed by temperature and catalyst (AC) interaction, Heating time (B) and catalyst ratio (C), and lastly catalyst- to catalyst ( $C^2$ ) interaction. All three parameters (reaction temperature, heating time, and catalyst ratio) had a significant effect on the PLO yield. The fit of the model is articulated by the coefficient of determination ( $R^2$ ), (0.9966), which indicated that 99.66% of the variability in the response could be explained by the model and which is in reasonable agreement with the predicted  $R^2$ , (0.9865 or 98.65%) as the difference in them is less than 0.2 showing the adequacy of the model. The Adequate Precision ratio of 95.481 during catalytic pyrolysis indicates an adequate signal. Thus, the model could be used to navigate the design matrix of PLO yield from catalytic pyrolysis of heavy distillate as a function of

significant variables A, B, C, AC, and C<sup>2</sup>. Table 4.13 gives the values of coefficients for the model of catalytic pyrolysis. From TP and CP ANOVA results, the PLOs yield highly depended on temperature followed by heating time, catalyst ratio and their interactions as clearly confirmed by large coefficient of temperature (A) in the model equations in Equations 4.1 and 4.3 as compared to others. Previous work has also observed the same for high dependence of pyrolytic liquid oil yield on temperature (Pan et al., 2021). Lack of fit was significant during both TP and CP which could suggest the models were not reasonably good to predict the PLO yields and this similar result on lack of fit has also been reported by Adeboye *et al.* (Adeboye et al., 2021). This prompted validation of the models by plotting actual verses predicted values which indicate that the model's prediction was accurate based on strong correlation between them as presented in Figure 4.9. There is a strong positive correlation between actual and predicted values obtained in both pyrolysis processes. This was evident with the high coefficient of determination, R<sup>2</sup> (> 0.9) for all cases thus the model in Eqn. 4.1, 4.2, 4.3, and 4.4 could be used to predict the response for maximum oil yield.

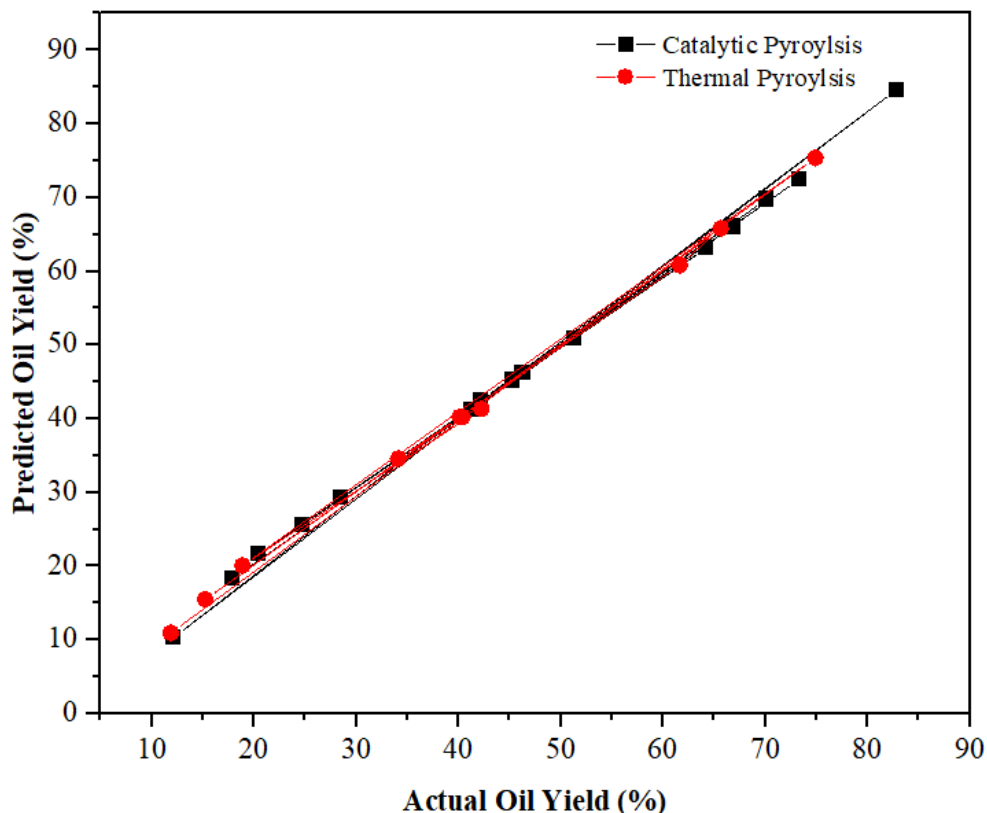


**Figure 4.9: Comparison of Predicted and actual oil yields from TP and CP**

Predicted liquid oil yields obtained during TP from Equation 4.1 and Equation 4.2 was given in Table 4.6. and during CP from Equation 4.3 and Equation 4.4 was given in Table 4.7. Equations 4.1 and 4.3 are in terms of coded factors which could be used to make predictions about the PLO yield from TP and CP, respectively for each factor levels given.

Equation 4.2 and 4.4 are in terms of uncoded (actual) factors which can be used to make predictions of PLO yield for given levels of each factor on TP and CP, respectively. In this, the levels are specified in the original units for each factor. Equations 4.2 and 4.4 cannot be used to determine the relative impact of each factor since the coefficients are scaled to accommodate the units of each factor and the intercept is not at the center of the design space.

$$\text{Oil Yield (\%)} = 40.25 + 22.78A + 2.39B + 1.45A^2 - 1.14B^2 \quad (4.1)$$

$$\text{Oil Yield (\%)} = 3.378 - 0.848A + 0.338B + 0.00233A^2 - 0.00127B^2 \quad (4.2)$$

$$\text{Oil Yield (\%)} = 46.27 + 22.09A + 2.51B + 1.17C - 2.58AC - 1.07 C^2 \quad (4.3)$$

$$\text{Oil Yield (\%)} = -238.022 + 0.475A - 0.340B + 8.762C - 0.021AC - 0.043C^2 \quad (4.4)$$

**Table 4.8: Sequential model sum of squares of PLO yield from TP**

Source	Sum of Squares	Df	Mean Square	F-value	p-value	Adj. R <sup>2</sup>	Pred. R <sup>2</sup>	Comment
Mean vs Total	21266.59	1	21266.59					
Linear vs Mean	4196.43	2	2098.21	663.86	<0.0001	0.9910	0.9836	
2FI vs Linear	0.0342	1	0.0342	0.0098	0.9235	0.9900	0.9820	
Quadratic vs 2FI	27.24	2	13.62	21.98	0.0010	0.9982	0.9928	suggested
Cubic vs Quadratic	3.89	2	1.95	21.84	0.0034	0.9997	0.9942	Aliased
Residual Total	0.4453	5	0.0891					
Adequate precision	25494.62	13	1961.12					120.4920

**Table 4.9: Sequential model sum of squares of PLO yield from CP**

Source	Sum of Squares	Df	Mean Squares	F-value	P-value	Adj. R <sup>2</sup>	Pred. R <sup>2</sup>	Comment
Mean vs Total	42196.81	1	42196.81					
Linear vs Mean	6767.32	3	2255.77	397.18	<0.0001	0.9843	0.9755	
2FI vs Linear	57.68	3	19.23	7.53	0.0036	0.9929	0.9864	
Quadratic vs 2FI	21.08	3	7.03	5.80	0.0146	0.9966	0.9865	Suggested
Residual Total	12.11	10	1.21					
Adequate precision	49055.01	20	2452.75					95.481

**Table 4.10: ANOVA for quadratic model of PLO yield from TP**

Source	Sum of Squares	Degree of Freedom	Mean Square	F-value	P-value	Comment
Model	4223.70	5	844.74	1363.70	<0.0001	significant
Temperature (A)	4150.76	1	4150.76	6700.76	<0.0001	significant
Heating Time (B)	45.67	1	45.67	73.72	<0.0001	significant
AB	0.0342	1	0.0342	0.0553	0.8209	Not Significant
A <sup>2</sup>	14.70	1	14.70	23.73	0.0018	significant
B <sup>2</sup>	9.06	1	9.06	14.63	0.0065	significant
Residual	4.34	7	0.6194			
Lack of Fit	4.27	3	1.42	91.14	0.0004	Significant
Pure Error	0.0625	4	0.0156			
Cor Total	4228.04	12				

**Table 4.11: ANOVA for quadratic model of PLO yield from CP**

Source	Sum of Squares	Df	Mean Square	F-value	p-value	Comment
Model	6846.09	9	760.68	628.22	<0.0001	S
Temperature (A)	6662.45	1	6662.45	5502.32	<0.0001	S
Heating time (B)	86.11	1	86.11	71.12	<0.0001	S
Catalyst ratio (C)	18.77	1	18.77	15.50	0.0028	S
AB	4.55	1	4.55	3.75	0.0814	NS
AC	53.10	1	53.10	43.85	<0.0001	S
BC	0.0406	1	0.0406	0.0335	0.8583	NS
A <sup>2</sup>	2.44	1	2.44	2.02	0.1858	NS
B <sup>2</sup>	0.3563	1	0.3563	0.2943	0.5994	NS
C <sup>2</sup>	16.49	1	16.49	13.62	0.0042	S
Residual	12.11	10	1.21			
Lack of Fit	12.11	5	2.42	5674.83	<0.0001	S
Pure Error	0.0021	5	0.0004			
Cor Total	6858.20	19				

**Key terms:** S - Significant, NS - Not Significant, A – Temperature (°C), B - Heating Time (min), C - Catalyst ratio (%), Df – Degree of Freedom

**Table 4.12: Coefficients for the quadratic model of PLO yield from TP**

Factor	Coded Coefficient Estimate	Uncoded Coefficient Estimate	DF	Standard Error	95% CI Low	95% CI High	VIF
Intercept	40.2500	3.378190	1	03520	39.420	41.0900	1.00
Temperature (A)	22.7800	-0.848023	1	0.2783	22.120	23.4400	1.00
Heating time (B)	2.3900	0.337756	1	0.2783	1.730	3.0500	1.00
AB	0.0925	0.000123	1	0.3935	-0.838	1.0200	1.00
A <sup>2</sup>	1.4500	0.002326	1	0.2984	0.748	2.1600	1.02
B <sup>2</sup>	-1.1400	-0.001268	1	02984	-1.850	-0.4358	1.02

**Table 4.13: Coefficients for a quadratic model of PLO yield from CP**

Factor	Coded Coefficient Estimate	Actual Coefficient Estimate	DF	Standard Error	95% CI Low	95% CI High	VIF
Intercept	46.2700	-238.02177	1	0.4488	45.2700	47.2700	1.00
A	22.0900	0.474826	1	0.2978	21.4200	22.7500	1.00
B	2.5100	-0.339855	1	0.2978	1.8500	3.1700	1.00
C	1.1700	8.761860	1	0.2978	0.5087	1.8400	1.00
AB	0.7538	0.001005	1	0.3890	-0.1131	1.6200	1.00
AC	-2.5800	-0.020610	1	0.3890	-3.4400	-1.7100	1.00
BC	0.0712	0.000475	1	0.3890	-0.7956	0.9381	1.00
A <sup>2</sup>	0.4118	0.000659	1	0.2899	-0.2341	1.0600	1.02
B <sup>2</sup>	0.1572	0.000175	1	0.2899	-0.4886	0.8031	1.02
C <sup>2</sup>	-1.0700	-0.042783	1	0.2899	-1.7200	-0.4237	1.02

**Key Terms:** A - Temperature (°C), B - Heating Time (min), C - Catalyst ratio (%), CI - Confident Interval, VIF - Variance Inflation Factor, DF – Degree of Freedom

#### 4.6.2 Pareto plot of oil yield from thermal pyrolysis of heavy distillate

Pareto chart is an important tool in the design of experiments (DOE). The chart permits one to distinguish the factor and interaction effects that are paramount to the process or design optimization study one has to deal with on response variable. It shows the absolute values of the effects and draws a reference line on the chart (Antony, 2014) and thus any effect that spreads past the reference line is very vital. This was employed to make it easier to visualize the main and interaction effects of all factors on the PLO yield. Figure 4.10 (a) shows a Pareto plot for standardized effects of temperature and heating time on oil yield from thermal pyrolysis where main and interaction effects were among the factors that mainly influenced the % of PLO yield. Factor A which is

temperature had a more positive effect compared to heating time. There was a small positive effect on heating time as it was quite closed to the mean value. A similar result was reported in literature where reaction time had a small positive effect on percentage oil yield (Deriase & El-Gendy, 2014). However, the second-order interaction effects of temperature and heating time also played some positive role in % oil yield during the pyrolysis process.

Figure 4.10 (b) shows a Pareto plot for standardized effects of different factors on diesel oil yield obtained from catalytic pyrolysis of heavy distillate. Factor A which is temperature had more effects compared to other factors followed by heating time and a combination of temperature and catalyst ratio. There were some small effects on the catalyst ratio and its interaction ( $B^2$ ) on oil yield as it was quite closed to the mean value of 2.23. However, the first-order interaction effect of catalyst ratio and temperature played a greater role during the pyrolysis process.

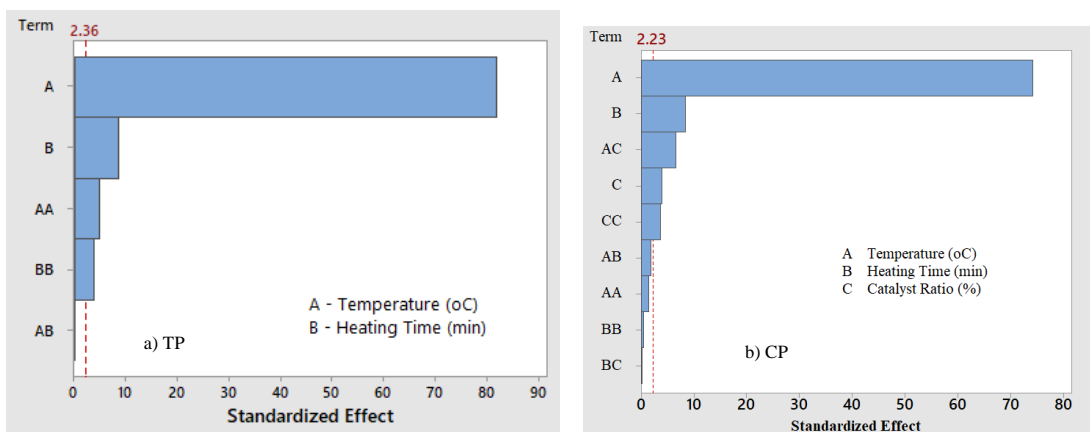


**Figure 4.10: Pareto plots (a, b) on oil yield from TP and CP of heavy distillate**

#### 4.6.3 Normal Plot of standardized effects on oil yield from thermal pyrolysis

The Normal probability plot (NPP) is normally generated to check the findings from a Pareto chart. The NPP is used to evaluate the magnitude, direction, and importance of the effects on one plot (Antony, 2014). Figure 4.11 (a) shows a normal plot for

standardized effects of temperature and heating time on oil yield produced from thermal pyrolysis of heavy distillate. On the NPP, effects that are further from zero (which in this case is the mean of 2.36) are statistically significant. The color and shape of the points differ between statistically significant and statistically insignificant effects. Factors A, B,  $A^2$ , and  $B^2$  had effects on the diesel oil yield as obtained in the Pareto chart since they are statistically significant at 95% confidence level. These points have a different color and shape from the points for the insignificant effects. The insignificant factor was AB while the rest were significant. Also, the NPP plot specifies the factor effect's direction. Processes (A, B, and  $A^2$ ) have positive standardized effects on oil yield. When the process changes from the low level to the high level of the factors (A, B, and  $A^2$ ), the % oil yield increases. The second-order interaction factor ( $B^2$ ) has a negative standardized effect. When the process factor ( $B^2$ ) increases, the % oil yield decreases. The wide variation of process factor A from the rest shows that diesel oil yield strongly depended on temperature. As temperature increased from 340 to 410 °C during thermal pyrolysis, the diesel oil yield increased from 11.88 to 74.88%, non-condensable gas increased from 2.12 to 6.37%, and non-volatile components reduced from 86 to 18.75%. These similar results on oil product yield have been reported for the batch pyrolysis (Pan et al., 2021).

Figure 4.11 (b) shows a normal plot for standardized effects of different factors on oil yield from catalytic pyrolysis. The normal plot indicates the direction of the effect. Factors A, C, and B had positive effects on diesel oil yield whereas factors AB and  $B^2$  had negative effects on the diesel oil yield. Processes (factors A, B, and C) have positive standardized effects on oil yield. When the process varies from the low level to the high level of the factors (A, B, and C), the % oil yield increases. The first and second-order interaction factors (AC and  $C^2$ ) have negative standardized effects. When the process



factors (AC and C<sup>2</sup>) increase, the % oil yield decreases. The wide variation of process factor A from the rest of the process parameters shows that diesel oil yield strongly depended on temperature during catalytic pyrolysis in a similar manner as observed in thermal pyrolysis ones. The positive effect of catalyst ratio (C) shows that kaolin can play a greater role in improving diesel oil yield during pyrolysis as a catalyst. The amount of catalyst ratio affects the oil yields. At a catalyst ratio of 18 %, oil yield was 45.32% compared to 46.25% with a 10% ratio. This decrease could have resulted due to too much catalyst ratio in the mixture which leads to low reactivity and degradation of the polymers.

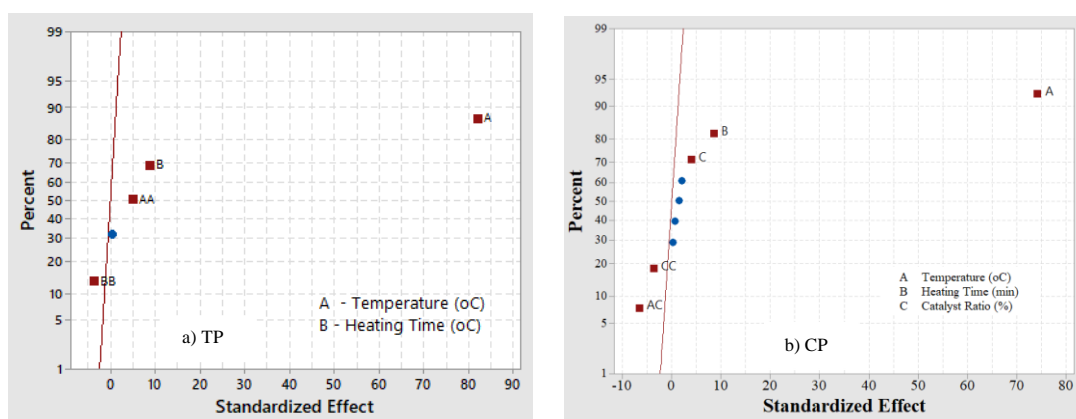


**Figure 4.11: Normal plots (a, b) on oil yield from TP and CP of heavy distillate**

#### 4.6.4 Contour Plots of oil yield generated from TP and CP

Contour plots are necessary to offer a direct interpretation of the interaction between two variables. Its shape provides a measure of the significance of the mutual interaction between the variables (Adeboye et al., 2021). For a circular contour plot, it shows that the interactions between variables are insignificant while for elliptical ones suggests that the interaction between variables is substantial. The contour plots for PLO yield obtained from thermal pyrolysis are presented as shown in Figure 4.12 (a) which shows that oil yield greater than 50% could be achieved between 390 and 400 °C with a heating

time of 120 min and more offering prominent results as it is colored yellow and red which is an indication of maximum oil yield. Between 375 and 390 °C, it is colored green showing low yield (30-50%) could be achieved and at less than 375 °C it is colored blue showing very low yield (less than 30%). From the contour plots, temperature increase results to a corresponding increase in the PLO yield as similarly observed in previous work (Adeboye et al., 2021). There was no prominent effect of heating time on the oil yield above 90 min which indicated that prolonging the heating time does not lead to a further increase in PLO yield. Figure 4.12 (b) shows contour plot result for diesel oil yield obtained from the catalytic pyrolysis process. There is a high yield as depicted from the contours during catalytic pyrolysis compared to thermal pyrolysis. In the figure, between 390 and 400 °C more than 60% of PLO yield was achieved which shows that there is a positive effect of kaolin catalyst during the pyrolysis.

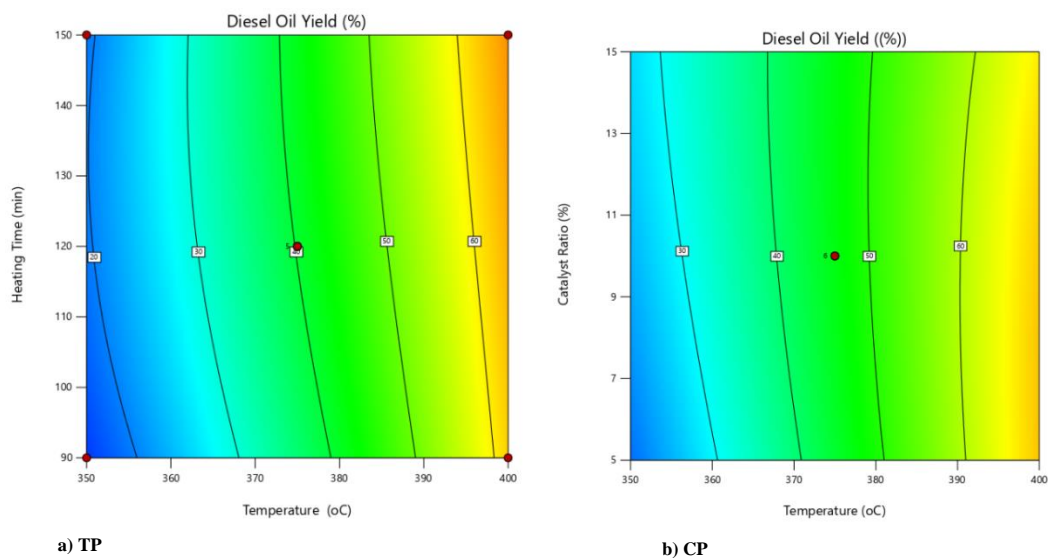


**Figure 4.12: Contour Plots on oil yield from TP and CP of Heavy Distillate**

#### **4.6.5 RSM of Diesel Oil yield from Thermal Pyrolysis of Heavy distillate**

Response surface model allows both the controlled variable (oil yield) and selected process variables to be statistically illustrated via a three-dimensional space and

contours which helps in visualizing the response surface (Te et al., 2021). It is used to study the corrections between the response variable and selected inferred properties. RSM is mostly used for the sequential experiments and can allow it to be split into sub-fractions which encourage the two-factor interaction model (Bhattacharya, 2021). In this study, the selected process parameters are temperature, heating time, and catalyst ratio which were known to affect the oil yield. Figure 4.13 gives a surface plot for PLO yield verses temperature and heating time. The figure showed both temperature and heating time had effects on PLO yield with temperature predominantly having a large effect on oil yield while heating time had a minimal effect as the surface gradually change across the respective axis. Figure 4.14 (a, b and c) shows a plot for PLO yield verses temperature and catalyst ratio, temperature and heating time, and catalyst ratio and heating time respectively. As observed in 4.14 (a, b), temperature had greater effect during pyrolysis compared to catalyst ratio and heating time. The oil yield was influenced by a combination of catalyst ratio and temperature (AC) as well as temperature and heating time (AB). This clearly shows that kaolin as a catalyst can affect pyrolysis process which thus enhances oil yield. There was not much interaction effect (between catalyst ratio and heating time) on oil yield.

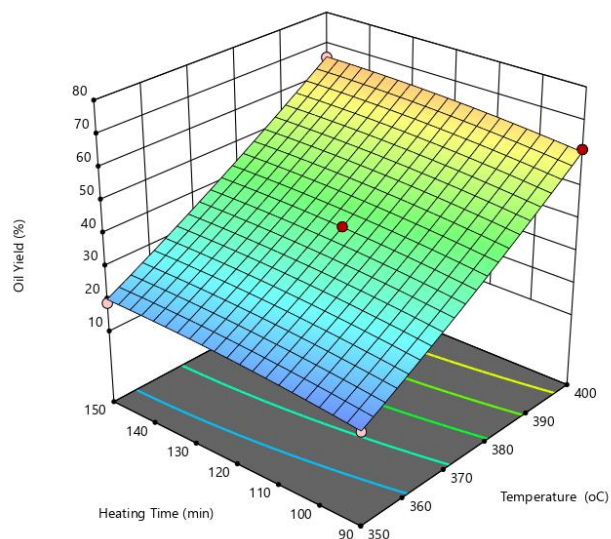


**Figure 4.13: RSM plot on oil yield from TP of Heavy distillate**

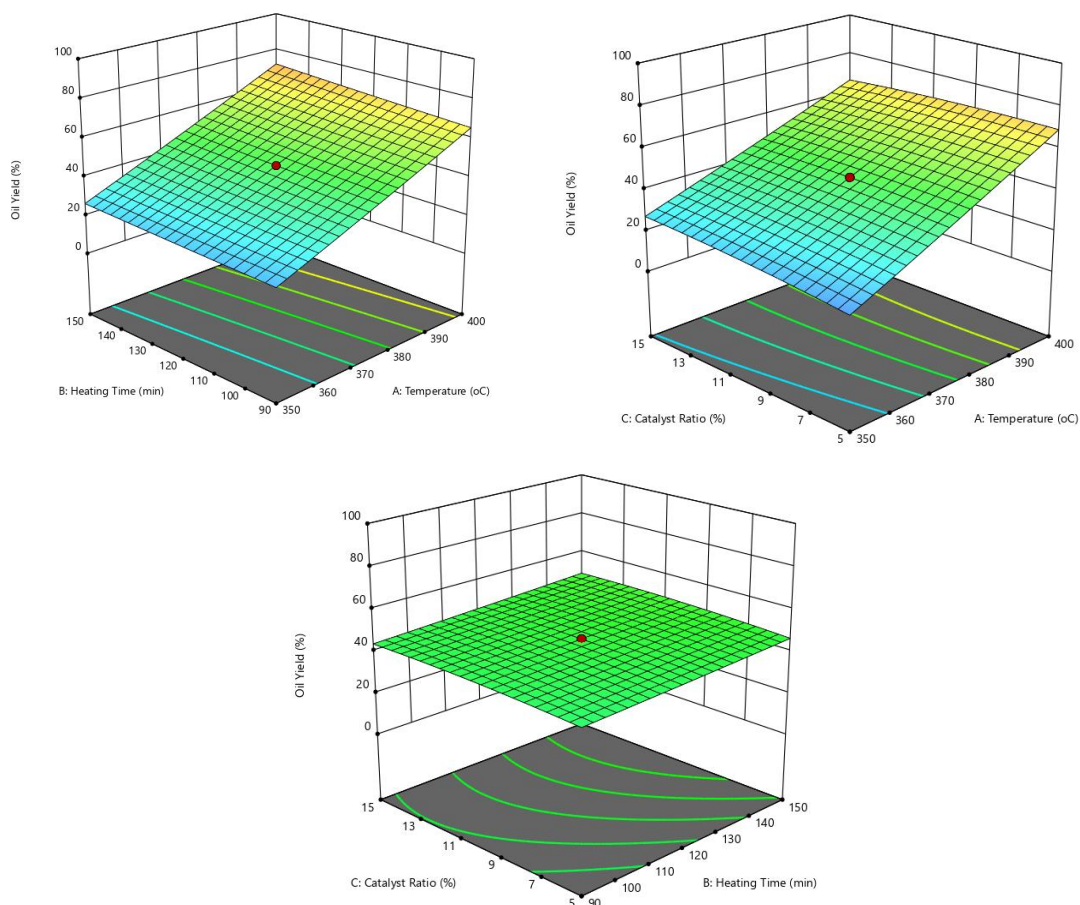


**Figure 4.14: RSM plot on oil yield from CP of heavy distillate**

## 4.7 Characterization results for Fuel Properties

The characterization results of the pyrolytic liquid oils (PLOs) obtained with and without catalyst are presented and discussed in this section. The characterizations

discussed in this section are based on physical properties and elemental and GC-MS analyses. Some of the heavy distillate properties are also included for comparison purposes and ease of data visualization.

#### 4.7.1 Physical Properties

The obtained results of the physical characteristics of the heavy distillate and pyrolytic liquid oils (PLOs) are presented in Table 4.14. The kinematic viscosity, density, and calorific values of the heavy distillate, pyrolytic liquid fuels produced with and without catalyst are 14.00, 2.88, 2.63 cSt; 864, 788, 779 kg m<sup>-3</sup>; and 44.52, 47.23, 46.62 MJ kg<sup>-1</sup> respectively. The results showed that PLO produced with catalyst had better characteristics than that produced without catalyst. Heavy distillate (HD) showed the lowest characteristics which indicate an improvement in the quality of PLOs (with and without catalyst) produced.

**Table 4.14: Physical properties of HD and PLOs**

Parameters	Test Method	Heavy Distillate (feedstock)	Liquid Oil (without Catalyst)	Liquid Oil (with catalyst)
Density at 20 °C	ASTM D4052*	864	779	788
Kinematic viscosity, cSt at 40 °C	ASTM D445	14.00	2.63	2.88
Dynamic viscosity, cP (By calculation)	-	12.10	2.05	2.27
Calorific value, MJ kg <sup>-1</sup>	ASTM D4868	44.52	46.62	47.23
Calorific value (Dulong's Formula), MJ kg <sup>-1</sup>	-	40.70	41.09	41.68
Flash Point, °C	ASTM D93	-	56	58
Freezing Point, °C	ASTM D97	-	-3	-3
Pour Point, °C	ASTM D97	-	-3	-3
pH value	ASTM D7946	-	6.34	7.45

The density of heavy distillate obtained in this study is slightly lower than the density of heavy crude oil which is reported by ASTM D 396 as greater than  $900 \text{ kg m}^{-3}$ , and is also in agreement as reported by other work (Al-salem & Dutta, 2021). This could be associated with lower asphaltene content and other products (lower molecular weights) present in heavy distillate compared to one of heavy crude oil. Density increases with carbon number for compound of same class whereas the order of increasing density is paraffin, naphthene, and aromatic for compounds with the same carbon number (Bacha et al., 2007). This possibly could be one of the reasons for the redistribution of the hydrocarbon compounds peak percentage from GC-MS analysis results obtained in pyrolytic light oils with and without catalyst. The liquid oil from the catalyst had a slightly higher density compared to that produced without catalyst.

Rullkotter and Farrington explicitly defined viscosity as a measure of resistance to fluid flow at a particular temperature and pressure which depends on the chemical composition of the petroleum and amount of dissolved gas it contains (Rullkötter & Farrington, 2016). The values of viscosity  $14.00 \text{ cSt}$  (or  $\text{mm}^2 \text{ s}^{-1}$ ) obtained in this study for heavy distillate is classified as fuel oil number (No.) 5 by ASTM D396 (ASTM, 2001) which is referred to as heavy fuel oil whereas PLOs with and without catalyst had values of  $2.88$  and  $2.63 \text{ cSt}$ , respectively all classified as No. 2 which is referred to as light fuel oil. Fuel oil with No. 2 is suitable for use as transport fuels on cars and trucks. The freezing and pour points ( $-3 \text{ }^\circ\text{C}$ ) of the PLOs are quite low. Other properties like pH (7.45, 6.34), density ( $0.788$ ,  $0.779 \text{ g cm}^{-3}$ ), dynamic viscosities ( $2.27$ ,  $2.05 \text{ cP}$ ) and flash points ( $58$ ,  $56 \text{ }^\circ\text{C}$ ) of the PLOs with and without catalyst, respectively are found to be very similar to conventional diesels.

The heating value of 44.52, 46.62, 47.23 MJ kg<sup>-1</sup> compares favourably to the commercial diesel value of 46 MJ kg<sup>-1</sup> as reported in literature (Madhu et al., 2022). The heating value of PLO with catalyst is slightly higher than diesel ones. Based on pH value and oxygen content, the PLO (with catalyst) are less acidic than PLO (without catalyst). These properties indicate that the scale-up of kaolin based product is realistic from an economic view point because of less requirement of additional equipment (Inayat et al., 2022).

#### **4.7.2 Elemental analysis results**

Elemental analysis is very important to understand the quality of the oil produced, method of up-gradation, and its appropriate applicability in real life. The elemental composition results of heavy distillate and pyrolytic liquid oils (HD & PLOs) are presented in Table 4.15. The carbon contents of the pyrolytic fuel oils obtained with and without catalyst, respectively are 84.83 and 83.24 wt% and that of heavy distillate is 77.21 wt%. The PLO generated with catalyst had the lowest oxygen content of 5.34 wt% compared to that without catalyst at 6.79 wt% and HD at 10.60 wt%. The pyrolysis oils had a decrease in oxygen content which could be related to the deoxygenation reactions (Madhu et al., 2022). Liquid oil produced with catalyst had slightly higher carbon content than one without catalyst. Additionally, the sulphur and nitrogen contents decreased in the pyrolytic liquid oils. Kaolin reduces sulfur content in heavy distillate as found previously in a similar work on crude oil (Ahmed et al., 2020). Kaolin had a positive effect on reducing sulphur contents in diesel oils and this could be due to the desulfurization of the oils as a result of partial and catalytic combustion (A. Demirbas et al., 2015). The presence of nitrogen-containing compounds in oil products can cause several problems such as acid catalyst inhibition

and deactivation, gum formation, metal complexation, and acid-base pair-related corrosion (Prado et al., 2017), thus its presence is unwanted in liquid fuels.

**Table 4.15: Elemental composition of HD and PLOs**

Parameters	Test Method	Heavy Distillate	Liquid Oil (without catalyst)	Liquid Oil (With catalyst)
Carbon (wt.%)	ASTM D5291	77.21	83.24	84.83
Sulphur (wt.%)	ASTM D2622	0.43	0.13	0.11
Hydrogen (wt.%)	ASTM D5291	11.42	9.78	9.68
Nitrogen (wt.%)	ASTM D5291	0.34	0.06	0.04
Oxygen (wt.%)	ASTM D3176	10.60	6.79	5.34

#### 4.7.3 GC-MS analysis results of HD and PLOs

The results from the gas chromatography-mass spectroscopy (GC-MS) analysis of heavy distillate and pyrolytic liquid oils with and without catalyst showing carbon number distribution and heavy carbon range are presented in Table 4.16.

**Table 4.16: Carbon distribution and heavy carbon (>C<sub>23</sub>) in HD and PLOs**

Sample	Carbon Number Distribution	Heavy Carbon range (> C <sub>23</sub> ) (%)
Heavy Distillate	C <sub>6</sub> -C <sub>54</sub>	41.82
PLO (without catalyst)	C <sub>6</sub> -C <sub>38</sub>	10.03
PLO (with catalyst)	C <sub>6</sub> -C <sub>44</sub>	8.88

The heavy carbon range (> C<sub>23</sub>) noticeably decreased from an area percentage of 41.82 wt% in heavy distillate to 10.03 wt% without a catalyst and 8.88 wt% with a catalyst. This undoubtedly revealed the thermal degradation of heavy components into lighter ones through pyrolysis with and without a catalyst. The carbon number distribution of diesel fractions ranges from C<sub>7</sub>-C<sub>23</sub> whereas those greater than C<sub>23</sub> are heavy fuel oil



fractions(Shuang Wang et al., 2021). Thus, kaolin favoured formations of light diesel oils with lower heavy carbon components.

The components with the lowest boiling points are represented by the first peaks in the chromatogram as shown in spectra for heavy distillate in Figure D.1, pyrolytic liquid oil produced without catalyst in Figure D.2 and that with catalyst in Figure D.3 (Appendix D). Earlier work by Demirbas *et al.* (2017) has shown that heavy components with larger molecular weights can be converted into lighter ones through dehydration, depolymerization, and decarboxylation. The ability of heavy oil to oxidize into lighter ones has been reported to be due to the catalytic effect of kaolinite which depends on the type and amount of acid sites and is linked to its thermal degradation, especially the dehydroxylation process (Zhang et al., 2022). Complex components such as naphthenes were observed in the diesel oils and this usually shows poorly defined and broad bumps beneath the sharp peaks which are in agreement with the previous work (Sorheim et al., 2020). The hydrocarbon distribution of carbon number in the heavy distillate, pyrolytic liquid oils with and without catalyst ranges from C<sub>6</sub> - C<sub>54</sub>, C<sub>6</sub> - C<sub>44</sub>, C<sub>6</sub> - C<sub>38</sub>, respectively having complicated mixtures of n-paraffins, iso-paraffins, naphthenes, olefins, diolefins, iso-olefins, and aromatics. The paraffin and iso-paraffin contents greatly improved with and without kaolin through the pyrolysis process. This shift toward the production of more aliphatic compounds could be due to the decomposition of aromatic and carbonyl compounds with the use of kaolin as a catalyst. In all cases (with and without catalyst), showed that the oil contains majorly aliphatic groups of compounds (paraffins and iso-paraffins), olefins, acids, and esters as shown in details in Appendix C (Table C.1-3) for HD and PLOs samples. The tables show the chromatographic area of compounds in the liquid oil samples identified as retention time increased with an area percentage greater than 0.00% which are reasonably

comparable to those greater than 0.5% as identified in previous work of Martin *et al.* (Martin et al., 2022). There is comparatively low abundance of heteroatoms compounds like nitrogen and sulfur containing compounds in the oil products.

The hydrocarbon group compositional analysis is presented in Figure 4.15. In Figure 4.15, the paraffin compositions of the pyrolytic liquid fuels obtained were greatly improved with kaolin catalyst (26.16%) as compared to without catalyst (25.15%) which could have resulted due to catalytic effect. There was no presence of benzene and naphthalene components in the HD and PLOs in this study which deviates from other work (Kar et al., 2018), as they obtained a significant amount of them in the pyrolytic oils and this could possibly be because the feedstock mostly used by the recycling industries to generate heavy distillate as a bi-product during pyrolysis are often soft plastics such as polyethylene (PE), low/high-density polyethylene (L/HDPE) and polypropylene (PP).

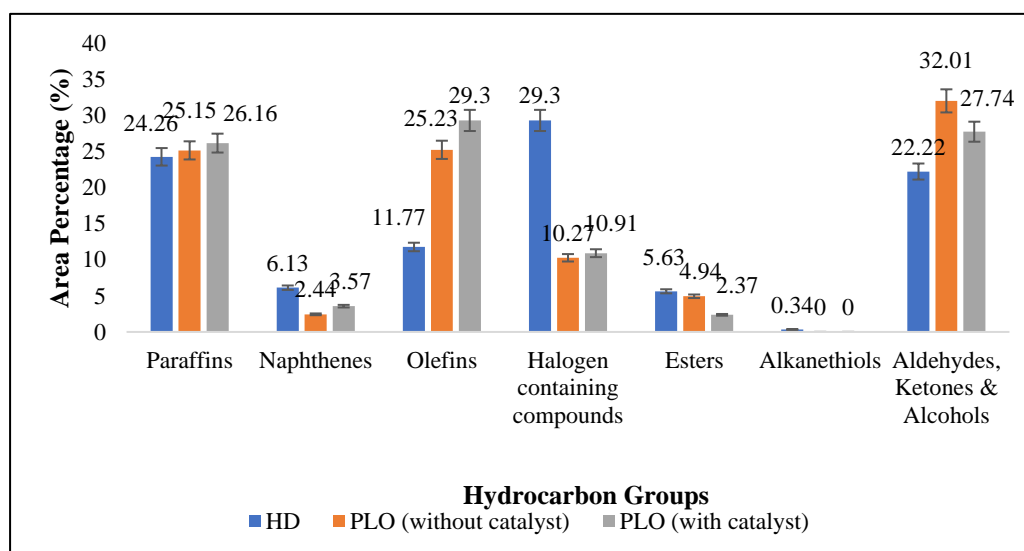


**Figure 4.15: Distribution of hydrocarbon groups in HD and PLOs**

The presence of esters and carbonyl compounds respectively were greatly reduced with catalyst (2.37% and 27.74%) compared to that without catalyst (4.94% and 32.01%).

The presence of alkanethiols was detected in heavy distillate sample with relatively low amount of approximately 0.34% and disappeared completely during pyrolysis with and without catalyst. The presence of esters was greatly reduced with catalyst (2.37%) as compared to that without catalyst (4.94%) and heavy distillate (5.63%), which could have resulted due to catalytic effect. Thus, kaolin could not only shift the organic chemical composition of oils during pyrolysis toward light carbon numbers which are in the diesel range but as well improve the quality of the liquid fuels by reducing the presence of unwanted impurities such as esters. There was also a decrease in content of halogen containing compounds from 29.3% in heavy distillate to 10.91% with catalyst and 10.27% without catalyst. Literature has revealed that the low amount of ketone, furan, styrene, and nitrogenated compounds could lead to the oil becoming lighter (Madhu et al., 2022).

## CHAPTER FIVE

### CONCLUSION AND RECOMMENDATIONS

#### 5.1 Conclusion

The study successfully investigated catalytic pyrolysis of heavy distillate from plastic waste into a diesel range fuel using response surface methodology central composite design as design matrix. Based on the findings, thermal characterization results showed that HD structure breaks at 285.77, 290.63, 327.02, 343.46 °C and fully decomposes at 365.83, 391.38, 412.42, 424.40 °C. The study also showed that use of kaolin as a catalyst during catalytic pyrolysis resulted into increased pyrolytic liquid oil yields (73.28, 66.80, 20.5, 17.88 wt.%) from design matrix (400 °C, 5%, 150 min; 400 °C, 5%, 90 min; 350 °C, 5%, 150 min; 350 °C, 5%, 90 min), as compared to that of thermal pyrolysis with oil yields (65.63, 61.63, 18.88, 15.25 wt.%) from design matrix (400 °C, 150 min; 400 °C, 90 min; 350 °C, 150 min; 350 °C, 90 min), respectively. The Pareto, normal, contour, and 3D surface plots revealed liquid oil yield from catalytic pyrolysis largely depended on temperature, with the ANOVA result at a 5% confidence level confirmed temperature had the most significance followed by catalyst and heating time; the interaction effect of temperature and catalyst (AC), and catalyst- to catalyst (C<sup>2</sup>) interactions were significant. The functional group analysis of the pyrolytic liquid oils (PLOs) showed a strong transmittance peak observed at 2954.4114, 2915.842, 2848.3457 cm<sup>-1</sup> which indicates the presence of symmetric and asymmetric stretching modes for methyl (CH<sub>3</sub>), methylene (CH<sub>2</sub>), methylidyne (CH). The heavy carbon range (> C<sub>23</sub>) decreased from an area percentage of 41.82 wt% in heavy distillate to 10.03 wt% without a catalyst and 8.88 wt% with a catalyst hence more diesel range fuels were favoured with use of kaolin as a catalyst. Paraffin compositions of diesel-like oils obtained were also greatly improved with kaolin catalyst (26.16%) as compared to

without catalyst (25.15%). The presence of unwanted impurities such as halogen containing compounds, esters and carbonyl compounds remained in the oil samples but decreased in chromatographic area percentages during catalytic pyrolysis compared to thermal pyrolysis. The study also found out that the fuel properties obtained were comparable with the distillation characteristics and the carbon number distribution of commercial diesel fuels which can be a potential substitute for transport grade fuels.

## **5.2 Recommendations**

In accordance to the research findings, the study recommends;

1. Desulfurization, dehalogenation and deoxygenation of the pyrolytic liquid oils to improve oil quality.
2. Structural modification of kaolin with mechanical or chemical activation to enhance kaolinite structure and improve its catalytic performance during pyrolysis process.
3. Engine performance testing with pyrolytic liquid oils from heavy distillate to understand its combustion characteristics.
4. Diesel fuels obtained from heavy distillate can be used as transport grade fuels.
5. Chemical recycling industries should scale-up pyrolysis technology for effective management of heavy distillate from plastic waste.

## **5.3 Research Contribution**

The following research contributions were made:

1. Characterized heavy distillate from plastic waste based on thermal properties, physical properties, elemental analysis and chemical compositions.
2. Upgraded heavy distillate from plastic waste into diesel-like oils by use of kaolin as a catalyst with pyrolysis technology.

3. Characterized diesel-like oils from heavy distillate based on the fuel properties.
4. Analyzed oil yields using Design Expert and Minitab statistical techniques.

## REFERENCES

- Abdul Jameel, A. G., Han, Y., Brignoli, O., Telalović, S., Elbaz, A. M., Im, H. G., Roberts, W. L., & Sarathy, S. M. (2017). Heavy fuel oil pyrolysis and combustion: Kinetics and evolved gases investigated by TGA-FTIR. *Journal of Analytical and Applied Pyrolysis*, 127, 183–195. <https://doi.org/10.1016/j.jaap.2017.08.008>
- Acomb, J. C., Wu, C., & Williams, P. T. (2014). Control of steam input to the pyrolysis-gasification of waste plastics for improved production of hydrogen or carbon nanotubes. *Applied Catalysis B: Environmental*, 147, 571–584. <https://doi.org/10.1016/j.apcatb.2013.09.018>
- Adams, C. J., Earle, M. J., & Seddon, K. R. (2000). Catalytic cracking reactions of polyethylene to light alkanes: In ionic liquids. *Green Chemistry*, 2(1), 21–23. <https://doi.org/10.1039/a908167d>
- Adebiyi, F. M. (2021). An insight into asphaltene precipitation, deposition and management stratagems in petroleum industry. *Journal of Pipeline Science and Engineering*, 1(4), 419–427. <https://doi.org/10.1016/j.jpse.2021.08.006>
- Adeboye, B. S., Adewole, B. Z., Adedoja, A. M., Obayopo, S. O., Asere, A. A., Kayode, O., Idris, M. O., & Okediran, I. K. (2021). Optimization and modeling of process parameters on the yield of enhanced pyrolysis oil during co-pyrolysis of cassava peel with polystyrene. *Environmental Challenges*, 5(February 2022), 100347. <https://doi.org/10.1016/j.envc.2021.100347>
- Sadan, Z., & De Kock, L. (2022). *Identifying Policy Gaps And Opportunities Plastic Pollution In Africa*. [www.wwf.org.za/report/plastic-pollution-policy-in-africa](http://www.wwf.org.za/report/plastic-pollution-policy-in-africa)
- Aguado, J., Serrano, D. P., Romero, M. D., & Escola, J. M. (1996). Catalytic conversion of polyethylene into fuels over mesoporous MCM-41. *Chemical Communications*, 6, 725–726. <https://doi.org/10.1039/cc9960000725>
- Ahmad, I., Ismail Khan, M., Khan, H., Ishaq, M., Tariq, R., Gul, K., & Ahmad, W. (2015). Pyrolysis study of polypropylene and polyethylene into premium oil products. *International Journal of Green Energy*, 12(7), 663–671. <https://doi.org/10.1080/15435075.2014.880146>
- Ahmed, H., Mustafa, B., Mohamed, A. M., & Lokman, A. (2020). *Preparation of Clay Catalyst from Natural Clay and its uses in Desulfurization of Crude Oil*. 9(9), 15–20. <https://doi.org/10.35629/6734-0909011520>
- Akhyar, M., Mehmood, K., & Chong, K. (2019a). Photoluminescence emission behavior on the reduced band gap of Fe doping in CeO<sub>2</sub>-SiO<sub>2</sub> nanocomposite and photophysical properties. *Journal of Saudi Chemical Society*, 23(5), 561–575. <https://doi.org/10.1016/j.jscs.2018.10.002>

- Akhyar, M., Mehmood, K., & Chong, K. (2019b). Photoluminescence emission behavior on the reduced band gap of Fe doping in CeO<sub>2</sub>-SiO<sub>2</sub> nanocomposite and photophysical properties. *Journal of Saudi Chemical Society*, 23(5), 561–575. <https://doi.org/10.1016/j.jscs.2018.10.002>
- Almeida, D., & Marque, M. de F. (2015). Thermal and Catalytic Pyrolysis of Polyethylene Plastic Waste in Semi. *Polimeros*, 26(1), 1–8.
- Al-Salem, S. M., Antelava, A., Constantinou, A., Manos, G., & Dutta, A. (2017). A review on thermal and catalytic pyrolysis of plastic solid waste (PSW). *Journal of Environmental Management*, 197(1408), 177–198. <https://doi.org/10.1016/j.jenvman.2017.03.084>
- Al-salem, S. M., & Dutta, A. (2021). *Wax Recovery from the Pyrolysis of Virgin and Waste Plastics*. <https://doi.org/10.1021/acs.iecr.1c01176>
- Amadala, V. (2021, September 11). *Global oil prices likely increase as demand grows 5%*.
- anne Fritt-Rasmussen, Susse Wegeberg, Kim Gustavson, Kristin Rist Sørheim, P. S. D., Kirsten Jørgensen, O. T. and J. P. H.-A., & Questions, O. (2018). *Heavy Fuel Oil (HFO)*.
- Anthony, J., Gopal, D. N., L, M. G., & Dheejaj, H. (2019). *a Review Paper on Extraction of Fuel From Waste Plastic By*. 06(1), 2348–2350.
- Antony, J. (2014). Design of Experiments for Engineers and Scientists: Second Edition. In *Design of Experiments for Engineers and Scientists: Second Edition* (Issue October). <https://doi.org/10.1016/C2012-0-03558-2>
- Asghar, A., Raman, A. A. A., & Daud, W. M. A. W. (2014). A Comparison of Central Composite Design and Taguchi Method for Optimizing Fenton Process. *Scientific World Journal*, 2014. <https://doi.org/10.1155/2014/869120>
- Aske, N., Kallevik, H., Einar, E. J., & Sjöblom, J. . (2002). Characterisation of Crude Oil Components , Asphaltene Aggregation and Emulsion Stability by means of Near Infrared Spectroscopy and Multivariate Analysis by Narve Aske Department of Chemical Engineering. *Advances in Colloid and Interface Science*, June, 3.
- ASTM, A. S. for T. M. (2001). *Standard Specification for Fuel Oils*. 05, 1–5.
- Augado, J., Serrano, D. P., & Escola, J. M. (2006). Catalytic Upgrading of Plastic Wastes. In *Feedstock Recycling and Pyrolysis of Waste Plastics: Converting Waste Plastics into Diesel and Other Fuels*. <https://doi.org/10.1002/0470021543.ch3>
- Bacha, J., Freel, J., Gibbs, A., Gibbs, L., Hemighaus, G., Hoekman, K., Horn, J., Ingham, M., Jossens, L., Kohler, D., Lesnini, D., McGeehan, J., Nikanjam, M., Olsen, E., Organ, R., Scott, B., Sztenderowicz, M., Tiedemann, A., Walker, C., ... Mills, J. (2007). Diesel Fuels Technical Review. *Chevron Global Marketing*, 1–116.



- Balan, V., Mihai, C. T., Cojocaru, F. D., Uritu, C. M., Dodi, G., Botezat, D., & Gardikiotis, I. (2019). Vibrational spectroscopy fingerprinting in medicine: From molecular to clinical practice. *Materials*, 12(18), 1–40. <https://doi.org/10.3390/ma12182884>
- Bartoli, M., Frediani, M., Briens, C., Berruti, F., & Rosi, L. (2019). An overview of temperature issues in microwave-assisted pyrolysis. *Processes*, 7(10), 1–14. <https://doi.org/10.3390/pr7100658>
- Behuria, P. (2019). The comparative political economy of plastic bag bans in East Africa: why implementation has varied in Rwanda, Kenya and Uganda. *Global Development Institute Working Paper Series, March*, 1–30.
- Bernardo, M. M. S. (2011). Physico-chemical characterization of chars produced in the co-pyrolysis of wastes and possible routes of valorisation. *Bioresource Technology*, 4(November), 89.
- Bett, R. K., Kumar, A., Siagi, Z. O., & Mibei, Z. C. (2022). *Thermal Pyrolysis of Used Tyres to Produce Liquid Fuel : Process Optimization Research Article Thermal Pyrolysis of Used Tyres to Produce Liquid Fuel : Process Optimization and How It Compares to Microwave Pyrolysis. 2022(March)*.
- Bhattacharya, S. (2021). Central Composite Design for Response Surface Methodology and Its Application in Pharmacy. *Response Surface Methodology in Engineering Science [Working Title]*, January. <https://doi.org/10.5772/intechopen.95835>
- Borchardt, T., & Borchardt, T. (1999). *A review of DSC kinetics methods. 1*, 1–6.
- Borkowski, J. J., Limmun, W., & Chomtee, B. (2021). Factorwise variance dispersion graphs. *Communications in Statistics - Theory and Methods*, 0(0), 1–22. <https://doi.org/10.1080/03610926.2021.1897144>
- Broido, A. (1969). Simple, Sensitive Graphical Method of Treating Thermogravimetric Analysis Data. *J Polym Sci Part A-2 Polym Phys*, 7(10), 1761–1773. <https://doi.org/10.1002/pol.1969.160071012>
- Budsaerechai, S., Hunt, A. J., & Ngernyen, Y. (2019a). Catalytic pyrolysis of plastic waste for the production of liquid fuels for engines. *RSC Advances*, 9(10), 5844–5857. <https://doi.org/10.1039/c8ra10058f>
- Budsaerechai, S., Hunt, A. J., & Ngernyen, Y. (2019b). Catalytic pyrolysis of plastic waste for the production of liquid fuels for engines. *RSC Advances*, 9(10), 5844–5857. <https://doi.org/10.1039/c8ra10058f>
- Burnham, A. K., & Dinh, L. N. (2007). A comparison of isoconversional and model-fitting approaches to kinetic parameter estimation and application predictions. *Journal of Thermal Analysis and Calorimetry*, 89(2), 479–490. <https://doi.org/10.1007/s10973-006-8486-1>

- Cai, N., Li, X., Xia, S., Sun, L., Hu, J., Bartocci, P., Fantozzi, F., Williams, P. T., Yang, H., & Chen, H. (2021). Pyrolysis-catalysis of different waste plastics over Fe/Al<sub>2</sub>O<sub>3</sub> catalyst: High-value hydrogen, liquid fuels, carbon nanotubes and possible reaction mechanisms. *Energy Conversion and Management*, 229, 113794. <https://doi.org/10.1016/j.enconman.2020.113794>
- Cardona, S. C., & Corma, A. (2000). Tertiary recycling of polypropylene by catalytic cracking in a semibatch stirred reactor. Use of spent equilibrium FCC commercial catalyst. *Applied Catalysis B: Environmental*, 25(2–3), 151–162. [https://doi.org/10.1016/S0926-3373\(99\)00127-7](https://doi.org/10.1016/S0926-3373(99)00127-7)
- Cebe, P. (2005). Recent developments in thermal analysis of polymers: Calorimetry in the limit of slow and fast heating rates. *Journal of Polymer Science, Part B: Polymer Physics*, 43(6), 629–636. <https://doi.org/10.1002/polb.20348>
- Chakma, A. (2000). Chapter 6 Kinetics and Mechanisms of Asphaltene Cracking During Petroleum Recovery and Processing Operations. In *Developments in Petroleum Science* (Vol. 40, Issue PART B). [https://doi.org/10.1016/S0376-7361\(09\)70277-8](https://doi.org/10.1016/S0376-7361(09)70277-8)
- Choi, I. H., Lee, H. J., Rhim, G. B., Chun, D. H., Lee, K. H., & Hwang, K. R. (2022). Catalytic hydrocracking of heavy wax from pyrolysis of plastic wastes using Pd/H $\beta$  for naphtha-ranged hydrocarbon production. *Journal of Analytical and Applied Pyrolysis*, 161, 105424. <https://doi.org/10.1016/j.jaap.2021.105424>
- Clapp, J., & Swanston, L. (2009). Doing away with plastic shopping bags: International patterns of norm emergence and policy implementation. *Environmental Politics*, 18(3), 315–332. <https://doi.org/10.1080/09644010902823717>
- Coates, J. (2000). Interpretation of Infrared Spectra, A practical Approach. In R. A. Meyers (Ed.), *John Wiley & Sons Ltd*. <https://doi.org/10.1097/00010694-197107000-00005>
- Coates, J. (2006). Interpretation of Infrared Spectra, A Practical Approach. *Encyclopedia of Analytical Chemistry*, 1–23. <https://doi.org/10.1002/9780470027318.a5606>
- Coats, A. W., & Redfern, J. P. (1964). *Kinetic Parameters from Thermogravimetric Data*.
- Coronado, M. A., Montero, G., García, C., Valdez, B., Ayala, R., & Pérez, A. (2017). Quality assessment of biodiesel blends proposed by the new Mexican policy framework. *Energies*, 10(5). <https://doi.org/10.3390/en10050631>
- Coskun, O. (2016). Separation Techniques: CHROMATOGRAPHY. *Northern Clinics of Istanbul, November 2016*. <https://doi.org/10.14744/nci.2016.32757>
- Dadario, N., Gabriel Filho, L. R. A., Cremasco, C. P., Santos, F. A. dos, Rizk, M. C., & Mollo Neto, M. (2023). Waste-to-Energy Recovery from Municipal Solid Waste: Global Scenario and Prospects of Mass Burning Technology in Brazil. In *Sustainability (Switzerland)* (Vol. 15, Issue 6). MDPI. <https://doi.org/10.3390/su15065397>

- Dafalla, M. A. (2013). *Effects of Clay and Moisture Content on Direct Shear Tests for Clay-Sand Mixtures*. 2013.
- De La Puente, G., & Sedran, U. (1998). Recycling polystyrene into fuels by means of FCC: Performance of various acidic catalysts. *Applied Catalysis B: Environmental*, 19(3–4), 305–311. [https://doi.org/10.1016/S0926-3373\(98\)00084-8](https://doi.org/10.1016/S0926-3373(98)00084-8)
- Demirbas, A., Alidrisi, H., & Balubaid, M. A. (2015). API gravity, sulfur content, and desulfurization of crude oil. *Petroleum Science and Technology*, 33(1), 93–101. <https://doi.org/10.1080/10916466.2014.950383>
- Demirbas, A., Bafail, A., & Nizami, A. S. (2016). Heavy oil upgrading: Unlocking the future fuel supply. *Petroleum Science and Technology*, 34(4), 303–308. <https://doi.org/10.1080/10916466.2015.1136949>
- Demirbas, Ayhan., Al-Ghamdi, K., Sen, N., Aslan, A., & Alalayah, W. M. (2017). Gasoline- and diesel-like products from heavy oils via catalytic pyrolysis. *Petroleum Science and Technology*, 35(15), 1607–1613. <https://doi.org/10.1080/10916466.2017.1336768>
- Demirbas & Taylan, O. (2016). Removing of resins from crude oils. *Petroleum Science and Technology*, 34(8), 771–777. <https://doi.org/10.1080/10916466.2016.1163397>
- Deriase, S. F., & El-Gendy, N. Sh. (2014). *Energy Sources , Part A : Recovery , Utilization , and Environmental Effects Waste Eggshells for Production of Biodiesel from Different Types of Waste Cooking Oil as Waste Recycling and a Renewable Energy Process*. January 2012. <https://doi.org/10.1080/15567036.2014.963745>
- Dewi, R., Agusnar, H., Alfian, Z., & Tamrin. (2018). Characterization of technical kaolin using XRF, SEM, XRD, FTIR and its potentials as industrial raw materials. *Journal of Physics: Conference Series*, 1116(4). <https://doi.org/10.1088/1742-6596/1116/4/042010>
- Diaz, A., Orea, M., Bazdikian, G., Bruzual, J., Mujica, Y., Benitez, N., Pacific, E., Arraga, T., & Pacific, E. (2015). *Laboratory simulation of chemical reactions occurring during the thermal recovery processes of heavy crude oil EOR* . November 2016.
- Ding, Z., Chen, H., Liu, J., Cai, H., Evrendilek, F., & Buyukada, M. (2021). Pyrolysis dynamics of two medical plastic wastes: Drivers, behaviors, evolved gases, reaction mechanisms, and pathways. *Journal of Hazardous Materials*, 402. <https://doi.org/10.1016/j.jhazmat.2020.123472>
- Dubdub, I., & Al-Yaari, M. (2020). Pyrolysis of mixed plastic waste: I. kinetic study. *Materials*, 13(21), 1–15. <https://doi.org/10.3390/ma13214912>
- Duncan, M. P., Hourston, D. J., & Dumont, F. (2000). Thermogravimetry of Polymers. *Encyclopedia of Analytical Chemistry*, 8094–8105. <https://doi.org/10.1002/9780470027318.a2037>

- Editor John Scheirs, S., & Polyesters, M. (2006). *Wiley Series in Polymer Science Metallocene-based polyolefins Preparations, Properties and Technology Polymer-Clay Nanocomposites Dendrimers and Other Dendritic Polymers Modern Styrenic Polymers Polystyrenes and Styrenic Copolymers Forthcoming Titles Ligh.*
- Ellen MacArthur Foundation. (2017). The New Plastics Economy: Rethinking the Future of Plastics & Catalysing Action. *Ellen MacArthur Foundation*, 68. <https://doi.org/10.1103/Physrevb.74.035409>
- Elordi, G., Olazar, M., Lopez, G., Artetxe, M., & Bilbao, J. (2011). Product yields and compositions in the continuous pyrolysis of high-density polyethylene in a conical spouted bed reactor. *Industrial and Engineering Chemistry Research*, 50(11), 6650–6659. <https://doi.org/10.1021/ie200186m>
- Eltohami, E. K., & Mustafa, M. A. (2019). Effect of Kaolin as a Catalyst on the Yield of Catalytic Pyrolysis of Waste Plastic Effect of Kaolin as a Catalyst on the Yield of Catalytic Pyrolysis Of Waste Plastic Mixtures. *UofKEJ*, 8(2), 17–24.
- EPRA, E. and P. R. A. (2020). *Energy and Petroelum Statistics Report 2020*. 1–70.
- Espinosa, M. J. C., Blanco, A. C., Schmidgall, T., Atanasoff-Kardjalieff, A. K., Kappelmeyer, U., Tischler, D., Pieper, D. H., Heipieper, H. J., & Eberlein, C. (2020). Toward Biorecycling: Isolation of a Soil Bacterium That Grows on a Polyurethane Oligomer and Monomer. *Frontiers in Microbiology*, 11. <https://doi.org/10.3389/fmicb.2020.00404>
- Fadillah, G., Fatimah, I., Sahroni, I., Musawwa, M. M., Mahlia, T. M. I., & Muraza, O. (2021). Recent progress in low-cost catalysts for pyrolysis of plastic waste to fuels. *Catalysts*, 11(7). <https://doi.org/10.3390/catal11070837>
- Fan, C., Zan, C., Zhang, Q., Ma, D., Chu, Y., Jiang, H., Shi, L., & Wei, F. (2013). The oxidation of heavy oil: Thermogravimetric analysis and non-isothermal kinetics using the distributed activation energy model. *Fuel Processing Technology*, 119, 146–150. <https://doi.org/10.1016/j.fuproc.2013.10.020>
- Fang, L. S. (2015). *Determination of Optimum Moisture Content for Aggregation of S300 Kaolin* (Vol. 7, Issue 1).
- Farhan, H. I., O. Mohammed, M., & Abdul-Jaleel, T. (2017). Fractionation and characterization of Crude Oil Components from Al-Rashidiya Field - Eastern Baghdad using Chromatography Method. *Kirkuk University Journal-Scientific Studies*, 12(2), 314–328. <https://doi.org/10.32894/kujss.2017.124966>
- Feist, M. (2015). Thermal analysis: basics, applications, and benefit. *ChemTexts*, 1(1), 1–12. <https://doi.org/10.1007/s40828-015-0008-y>
- Fernandez, Y., Arenillas, A., & Angel, J. (2011). Microwave Heating Applied to Pyrolysis. *Advances in Induction and Microwave Heating of Mineral and Organic Materials*. <https://doi.org/10.5772/13548>

- Feyisayo, V. A., E. Chukwuneke, C., & O. Agboola, B. (2019). Recent Techniques for the Removal of Naphthenic Acid from Heavy Crude Oils. *Processing of Heavy Crude Oils - Challenges and Opportunities*. <https://doi.org/10.5772/intechopen.89585>
- Freeman, E. S., & Carroll, B. (1975). The Application Of Thermoanalytical Techniques To Reaction Kinetics.' The Thermogravimetric Evaluation Of The Kinetics Of The Decomposition Of Calcium Oxalate Monohydrate. *Mod.Healthcare*, 4(6), 6–8.
- Friedman, H. L. (1964). Kinetics of thermal degradation of char-forming plastics from thermogravimetry. Application to a phenolic plastic. *Journal of Polymer Science Part C: Polymer Symposia*, 6(1), 183–195. <https://doi.org/10.1002/polc.5070060121>
- Gandidi, I. M., Susila, M. D., & Rustamaji, H. (2018a). Effect of natural zeolite and kaolin as a catalyst in the isothermal-catalytic cracking of real municipal solid waste (MSW) for bio-oil production. *IOP Conference Series: Earth and Environmental Science*, 160(1). <https://doi.org/10.1088/1755-1315/160/1/012018>
- Gandidi, I. M., Susila, M. D., & Rustamaji, H. (2018b). Effect of natural zeolite and kaolin as a catalyst in the isothermal-catalytic cracking of real municipal solid waste (MSW) for bio-oil production. *IOP Conference Series: Earth and Environmental Science*, 160(1). <https://doi.org/10.1088/1755-1315/160/1/012018>
- Gao, J., & Xu, C. (1999). Review of the chemistry for catalytic cracking of heavy oils. *Petroleum Science and Technology*, 17(5), 471–490.
- Geyer, R., Jambeck, J. R., & Law, K. L. (2017). Production, use, and fate of all plastics ever made. *Science Advances*, 3(7), 25–29. <https://doi.org/10.1126/sciadv.1700782>
- Gill, P., Moghadam, T., & Ranjbar, B. (2010). Differential Scanning Calorimetry Techniques: Applications in Biology and Nanoscience. *JOURNAL OF BIOMOLECULAR TECHNIQUES*, 21(4), 167–193. <https://doi.org/10.1111/dme.13173>
- Goodfellow, T. (2014). Rwanda's political settlement and the urban transition: expropriation, construction and taxation in Kigali. *Journal of Eastern African Studies*, 8(2), 311–329. <https://doi.org/10.1080/17531055.2014.891714>
- Grabarics, M., Lettow, M., Kirschbaum, C., Greis, K., Manz, C., & Pagel, K. (2022). Mass Spectrometry-Based Techniques to Elucidate the Sugar Code. *Chemical Reviews*, 122(8), 7840–7908. <https://doi.org/10.1021/acs.chemrev.1c00380>
- Graciani, D. M., María, Rodríguez, A., Muñoz, M., & Moyá, M. L. (2005). Micellar solutions of sulfobetaine surfactants in water-ethylene glycol mixtures: Surface tension, fluorescence, spectroscopic, conductometric, kinetic studies. *Langmuir*, 21(16), 7161–7169. <https://doi.org/10.1021/la050862j>

- Gul, S., Shah, A. A., & Bilal, S. (2013). *Calculation of Activation Energy of Degradation of Polyaniline-Dodecylbenzene Sulfonic Acid Salts via.* 2(3), 673–684.
- Hadi, B., Sokoto, A. M., Garba, M. M., & Muhammad, A. B. (2017). Effect of neat kaolin and CuO/Kaolin on the yield and composition of products from pyrolysis of polystyrene waste. *Energy Sources, Part A: Recovery, Utilization and Environmental Effects*, 39(2), 148–153. <https://doi.org/10.1080/15567036.2016.1201548>
- Hakeem, I. G., Aberuagba, F., & Musa, U. (2018). Catalytic pyrolysis of waste polypropylene using Ahoko kaolin from Nigeria. *Applied Petrochemical Research*, 8(4), 203–210. <https://doi.org/10.1007/s13203-018-0207-8>
- Hariadi, D., Saleh, S. M., Yamin, R. A., & Aprilia, S. (2021). Utilization of LDPE plastic waste on the quality of pyrolysis oil as an asphalt solvent alternative. *Thermal Science and Engineering Progress*, 23, 100872. <https://doi.org/10.1016/j.tsep.2021.100872>
- Hartulistiyoso, E., Sigiro, F. A. P. A. G., & Yulianto, M. (2015). Temperature Distribution of the Plastics Pyrolysis Process to Produce Fuel at 450oC. *Procedia Environmental Sciences*, 28(Sustain 2014), 234–241. <https://doi.org/10.1016/j.proenv.2015.07.030>
- Hashimoto, K., & Al, S. (1994). Waste Plastics over REY Zeolite. *Energy*, 131–135.
- Hassan, S. Y. (2014). *Effect of Refining on Asphaltene Property Distributions.* 204. <https://doi.org/10.11575/PRISM/25805>
- Hatakeyama, T., & Quinn, F. X. (1999). Thermal analysis: Fundamentals and applications to polymer science. In *Thermochemica Acta: Vol. second edi* (Issue second edition). [https://doi.org/10.1016/0040-6031\(95\)91503-6](https://doi.org/10.1016/0040-6031(95)91503-6)
- Helaluddin, A. B. M., Khalid, R. S., Alaama, M., & Abbas, S. A. (2016). Main analytical techniques used for elemental analysis in various matrices. *Tropical Journal of Pharmaceutical Research*, 15(2), 427–434. <https://doi.org/10.4314/tjpr.v15i2.29>
- Hong, T., Yin, J. Y., Nie, S. P., & Xie, M. Y. (2021). Applications of infrared spectroscopy in polysaccharide structural analysis: Progress, challenge and perspective. *Food Chemistry: X*, 12(November), 100168. <https://doi.org/10.1016/j.fochx.2021.100168>
- Huang, Y. F., Chiueh, P. Te, & Lo, S. L. (2016). A review on microwave pyrolysis of lignocellulosic biomass. *Sustainable Environment Research*, 26(3), 103–109. <https://doi.org/10.1016/j.serj.2016.04.012>
- Hubadillah, K. S., Harun, Z., Hafiz, M., Othman, D., & Ismail, A. F. (2016). Effect of kaolin particle size and loading on the characteristics of kaolin ceramic support prepared via phase inversion technique. *Journal of Asian Ceramic Societies*, 4(2), 164–177. <https://doi.org/10.1016/j.jascer.2016.02.002>

- Huth, M., & Heilos, A. (2013). Fuel flexibility in gas turbine systems: Impact on burner design and performance. In *Modern Gas Turbine Systems: High Efficiency, Low Emission, Fuel Flexible Power Generation* (pp. 635–684). Elsevier Ltd. <https://doi.org/10.1533/9780857096067.3.635>
- Inayat, A., Ahmed, A., Tariq, R., Waris, A., Jamil, F., Ahmed, S. F., Ghenai, C., & Park, Y. K. (2022). Techno-Economical Evaluation of Bio-Oil Production via Biomass Fast Pyrolysis Process: A Review. *Frontiers in Energy Research*, 9(January), 1–9. <https://doi.org/10.3389/fenrg.2021.770355>
- International Organization for Standardization [ISO]. (2020). *Petroleum products-Transparent and opaque liquids-Determination of kinematic viscosity and calculation of dynamic viscosity*. 2020.
- IUCN, EA, & QUANTIS. (2020). National Guidance for Plastic Pollution Hotspotting and Shaping Action, Country Report Thailand. *United Nations Environment Programme, October*, 48.
- Ivanova, S. R., Gumerova, E. F., Minsker, K. S., Zaikov, G. E., & Berlin, A. A. (1990). Selective catalytic degradation of polyolefins. *Progress in Polymer Science*, 15(2), 193–215. [https://doi.org/10.1016/0079-6700\(90\)90028-Y](https://doi.org/10.1016/0079-6700(90)90028-Y)
- Ivanova, S. R., Minsker, K. S., & Zaikov, G. E. (2002). Catalytic degradation of polyolefins. *Oxidation Communications*, 25(3), 325–349. <https://doi.org/10.1002/masy.19920570117>
- Jaiswal, A. K., Mohrana, M., Krishna, P. H. R., Moon, D. V., Millo, T., & Murty, O. P. (2010). Atomic absorption spectrometry - A review. *Journal of Forensic Medicine and Toxicology*, 27(2), 64–71. <https://doi.org/10.5505/adlitip.2013.70299>
- Jankovic, A., Chaudhary, G., & Goia, F. (2021). Designing the design of experiments (DOE) – An investigation on the influence of different factorial designs on the characterization of complex systems. *Energy and Buildings*, 250, 111298. <https://doi.org/10.1016/j.enbuild.2021.111298>
- Kaminsky, W. (2006). The Hamburg Fluidized-bed Pyrolysis Process to Recycle Polymer Wastes and Tires. *Feedstock Recycling and Pyrolysis of Waste Plastics: Converting Waste Plastics into Diesel and Other Fuels, Lws 1*, 475–491. <https://doi.org/10.1002/0470021543.ch17>
- Kar, Y. (2011). Catalytic pyrolysis of car tire waste using expanded perlite. *Waste Management*, 31(8), 1772–1782. <https://doi.org/10.1016/j.wasman.2011.04.005>
- Kar, Y., Dilek, S., & Yalman, Y. (2018). *Characterization of light diesel fraction obtained from upgraded heavy oil*. 1–4. <https://doi.org/10.1016/j.ejpe.2018.08.001>
- Karimian, M., Schaffie, M., & Fazaelpoor, M. H. (2016). Determination of activation energy as a function of conversion for the oxidation of heavy and light crude oils in relation to in situ combustion. *Journal of Thermal Analysis and Calorimetry*, 125(1), 301–311. <https://doi.org/10.1007/s10973-016-5439-1>

- Kasar, P., & Ahmaruzzaman, M. (2022). Characterization of liquid products obtained from catalytic binary co-cracking of residual fuel oil with various waste plastics. *Scientific Reports*, *12*(1), 1–15. <https://doi.org/10.1038/s41598-022-15371-8>
- Kenya Association of Manufacturers (KAM). (2019). Accelerating a Circular Economy in Kenya. *Kenya Plastic Action Plan, November*.
- Khelkhal, M. A., Lapuk, S. E., Buzyurov, A. V., Ignashev, N. E., Shmeleva, E. I., Mukhamatdinov, I. I., & Vakhin, A. V. (2022). Thermal Behavior of Heavy Oil Catalytic Pyrolysis and Aquathermolysis. *Catalysts*, *12*(4), 2–6. <https://doi.org/10.3390/catal12040449>
- Kibria, M. G., Masuk, N. I., Safayet, R., Nguyen, H. Q., & Mourshed, M. (2023). Plastic Waste: Challenges and Opportunities to Mitigate Pollution and Effective Management. In *International Journal of Environmental Research* (Vol. 17, Issue 1). Springer Science and Business Media Deutschland GmbH. <https://doi.org/10.1007/s41742-023-00507-z>
- Kissinger, H. E. (1957). Reaction Kinetics in Differential Thermal Analysis. *Guang Pu Xue Yu Guang Pu Fen Xi/Spectroscopy and Spectral Analysis*, *29*(11), 1702–1706. <https://doi.org/https://sci-hub.hkvisa.net/10.1021/ac60131a045>
- Klancnik, G., Medved, J., & Mrvar, P. (2010). Differential thermal analysis (DTA) and differential scanning calorimetry (DSC) as a method of material investigation. *Materials and Geoenvironment*, *57*(1), 127–142.
- Kök, M. V. K., Varfolomeev, M. A., & Nurgaliev, D. K. (2017). Crude oil characterization using TGA-DTA, TGA-FTIR and TGA-MS techniques. *Journal of Petroleum Science and Engineering*, *154*, 537–542. <https://doi.org/10.1016/j.petrol.2016.12.018>
- Kok, M. V., Varfolomeev, M. A., & Nurgaliev, D. K. (2018). Wax appearance temperature (WAT) determinations of different origin crude oils by differential scanning calorimetry. *Journal of Petroleum Science and Engineering*, *168*(March), 542–545. <https://doi.org/10.1016/j.petrol.2018.05.045>
- Kumagai, S., Hasegawa, I., Grause, G., Kameda, T., & Yoshioka, T. (2015). Thermal decomposition of individual and mixed plastics in the presence of CaO or Ca(OH)<sub>2</sub>. *Journal of Analytical and Applied Pyrolysis*, *113*, 584–590. <https://doi.org/10.1016/j.jaap.2015.04.004>
- Kumar, S., Panda, A. K., & Singh, R. K. (2011). A review on tertiary recycling of high-density polyethylene to fuel. *Resources, Conservation and Recycling*, *55*(11), 893–910. <https://doi.org/10.1016/j.resconrec.2011.05.005>
- Kumar, S., & Singh, R. K. (2011). Recovery of hydrocarbon liquid from waste high density polyethylene by thermal pyrolysis. *Brazilian Journal of Chemical Engineering*, *28*(4), 659–667. <https://doi.org/10.1590/S0104-66322011000400011>



- Lange, J. P. (2021). Managing Plastic Waste-Sorting, Recycling, Disposal, and Product Redesign. In *ACS Sustainable Chemistry and Engineering* (Vol. 9, Issue 47, pp. 15722–15738). American Chemical Society. <https://doi.org/10.1021/acssuschemeng.1c05013>
- Li, Y. B., Zhao, J. Z., Pu, W. F., Jia, H., Peng, H., Zhong, D., & Wang, S. K. (2013). Catalytic effect analysis of metallic additives on light crude oil by TG and DSC tests. *Journal of Thermal Analysis and Calorimetry*, 113(2), 579–587. <https://doi.org/10.1007/s10973-012-2759-7>
- Lim, A. C. R., Chin, B. L. F., Jawad, Z. A., & Hii, K. L. (2016). Kinetic Analysis of Rice Husk Pyrolysis Using Kissinger-Akahira-Sunose (KAS) Method. *Procedia Engineering*, 148(January), 1247–1251. <https://doi.org/10.1016/j.proeng.2016.06.486>
- Lin, R., Negelein, D. L., & White, R. L. (1997). Effects of catalyst acidity and structure on polymer cracking mechanisms. *ACS Division of Fuel Chemistry, Preprints*, 42(4), 982–984.
- Liu, W., Zhang, N., Li, Z., & Yao, Z. (2020). Reaction Behavior of a Trace Element during the Pitch Pyrolysis Process. *ACS Omega*, 5(30), 18731–18737. <https://doi.org/10.1021/acsomega.0c01751>
- Liu, Z., Meng, X., Xu, C., & Gao, J. (2007). Secondary Cracking of Gasoline and Diesel from Heavy Oil Catalytic Pyrolysis. *Chinese Journal of Chemical Engineering*, 15(3), 309–314. [https://doi.org/10.1016/s1004-9541\(07\)60085-8](https://doi.org/10.1016/s1004-9541(07)60085-8)
- Loganathan, S., Valapa, R. B., Mishra, R., & Pugazhenth, G. (2017). Thermogravimetry Analysis for Characterization of Nanomaterials. In *Thermal and Rheological Measurement Techniques for Nanomaterials Characterization* (Issue March 2018). <https://doi.org/10.1016/b978-0-323-46139-9.12001-8>
- López, A., de Marco, I., Caballero, B. M., Laresgoiti, M. F., & Adrados, A. (2011). Influence of time and temperature on pyrolysis of plastic wastes in a semi-batch reactor. *Chemical Engineering Journal*, 173(1), 62–71. <https://doi.org/10.1016/j.cej.2011.07.037>
- Lordeiro, F. B., Altoé, R., Hartmann, D., Filipe, E. J. M., González, G., & Lucas, E. F. (2021). The Stabilization of Asphaltenes in Different Crude Fractions: A Molecular Approach. *Journal of the Brazilian Chemical Society*, 32(4), 741–756. <https://doi.org/10.21577/0103-5053.20200226>
- Lucena, M. da C. C., Soares, S. de A., & Soares, J. B. (2004). Characterization and thermal behavior of polymer-modified asphalt. *Materials Research*, 7(4), 529–534. <https://doi.org/10.1590/s1516-14392004000400004>
- Luo, W., Fan, Z., Wan, J., Hu, Q., Dong, H., Zhang, X., & Zhou, Z. (2021). Study on the reusability of kaolin as catalysts for catalytic pyrolysis of low-density polyethylene. *Fuel*, 302(January), 121164. <https://doi.org/10.1016/j.fuel.2021.121164>

- Luo, W., Hu, Q., Fan, Z. yi, Wan, J., He, Q., Huang, S. xiong, Zhou, N., Song, M., Zhang, J. chao, & Zhou, Z. (2020). The effect of different particle sizes and HCl-modified kaolin on catalytic pyrolysis characteristics of reworked polypropylene plastics. *Energy*, 213, 119080. <https://doi.org/10.1016/j.energy.2020.119080>
- Madhu, P., Sasireka, M., Samikannu, R., Vinoth, K., Kumar, A. U., Patil, P. P., Kaliappan, S., & Gebrekidan, A. M. (2022). Production and Characterization of Maximum Liquid Oil Products through Individual and Copyrolysis of Pressed Neem Oil Cake and Waste Thermocol Mixture. *Advances in Polymer Technology*, 2022. <https://doi.org/10.1155/2022/5258130>
- Maitlo, G., Ali, I., Maitlo, H. A., Ali, S., Unar, I. N., Ahmad, M. B., Bhutto, D. K., Karmani, R. K., Naich, S. ur R., Sajjad, R. U., Ali, S., & Afridi, M. N. (2022). Plastic Waste Recycling, Applications, and Future Prospects for a Sustainable Environment. In *Sustainability (Switzerland)* (Vol. 14, Issue 18). MDPI. <https://doi.org/10.3390/su141811637>
- Mansoori, G. A., Vazquez, D., & Shariaty-Niassar, M. (2013). Polydispersity of Heavy Organics in Crude Oils and their Role in Oil Well Fouling. *Journal of Petroleum Science and Engineering*, 58(September 2003), 1–7.
- Mark, L. O., Cendejas, M. C., & Hermans, I. (2020). The Use of Heterogeneous Catalysis in the Chemical Valorization of Plastic Waste. *ChemSusChem*, 13(22), 5808–5836. <https://doi.org/10.1002/cssc.202001905>
- Martin, M. T., Aguirre, J. L., Baena-gonz, J., Gonz, S., Roberto, P., & Saiz-rodr, L. (2022). *Influence of Specific Power on the Solid and Liquid Products Obtained in the Microwave-Assisted Pyrolysis of*.
- Matheka, M. N. (2012). *Mechanical Properties and Thermal Degradation of Bitumen-Acacia Sap Composites*. November, 1–102.
- Matthews, C. N., & Minard, R. D. (2006). Hydrogen cyanide polymers, comets and the origin of life. *Faraday Discussions*, 133(January), 393–401. <https://doi.org/10.1039/b516791d>
- MEF, M. of E. and F. (2021). National Sustainable Waste Management Policy, February 2021. *Government of Kenya, April*, 1–49.
- Meng, X., Xu, C., & Gao, J. (2006). Production of light olefins by catalytic pyrolysis of heavy oil. *Petroleum Science and Technology*, 24(3–4), 413–422. <https://doi.org/10.1080/10916460500281090>
- Mertinkat, J., Kirsten, A., Predel, M., & Kaminsky, W. (1999). Cracking catalysts used as fluidized bed material in the Hamburg pyrolysis process. *Journal of Analytical and Applied Pyrolysis*, 49(1), 87–95. [https://doi.org/10.1016/S0165-2370\(98\)00103-X](https://doi.org/10.1016/S0165-2370(98)00103-X)
- Miandad, R., Barakat, M. A., Aburizaiza, A. S., Rehan, M., & Nizami, A. S. (2016). Catalytic pyrolysis of plastic waste: A review. *Process Safety and Environmental Protection*, 102, 822–838. <https://doi.org/10.1016/j.psep.2016.06.022>

- Miandad, R., Rehan, M., Barakat, M. A., Aburiazaiza, A. S., Khan, H., Ismail, I. M. I., Dhavamani, J., Gardy, J., Hassanpour, A., & Nizami, A. S. (2019). Catalytic pyrolysis of plastic waste: Moving toward pyrolysis based biorefineries. *Frontiers in Energy Research*, 7(MAR). <https://doi.org/10.3389/fenrg.2019.00027>
- Miandad, Rashid; Mohammad, R. M. A. B., Aburiazaiza, A. S., , Hizbullah Khan, Iqbal M. I. Ismail, Jeya Dhavamani, J. G., & Hassanpour, Ali, and A.-S. N. (2019). Catalytic pyrolysis of plastic waste: Moving toward pyrolysis based biorefineries. *Frontiers in Energy Research*, 7(MAR), 1–17. <https://doi.org/10.3389/fenrg.2019.00027>
- Mibei, Z. C., Kumar, A., & Talai, S. M. (2023). Catalytic Pyrolysis of Plastic Waste to Liquid Fuel Using Local Clay Catalyst. *Journal of Energy*, 2023, 1–11. <https://doi.org/10.1155/2023/7862293>
- Motawie, M., Hanafi, S. A., Elmelawy, M. S., Ahmed, S. M., Mansour, N. A., Darwish, M. S. A., & Abulyazied, D. E. (2015). Wax co-cracking synergism of high density polyethylene to alternative fuels. *Egyptian Journal of Petroleum*, 24(3), 353–361. <https://doi.org/10.1016/j.ejpe.2015.07.004>
- Mothé, M. G., Perin, M., & Mothé, C. G. (2016). *Comparative thermal study of heavy crude oils by DSC*. 6466(March). <https://doi.org/10.1080/10916466.2015.1136328>
- Muhammad, I., Tijjani, N., Dioha, I., & Musa, A. (2013). SARA Separation and Determination of Concentration Levels of Some Heavy Metals in Organic Fractions of Nigerian Crude Oil. *Chemistry and Materials Research*, 3(4), 7–15.
- Nandiyanto, A. B. D., Oktiani, R., & Ragadhita, R. (2019). How to read and interpret ftir spectroscopy of organic material. *Indonesian Journal of Science and Technology*, 4(1), 97–118. <https://doi.org/10.17509/ijost.v4i1.15806>
- Ng, H. M., Saidi, N. M., Omar, F. S., Ramesh, K., Ramesh, S., & Bashir, S. (2018). Thermogravimetric Analysis of Polymers. *Encyclopedia of Polymer Science and Technology*, January 2019, 1–29. <https://doi.org/10.1002/0471440264.pst667>
- Nugroho, A. S., Rahmad, Chamim, M., & Hidayah, F. N. (2018). Plastic waste as an alternative energy. *AIP Conference Proceedings*, 1977(June). <https://doi.org/10.1063/1.5043022>
- OECD, O. for E. C. and D. (2018). Improving plastics management: trends, policy responses, and the role of international co-operation and trade. *Environmental Policy Paper No. 12*, 12, 20.
- Ojo, G. P., Igbokwe, U. G., Egbuachor, C. J., & Nwozor, K. K. (2017). *Geotechnical Properties and Geochemical Composition of Kaolin Deposits in American Journal of Engineering Research (AJER) Open Access Geotechnical Properties and Geochemical Composition of Kaolin Deposits in Parts of Ifon , Southwestern Nigeria. January.*

- Olori, A., Di Pietro, P., & Campopiano, A. (2021). Preparation of Ultrapure KBr Pellet: New Method for FTIR Quantitative Analysis. *International Journal of Science Academic Research*, 02(02), 1015–1020.
- Omar, S., Alsamaq, S., Yang, Y., & Wang, J. (2019). Production of renewable fuels by blending bio-oil with alcohols and upgrading under supercritical conditions. *Frontiers of Chemical Science and Engineering*, 13(4), 702–717. <https://doi.org/10.1007/s11705-019-1861-9>
- Omol, D. K., Acaye, O., Okot, D. F., & Bongomin, O. (2020). Production of Fuel Oil from Municipal Plastic Wastes Using Thermal and Catalytic Pyrolysis. *Journal of Energy Research and Reviews*, January, 1–8. <https://doi.org/10.9734/jenrr/2020/v4i230120>
- Ore, O. T., & Adebisi, F. M. (2021). A review on current trends and prospects in the pyrolysis of heavy oils. *Journal of Petroleum Exploration and Production*, 11(3), 1521–1530. <https://doi.org/10.1007/s13202-021-01099-0>
- Owino, O. M., Muriithi, T. Naftali., & Mbuvi, M. H. (2016). *Chemical And Mineral Analysis Of Raw And Acid-Treated Clays From Kano Plains, Kisumu County, Kenya* (Issue April).
- Oyedotun, T. D. T. (2018). X-ray fluorescence (XRF) in the investigation of the composition of earth materials: a review and an overview. *Geology, Ecology, and Landscapes*, 2(2), 148–154. <https://doi.org/10.1080/24749508.2018.1452459>
- Oyeleke, O. O., Ohunakin, O. S., & Adelekan, D. S. (2021). Catalytic Pyrolysis in Waste to Energy Recovery Applications: A Review. *IOP Conference Series: Materials Science and Engineering*, 1107(1), 012226. <https://doi.org/10.1088/1757-899x/1107/1/012226>
- Pal, R. kumar, & Tiwari, A. C. (2020). *Comparative Study Of Catalytic Pyrolysis Of Waste Polypropylene ( Pp ) Using Silica – Alumina , Kaolin Clay*. 7(9), 342–347.
- Pan, R., Martins, M. F., Debenest, G., Pan, R., Martins, M. F., & Debenest, G. (2021). *Pyrolysis of waste polyethylene in a semi-batch reactor to produce liquid fuel : optimization of operating conditions To cite this version : HAL Id : hal-03382557*.
- Panda, A. K., Alotaibi, A., Kozhevnikov, I. V., & Shiju, N. R. (2020). Pyrolysis of Plastics to Liquid Fuel Using Sulphated Zirconium Hydroxide Catalyst. *Waste and Biomass Valorization*, 11(11), 6337–6345. <https://doi.org/10.1007/s12649-019-00841-4>
- Panda, A. K., Murugan, S., & Singh, R. K. (2016). Performance and emission characteristics of diesel fuel produced from waste plastic oil obtained by catalytic pyrolysis of waste polypropylene. *Energy Sources, Part A: Recovery, Utilization and Environmental Effects*, 38(4), 568–576. <https://doi.org/10.1080/15567036.2013.800924>

- Panda, A. K., & Singh, R. K. (2013). Optimization of Process Parameters in the Catalytic Degradation of Polypropylene to Liquid Fuel by Taguchi Method. *Advanced Chemical Engineering Research*, 2(4), 50–54.
- Panda, A. K., Singh, R. K., & Mishra, D. K. (2010). Thermolysis of waste plastics to liquid fuel. A suitable method for plastic waste management and manufacture of value added products-A world prospective. *Renewable and Sustainable Energy Reviews*, 14(1), 233–248. <https://doi.org/10.1016/j.rser.2009.07.005>
- Pandey, P., Dhiman, M., Kansal, A., & Subudhi, S. P. (2023). Plastic waste management for sustainable environment: techniques and approaches. In *Waste Disposal and Sustainable Energy* (Vol. 5, Issue 2, pp. 205–222). Springer. <https://doi.org/10.1007/s42768-023-00134-6>
- Papari, S., Bamdad, H., & Berruti, F. (2021). Pyrolytic conversion of plastic waste to value-added products and fuels: A review. *Materials*, 14(10). <https://doi.org/10.3390/ma14102586>
- Prado, G. H. C., Rao, Y., & De Klerk, A. (2017). Nitrogen removal from oil: A review. *Energy and Fuels*, 31(1), 14–36. <https://doi.org/10.1021/acs.energyfuels.6b02779>
- Pujro, R. A., Falco, M. G., Pedrosa, A. M. G., Souza, M. J. B., Morgado, E., & Sedran, U. (2012). Yield of aromatics from naphthenics upon catalytic cracking. *Journal of the Brazilian Chemical Society*, 23(7), 1378–1387. <https://doi.org/10.1590/S0103-50532012000700023>
- Quesada, L., Calero, M., Martín-Lara, M. Á., Pérez, A., Paucar-Sánchez, M. F., & Blázquez, G. (2022). Characterization of the Different Oils Obtained through the Catalytic In Situ Pyrolysis of Polyethylene Film from Municipal Solid Waste. *Applied Sciences (Switzerland)*, 12(8). <https://doi.org/10.3390/app12084043>
- Rafey, A., Pal, K., Bohre, A., & Modak, A. (2023). *A State-of-the-Art Review on the Technological Advancements for the Sustainable Management of Plastic Waste in Consort with the Generation of Energy and Value-Added Chemicals*.
- Ragaert, K., Delva, L., & Van Geem, K. (2017). Mechanical and chemical recycling of solid plastic waste. In *Waste Management* (Vol. 69, pp. 24–58). Elsevier Ltd. <https://doi.org/10.1016/j.wasman.2017.07.044>
- Rahman, M., Roy, S. C., Hassan, M. M., Mondal, B. K., Faruk, M. O., Rahman, M. A., Zahiduzzaman, M., Sharmin, A., Hosen, M. J., Afroze, M., Khan, M., Nasreen, Z., & Matin, M. A. (2020). Catalytic Pyrolysis of Waste Plastics into Liquid Hydrocarbon using Mesoporous Kaolin Clay. *Journal of Bangladesh Academy of Sciences*, 44(1), 1–12. <https://doi.org/10.3329/jbas.v44i1.48559>
- Rathod, et al. (2020). Diesel From Plastic Polyethene. *International Journal for Research in Applied Science & Engineering Technology*, 8(V), 576–581. <https://doi.org/http://doi.org/10.22214/ijraset.2020.5090>

- Rivas-perez, R., Feliu, V., Jose, F., & Garcia, C. (2014). *Temperature control of a crude oil preheating furnace using a modified Smith predictor improved with a disturbance rejection term* *Temperature control of a crude oil preheating furnace using a modified Smith predictor improved with a disturbance rejection*. *August*. <https://doi.org/10.3182/20140824-6-ZA-1003.01999>
- Rullkötter, J., & Farrington, J. W. (2016). What Was Released? Assessing the Physical Properties and Chemical Composition of Petroleum and Products of Burned Oil. *Oceanography*, *34*(1), 14.
- Sánchez-Lemus, M. C., Schoeggl, F. F., Taylor, S. D., Andersen, S. I., Mapolelo, M. M., Mahavadi, S. C., & Yarranton, H. W. (2016). Characterization of Heavy Distillation Cuts Using Fourier Transform Infrared Spectrometry: Proof of Concept. *Energy and Fuels*, *30*(12), 10187–10199. <https://doi.org/10.1021/acs.energyfuels.6b01912>
- Sankaran, R., Show, P. L., Nagarajan, D., & Chang, J. S. (2018). Exploitation and biorefinery of microalgae. In *Waste Biorefinery: Potential and Perspectives*. Elsevier B.V. <https://doi.org/10.1016/B978-0-444-63992-9.00019-7>
- Santhoshkumar, A., & Anand, R. (2019). Microwave-assisted fast pyrolysis of hazardous waste engine oil into green fuels. In *Advances in Eco-Fuels for a Sustainable Environment*. Elsevier Ltd. <https://doi.org/10.1016/b978-0-08-102728-8.00005-x>
- Savage, P. E., Klein, M. T., & Kukes, S. G. (1985). Asphaltene Reaction Pathways. 1. Thermolysis. *Industrial and Engineering Chemistry Process Design and Development*, *24*(4), 1169–1174. <https://doi.org/10.1021/i200031a046>
- Senthil Kumar, P., Bharathikumar, M., Prabhakaran, C., Vijayan, S., & Ramakrishnan, K. (2017). Conversion of waste plastics into low-emissive hydrocarbon fuels through catalytic depolymerization in a new laboratory scale batch reactor. *International Journal of Energy and Environmental Engineering*, *8*(2), 167–173. <https://doi.org/10.1007/s40095-015-0167-z>
- Serrano, D. P., Aguado, J., Escola, J. M., & Garagorri, E. (2003). Performance of a continuous screw kiln reactor for the thermal and catalytic conversion of polyethylene-lubricating oil base mixtures. *Applied Catalysis B: Environmental*, *44*(2), 95–105. [https://doi.org/10.1016/S0926-3373\(03\)00024-9](https://doi.org/10.1016/S0926-3373(03)00024-9)
- Serrano, D. P., Aguado, J., Escola, J. M., & Rodríguez, J. M. (2002). Nanocrystalline ZSM-5: A highly active catalyst for polyolefin feedstock recycling. *Studies in Surface Science and Catalysis*, *142 A*, 77–84. [https://doi.org/10.1016/s0167-2991\(02\)80014-3](https://doi.org/10.1016/s0167-2991(02)80014-3)
- Shang, J., Chai, M., & Zhu, Y. (2003). Photocatalytic degradation of polystyrene plastic under fluorescent light. *Environmental Science and Technology*, *37*(19), 4494–4499. <https://doi.org/10.1021/es0209464>

- Sharma, B., Shekhar, S., Sharma, S., & Jain, P. (2021). The paradigm in conversion of plastic waste into value added materials. *Cleaner Engineering and Technology*, 4, 100254. <https://doi.org/10.1016/j.clet.2021.100254>
- Shen, M., Zeng, G., Zhang, Y., Wen, X., Song, B., & Tang, W. (2019). Can biotechnology strategies effectively manage environmental (micro)plastics? In *Science of the Total Environment* (Vol. 697). Elsevier B.V. <https://doi.org/10.1016/j.scitotenv.2019.134200>
- Shirley, B., & Jarochowska, E. (2022). Chemical characterisation is rough: the impact of topography and measurement parameters on energy-dispersive X-ray spectroscopy in biominerals. *Facies*, 68(2), 1–15. <https://doi.org/10.1007/s10347-022-00645-4>
- Simanzhenkov, V., & Idem, R. (2003). Processing of Heavy Crude Oils and Crude Oil Residues. In *Crude Oil Chemistry*. <https://doi.org/10.1201/9780203014042.ch9>
- Singh, S., Chakraborty, J. P., & Mondal, M. K. (2020). Pyrolysis of torrefied biomass: Optimization of process parameters using response surface methodology, characterization, and comparison of properties of pyrolysis oil from raw biomass. *Journal of Cleaner Production*, 272, 122517. <https://doi.org/10.1016/j.jclepro.2020.122517>
- Soleymanzadeh, A., Yousefi, M., Kord, S., & Mohammadzadeh, O. (2019). A review on methods of determining onset of asphaltene precipitation. *Journal of Petroleum Exploration and Production Technology*, 9(2), 1375–1396. <https://doi.org/10.1007/s13202-018-0533-5>
- Soliman, E. (2019). Flow of Heavy Oils at Low Temperatures: Potential Challenges and Solutions. *Processing of Heavy Crude Oils - Challenges and Opportunities*, 1–28. <https://doi.org/10.5772/intechopen.82286>
- Soni, A. (2020). Plastics as A Potential Source of Energy: A Review. *SSRN Electronic Journal*. <https://doi.org/10.2139/ssrn.3707343>
- Sorheim, K. R., Daling, P. S., Cooper, D., Buist, I., Faksness, L., Altin, D., Pettersen, T., & Bakken, O. M. (2020). *Report Characterization of Low Sulfur Fuel Oils*.
- Stanlick, C., Berruti, F., & Briens, C. (2017). Effect of mixing and vapor residence time on thermal cracking of bitumen in a Mechanically Fluidized Reactor. *Fuel*, 200, 481–487. <https://doi.org/10.1016/j.fuel.2017.03.025>
- Sun, X., Li, X., Tan, X., Zheng, W., Zhu, G., Cai, J., & Zhang, Y. (2021). Pyrolysis of heavy oil in supercritical multi-thermal fluid: An effective recovery agent for heavy oils. *Journal of Petroleum Science and Engineering*, 196(April 2020), 107784. <https://doi.org/10.1016/j.petrol.2020.107784>
- Syamsiro, M., Saptoadi, H., Norsujianto, T., & Noviasri, P. (2014). Fuel Oil Production from Municipal Plastic Wastes in Sequential Pyrolysis and Catalytic Reforming Reactors. *Energy Procedia*, 47, 180–188. <https://doi.org/10.1016/j.egypro.2014.01.212>

- Takouleu, J. M. (2018, June 11). *KENYA: Alternative Energy Systems manufactures diesel from plastic wasteitle.*
- Tampieri, A., Szabó, M., Medina, F., & Gulyás, H. (2021). A brief introduction to the basics of NMR spectroscopy and selected examples of its applications to materials characterization. *Physical Sciences Reviews*, 6(1), 1–41. <https://doi.org/10.1515/psr-2019-0086>
- Tan, Y. L., Abdullah, A. Z., & Hameed, B. H. (2018). Catalytic fast pyrolysis of durian rind using silica-alumina catalyst: Effects of pyrolysis parameters. *Bioresource Technology*, 264(May), 198–205. <https://doi.org/10.1016/j.biortech.2018.05.058>
- Te, W. Z., Nair, K., Muhanin, M., Chu, Y., & Selvarajoo, A. (2021). *Optimization of Pyrolysis Parameters for Production of Biochar From Banana Peels: Evaluation of Biochar Application on the Growth of Ipomoea aquatica.* 8(February), 1–16. <https://doi.org/10.3389/fenrg.2020.637846>
- Thomas, A., Moinuddin, K., Tretsiakova-McNally, S., & Joseph, P. (2020). A kinetic analysis of the thermal degradation behaviours of some bio-based substrates. *Polymers*, 12(8). <https://doi.org/10.3390/POLYM12081830>
- Tofa, T. S., Kunjali, K. L., Paul, S., & Dutta, J. (2019). Visible light photocatalytic degradation of microplastic residues with zinc oxide nanorods. *Environmental Chemistry Letters*, 17(3), 1341–1346. <https://doi.org/10.1007/s10311-019-00859-z>
- Tsizin, S., Fialkov, A. B., & Amirav, A. (2020). Electron Ionization Mass Spectrometry for Both Liquid and Gas Chromatography in One System without the Need for Hardware Adjustments. *Journal of the American Society for Mass Spectrometry*, 31(8), 1713–1721. <https://doi.org/10.1021/jasms.0c00136>
- Tun, U., & Onn, H. (2020). *Muhammad Ukasyah Irfan Bin Mat Rahimi.* May, 1–4.
- Uemichi, Y., Makino, Y., & Kanazuka, T. (1989). Degradation of polypropylene to aromatic hydrocarbons over Pt- and Fe-containing activated carbon catalysts. *Journal of Analytical and Applied Pyrolysis*, 16(3), 229–238. [https://doi.org/10.1016/0165-2370\(89\)80027-0](https://doi.org/10.1016/0165-2370(89)80027-0)
- Vakhin, A. V., Aliev, F. A., Mukhamatdinov, I. I., Sitnov, S. A., Sharifullin, A. V., Kudryashov, S. I., Afanasiev, I. S., Petrashov, O. V., & Nurgaliev, D. K. (2020). Catalytic aquathermolysis of boca de jaruco heavy oil with nickel-based oil-soluble catalyst. *Processes*, 8(5). <https://doi.org/10.3390/PR8050532>
- Varma, A. K., & Mondal, P. (2017). Pyrolysis of sugarcane bagasse in semi batch reactor: Effects of process parameters on product yields and characterization of products. *Industrial Crops and Products*, 95, 704–717. <https://doi.org/10.1016/j.indcrop.2016.11.039>
- Wang, D., Li, D., & Liu, Y. (2013). High Quality Bio-Oil Production via Catalytic Pyrolysis of Pine Sawdust. *BioResources*, 8(2), 4142–4154. <https://doi.org/10.15376/biores.8.3.4142-4154>



- Wang, S., Jiang, X., Han, X., & Tong, J. (2014). Effect of retorting temperature on product yield and characteristics of non-condensable gases and shale oil obtained by retorting Huadian oil shales. *Fuel Processing Technology*, *121*, 9–15. <https://doi.org/10.1016/j.fuproc.2014.01.005>
- Wang, S., Kim, H., Lee, D., Lee, Y. R., Won, Y., Hwang, B. W., Nam, H., Ryu, H. J., & Lee, K. H. (2021). Drop-in fuel production with plastic waste pyrolysis oil over catalytic separation. *Fuel*, *305*(August), 121440. <https://doi.org/10.1016/j.fuel.2021.121440>
- Wang, X. C., Fang, J. H., Chen, B. S., Wang, J., Wu, J., & Xia, D. (2015). Thermal decomposition characteristics and kinetics of methyl linoleate under nitrogen and oxygen atmospheres. *Petroleum Science*, *12*(3), 518–524. <https://doi.org/10.1007/s12182-015-0034-9>
- Wang, Z., Fingas, M., & Li, K. (1994). Fractionation of a light crude oil and identification and quantitation of aliphatic, aromatic, and biomarker compounds by gc-fid and gc-ms, part I. *Journal of Chromatographic Science*, *32*(9), 361–366. <https://doi.org/10.1093/chromsci/32.9.361>
- WEF, W. E. F. (2016). *The New Plastics Economy Rethinking the future of plastics*. January.
- Wei, F., Cao, J. P., Zhao, X. Y., Ren, J., Wang, J. X., Fan, X., & Wei, X. Y. (2017). Nitrogen Evolution during Fast Pyrolysis of Sewage Sludge under Inert and Reductive Atmospheres. *Energy and Fuels*, *31*(7), 7191–7196. <https://doi.org/10.1021/acs.energyfuels.7b00920>
- Yamada, H., Kiatkittipong, W., & Tagawa, T. (2022). Catalyst screening for heavy oil production from waste plastic. *Environmental Challenges*, *6*(January), 100444. <https://doi.org/10.1016/j.envc.2022.100444>
- Yang, R.-X., Jan, K., Chen, C.-T., Chen, W.-T., & Wu, K. C. W. (2022). Thermochemical Conversion of Plastic Waste into Fuels, Chemicals, and Value-Added Materials: A Critical Review and Outlooks. *ChemSusChem*, *15*(11), 1–39. <https://doi.org/doi.org/10.1002/cssc.202200171>
- Yang, Z., Lü, F., Zhang, H., Wang, W., Shao, L., Ye, J., & He, P. (2021). Is incineration the terminator of plastics and microplastics? *Journal of Hazardous Materials*, *401*. <https://doi.org/10.1016/j.jhazmat.2020.123429>
- Yogalakshmi, K. N., & Singh, S. (2020). Plastic Waste: Environmental Hazards, Its Biodegradation, and Challenges. In *Bioremediation of Industrial Waste for Environmental Safety* (pp. 99–133). Springer Singapore. [https://doi.org/10.1007/978-981-13-1891-7\\_6](https://doi.org/10.1007/978-981-13-1891-7_6)
- You, Y., Liu, C., Xu, Q., Hu, X., Zhang, S., Wang, C., Guo, H., & Tang, C. (2022). Response surface methodology to optimize ultrasonic-assisted extraction of crude oil from oily sludge. *Petroleum Science and Technology*. <https://doi.org/10.1080/10916466.2022.2036758>

- Yuan, J., Ma, J., Sun, Y., Zhou, T., Zhao, Y., & Yu, F. (2020). Microbial degradation and other environmental aspects of microplastics/plastics. *Science of the Total Environment*, 715. <https://doi.org/10.1016/j.scitotenv.2020.136968>
- Zevenhoven, M., Savolahti, J., Saeed, L., Backman, R., Zevenhoven, R., & Hupa, M. (2006). Trace elements from fluidised bed pyrolysis of coal-sewage sludge mixture. *The International Conference on Fluidized Bed Combustion (FBC19)*, 21–24.
- Zhang, X., Wang, J., Wang, L., Li, Z., Wang, R., Li, H., Luo, M., Liu, H., Hu, W., & Feng, Q. (2022). Effects of kaolinite and its thermal transformation on oxidation of heavy oil. *Applied Clay Science*, 223(106507). <https://doi.org/https://doi.org/10.1016/j.clay.2022.106507>
- Zhao, F., Liu, Y., Lu, N., Xu, T., Zhu, G., & Wang, K. (2021). A review on upgrading and viscosity reduction of heavy oil and bitumen by underground catalytic cracking. *Energy Reports*, 7, 4249–4272. <https://doi.org/10.1016/j.egy.2021.06.094>
- Zhi, W. J., Wang, L. F., & Hu, X. J. (2017). Recent advances in the effects of microwave radiation on brains. *Military Medical Research*, 4(1), 1–14. <https://doi.org/10.1186/s40779-017-0139-0>
- Zhou, X., Liu, D., Bu, H., Deng, L., Liu, H., Yuan, P., Du, P., & Song, H. (2018). XRD-based quantitative analysis of clay minerals using reference intensity ratios, mineral intensity factors, Rietveld, and full pattern summation methods: A critical review. *Solid Earth Sciences*, 3(1), 16–29. <https://doi.org/10.1016/j.sesci.2017.12.002>

## APPENDICES

### Appendix A: Kaolin Preparation and Sieving



**Plate A. 1: Sundrying of Kaolin Clay**



**Plate A. 2: Sieving of Kaolin**



**Plate A. 3: Kaolin sieved to 400  $\mu\text{m}$**

**Table A. 1: Moisture Content of Kaolin Clay**

Run	Weight of Crucible ( $W_1$ )	Weight of Crucible + Kaolin clay before drying ( $W_2$ )	Weight of Crucible + Kaolin clay after drying ( $W_3$ )	Weight of moisture (g)	Percent of Moisture in Kaolin Clay (%)
1	42.101	60.557	54.588	5.969	32.342
2	43.125	63.563	57.176	6.387	31.251
3	44.234	63.866	58.249	5.617	28.611

## Appendix B: Heavy Distillate sample and Pyrolysis of HD into Diesel Fuel



**Plate B. 1: Heavy Distillate Sample from AESL**

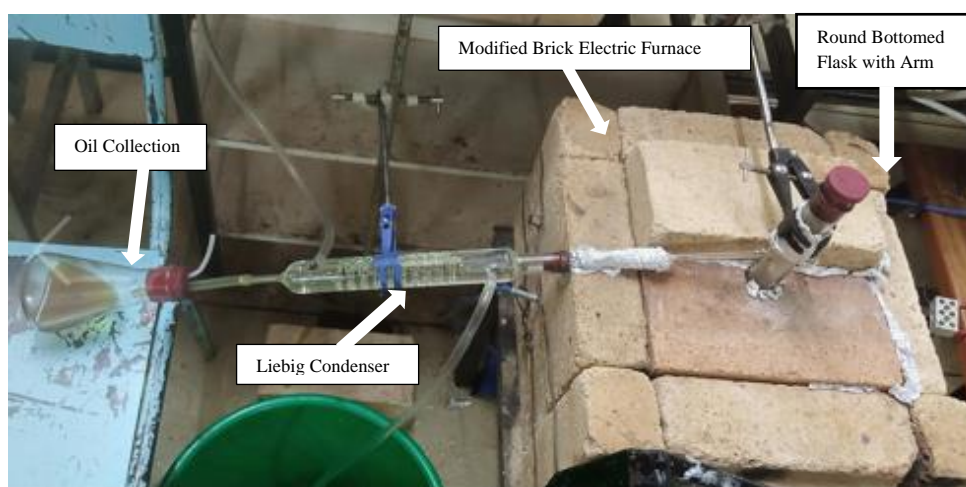


**Plate B. 2: Pyrolysis setup**



**Plate B. 3: Monitoring with Power Meter and Electronic Balance**



**Plate B. 4: Diesel oil from HD pyrolysis**

**Table B. 1: Density of Heavy Distillate**

S/N	Item	Sample 1	Sample 2	Sample 3	Average
1	Volume of Water (mL)	40	40	40	40
2	Volume of Water and Heavy distillate (mL)	43	43	43	43
3	Volume of heavy distillate (mL)	3	3	3	3
4	Mass of Cylinder (g)	66.184	66.186	66.184	66.185
5	Mass of Cylinder and Heavy distillate (g)	68.776	68.781	68.772	68.776
6	Mass of Heavy distillate (g)	2.592	2.595	2.588	2.592
7	Density of Heavy distillate (g/mL)	0.864	0.865	0.863	0.864

## Appendix C: GC-MS Analysis results of HD and PLOs

Table C. 1: GC-MS analysis results of organic compounds identified in HD

Peak Number	Retention Time (min)	Organic Compound	Molecular Formula	Molecular Weight	Area (%)
		<b>Paraffin (n- and iso-paraffins)</b>			
12	36.250	Octane,3,4,5,6- tetramethyl-	C <sub>12</sub> H <sub>26</sub>	170	0.04
13	38.393	Dodecane,2,6,11-trimethyl-	C <sub>15</sub> H <sub>32</sub>	212	0.33
14	39.136	Dodecane,2,6,11-trimethyl-	C <sub>15</sub> H <sub>32</sub>	212	0.52
16	40.436	Dodecane	C <sub>12</sub> H <sub>26</sub>	170	0.70
24	44.387	Eicosane, 10-methyl-	C <sub>21</sub> H <sub>44</sub>	296	1.03
26	48.141	Tetradecane	C <sub>14</sub> H <sub>30</sub>	198	1.13
35	51.707	Hexadecane	C <sub>16</sub> H <sub>34</sub>	226	1.16
37	53.669	Nonane, 5-butyl-	C <sub>13</sub> H <sub>28</sub>	184	0.34
39	55.095	Eicosane, 10-methyl-	C <sub>21</sub> H <sub>44</sub>	296	1.74
45	58.326	Pentadecane	C <sub>15</sub> H <sub>32</sub>	212	0.92
48	61.121	Eicosane, 10-methyl-	C <sub>21</sub> H <sub>44</sub>	296	2.65
56	63.488	Pentadecane	C <sub>15</sub> H <sub>32</sub>	212	1.23
60	65.569	Heptadecane	C <sub>17</sub> H <sub>36</sub>	240	2.83
65	67.451	Hexadecane	C <sub>16</sub> H <sub>34</sub>	226	0.11
68	68.882	2,6,10-Trimethyltridecane	C <sub>16</sub> H <sub>34</sub>	226	0.68
69	69.293	2-methyloctacosane	C <sub>29</sub> H <sub>60</sub>	408	4.02
73	71.481	Heptadecane	C <sub>17</sub> H <sub>36</sub>	240	1.36
75	74.170	2-methyloctacosane	C <sub>29</sub> H <sub>60</sub>	408	2.23
77	77.617	Tetratetraacontane	C <sub>44</sub> H <sub>90</sub>	618	1.24
				<b>Sum</b>	<b>24.26</b>
		<b>Naphthenes (Cyclo-alkanes or cycloparaffins)</b>			
46	58.402	Cyclooctane, 1-methyl-3-propyl-	C <sub>12</sub> H <sub>24</sub>	168	0.85
57	63.760	1-Cyclopentyleicosane	C <sub>25</sub> H <sub>50</sub>	350	2.67
66	67.850	Cyclohexane, 1,2,3,5-tetraisopropyl-	C <sub>18</sub> H <sub>36</sub>	252	1.12
67	68.270	1-Cyclopentyleicosane	C <sub>25</sub> H <sub>50</sub>	350	0.43
74	72.254	Cyclohexane, 1,2,3,5-tetraisopropyl-	C <sub>18</sub> H <sub>36</sub>	252	1.06
				<b>sum</b>	<b>6.13</b>
		<b>Olefins (Alkenes and iso-olefins)</b>			
1	8.963	2,4-Dimethylhept-1-ene	C <sub>9</sub> H <sub>18</sub>	126	1.30
7	32.068	1-undecene, 7-methyl-	C <sub>12</sub> H <sub>24</sub>	168	1.90
8	32.442	1-undecene, 7-methyl-	C <sub>12</sub> H <sub>24</sub>	168	3.03
11	35.960	1-Tridecene	C <sub>13</sub> H <sub>26</sub>	182	0.31
15	40.185	3-Octadecene, (E)-	C <sub>18</sub> H <sub>36</sub>	252	0.59
23	44.159	3-Octadecene, (E)-	C <sub>18</sub> H <sub>36</sub>	252	0.87
31	50.195	Nonacos-1-ene	C <sub>29</sub> H <sub>58</sub>	406	0.31
38	54.919	10-Heneicosene (c,t)	C <sub>21</sub> H <sub>42</sub>	294	1.07
44	58.185	10-Heneicosene (c,t)	C <sub>21</sub> H <sub>42</sub>	294	1.42
59	65.493	1-Tricosene	C <sub>23</sub> H <sub>46</sub>	322	0.97
				<b>sum</b>	<b>11.77</b>
		<b>Halogen-containing compounds</b>			
27	48.887	Tricosyl trifluoroacetate	C <sub>25</sub> H <sub>47</sub> F <sub>3</sub> O <sub>2</sub>	436	2.39
28	49.249	Octacosyl trifluoroacetate	C <sub>30</sub> H <sub>57</sub> F <sub>3</sub> O <sub>2</sub>	506	0.50
30	49.964	Tricosyl trifluoroacetate	C <sub>25</sub> H <sub>47</sub> F <sub>3</sub> O <sub>2</sub>	436	3.42
32	50.374	Tricosyl trifluoroacetate	C <sub>25</sub> H <sub>47</sub> F <sub>3</sub> O <sub>2</sub>	436	0.82

34	51.331	Heneicosyl heptafluorobutyrate	$C_{25}H_{43}F_7O_2$	508	0.45
36	52.716	Tricosyl trifluoroacetate	$C_{25}H_{47}F_3O_2$	436	0.77
40	56.069	Octacosyl trifluoroacetate	$C_{30}H_{57}F_3O_2$	506	2.66
41	56.351	Octacosyl trifluoroacetate	$C_{30}H_{57}F_3O_2$	506	0.96
42	56.965	Hexacosyl trifluoroacetate	$C_{28}H_{53}F_3O_2$	478	1.38
49	62.060	Triacontyl pentafluoropropionate	$C_{33}H_{61}F_5O_2$	584	2.80
50	62.249	Octacosyl trifluoroacetate	$C_{30}H_{57}F_3O_2$	506	0.60
51	62.650	Octacosyl trifluoroacetate	$C_{30}H_{57}F_3O_2$	506	2.67
52	62.921	Tetracosyl trifluoroacetate	$C_{26}H_{49}F_3O_2$	450	0.77
54	63.274	Tricosyl pentafluoropropionate	$C_{26}H_{47}F_5O_2$	486	0.50
61	66.469	Triacontyl pentafluoropropionate	$C_{33}H_{61}F_5O_2$	584	1.96
63	66.914	Tetratriacontyl heptafluorobutyrate	$C_{38}H_{69}F_7O_2$	690	1.38
70	70.440	Octatriacontyl trifluoroacetate	$C_{40}H_{77}F_3O_2$	646	2.57
71	70.954	Triacontyl pentafluoropropionate	$C_{33}H_{61}F_5O_2$	584	0.86
72	71.165	Tetrapentacontane, 1,54-dibromo-	$C_{54}H_{108}Br_2$	914	0.76
76	76.163	Octatriacontyl trifluoroacetate	$C_{40}H_{77}F_3O_2$	646	1.08
				<b>sum</b>	<b>29.30</b>
		<b>Esters</b>			
5	21.005	Acetic acid, trichloro, octyl ester	$C_{10}H_{17}Cl_3O_2$	274	0.74
9	33.595	Pentadecafluorooctanoic acid, tetradecyl ester	$C_{22}H_{29}F_{15}O_2$	610	1.32
20	42.378	Trichloroacetic acid, hexadecyl ester	$C_{18}H_{33}Cl_3O_2$	386	0.92
21	42.525	Pentadecafluorooctanoic acid, tetradecyl ester	$C_{22}H_{29}F_{15}O_2$	610	0.69
43	57.404	Pentadecafluorooctanoic acid, tetradecyl ester	$C_{22}H_{29}F_{15}O_2$	610	0.98
55	63.396	Trifluoroacetic acid, pentadecyl ester	$C_{17}H_{31}F_3O_2$	324	0.35
58	65.005	Carbonic acid, decyl nonyl ester	$C_{20}H_{40}O_3$	328	0.13
64	67.226	Pentadecafluorooctanoic acid, octadecyl ester	$C_{26}H_{37}F_{15}O_2$	666	0.85
				<b>sum</b>	<b>5.63</b>
		<b>Alkanethiols</b>			
29	49.550	Tert-Hexadecanethiol	$C_{16}H_{34}S$	258	0.34
				<b>sum</b>	<b>0.34</b>
		<b>Aldehydes, Ketones, Alcohol</b>			
2	9.536	2-Pentanone,4-hydroxy-4-methyl	$C_6H_{12}O_2$	116	8.34
3	11.330	2-Pentanone,3-[(acetyloxy)methyl]-3,4-dimethyl-, (+-)-	$C_{10}H_{18}O_3$	186	0.52
4	20.779	11-Methyldodecanol	$C_{13}H_{28}O$	200	0.90
6	31.670	11-Methyldodecanol	$C_{13}H_{28}O$	200	2.83
10	34.586	1-Octanol, 2-butyl	$C_{12}H_{26}O$	186	1.06
17	40.869	1-Dodecanol, 2-hexyl-	$C_{18}H_{38}O$	270	1.59
18	41.285	11-Methyldodecanol	$C_{13}H_{28}O$	200	0.94
19	41.980	2-Hexyl-1-octanol	$C_{14}H_{30}O$	214	1.20
22	43.674	11-Dodecen-1-ol, 2,4,6-trimethyl-, (R,R,R)-	$C_{15}H_{30}O$	226	0.43
25	47.929	E-14-Hexadecanal	$C_{16}H_{30}O$	238	0.98
33	51.087	1-Dodecanol, 2-hexyl-	$C_{18}H_{38}O$	270	0.82
47	61.005	1-Heneicosanol	$C_{21}H_{44}O$	312	1.21

53	63.020	1-Dodecanol, 2-octyl-	C <sub>20</sub> H <sub>42</sub> O	298	0.63
62	66.612	Octadecyl octyl ether	C <sub>26</sub> H <sub>54</sub> O	382	0.77
				<b>sum</b>	<b>22.22</b>

**Table C. 2: GC-MS Analysis of PLO obtained from thermal pyrolysis**

Peak Number	Retention Time (min)	Organic Compound	Molecular Formula	Molecular Weight	Area (%)
		<b>Paraffin (n- and iso-paraffins)</b>			
1	2.340	Pentane, 2-methyl-	C <sub>6</sub> H <sub>14</sub>	86	0.31
3	2.596	n-Hexane	C <sub>6</sub> H <sub>14</sub>	86	3.78
5	6.029	Hexane, 2,3-dimethyl-	C <sub>8</sub> H <sub>18</sub>	114	0.97
7	8.075	Hexane, 2,3,4-trimethyl-	C <sub>9</sub> H <sub>20</sub>	128	0.40
15	17.186	Decane, 4-methyl-	C <sub>11</sub> H <sub>22</sub>	156	1.14
16	17.411	Decane, 4-methyl-	C <sub>11</sub> H <sub>24</sub>	156	0.87
19	19.609	Decane, 3,7-dimethyl-	C <sub>12</sub> H <sub>26</sub>	170	0.23
24	22.085	Undecane	C <sub>11</sub> H <sub>24</sub>	156	0.44
29	27.083	Dodecane	C <sub>12</sub> H <sub>26</sub>	170	0.63
30	28.432	Dodecane,2,6,11-trimethyl-	C <sub>15</sub> H <sub>32</sub>	212	0.60
31	28.842	Dodecane,4,6-dimethyl-	C <sub>14</sub> H <sub>30</sub>	198	0.58
32	29.160	Tetradecane,4-methyl-	C <sub>15</sub> H <sub>32</sub>	212	0.69
43	36.236	Tetradecane	C <sub>14</sub> H <sub>30</sub>	198	1.03
44	37.957	Dodecane, 4,6-dimethyl-	C <sub>14</sub> H <sub>30</sub>	198	0.52
45	38.381	2,6,10-Trimethyltridecane	C <sub>16</sub> H <sub>34</sub>	226	0.82
46	39.134	Tetradecane, 4-methyl-	C <sub>15</sub> H <sub>32</sub>	212	0.73
47	39.485	10-Methylnonadecane	C <sub>20</sub> H <sub>42</sub>	282	0.54
49	40.417	Pentadecane	C <sub>15</sub> H <sub>32</sub>	212	0.62
58	44.383	Hexadecane	C <sub>16</sub> H <sub>34</sub>	226	1.34
59	46.251	Eicosane	C <sub>20</sub> H <sub>42</sub>	282	0.38
61	48.133	Heptadecane	C <sub>17</sub> H <sub>36</sub>	240	1.45
69	51.696	Tetradecane	C <sub>14</sub> H <sub>30</sub>	198	0.98
72	55.088	Eicosane, 10-methyl-	C <sub>21</sub> H <sub>44</sub>	296	1.11
77	58.315	Heptadecane	C <sub>17</sub> H <sub>36</sub>	240	0.77
78	61.114	Heptadecane	C <sub>17</sub> H <sub>36</sub>	240	0.87
81	63.473	Eicosane, 10-methyl-	C <sub>21</sub> H <sub>44</sub>	296	0.76
83	65.556	Eicosane	C <sub>20</sub> H <sub>42</sub>	282	0.64
85	67.438	Heptadecane	C <sub>17</sub> H <sub>36</sub>	240	0.68
86	69.284	Heneicosane	C <sub>21</sub> H <sub>44</sub>	296	0.65
88	71.468	2-methtyloctacosane	C <sub>29</sub> H <sub>60</sub>	408	0.34
89	74.161	Heptadecane, 2,6,10, 15-tetramethyl-	C <sub>21</sub> H <sub>44</sub>	296	0.28
				<b>sum</b>	<b>25.15</b>
		<b>Naphthenes (Cycloalkanes or cycloparaffins)</b>			
6	7.731	Cyclopentane, 1,1,3,4-tetramethyl, cis-	C <sub>9</sub> H <sub>24</sub>	126	0.25
8	8.683	Cyclohexane, 1,3,5-trimethyl-	C <sub>9</sub> H <sub>18</sub>	126	0.55



11	9.772	Cyclohexane,1,3,5-trimethyl-,(1.alpha,3.alpha,5.beta.)	C <sub>9</sub> H <sub>18</sub>	126	0.65
12	10.447	1,2,4,4-Tetramethylcyclopentene	C <sub>9</sub> H <sub>16</sub>	124	0.20
82	63.745	Cyclohexane,1,2,3,5-tetraisopropyl-	C <sub>18</sub> H <sub>36</sub>	252	0.79
				<b>sum</b>	<b>2.44</b>
		<b>Olefins (Alkenes and iso-olefins)</b>			
2	2.521	1-Pentene, 2-methyl-	C <sub>6</sub> H <sub>12</sub>	84	1.08
4	3.181	1-Pentene, 2-methyl-	C <sub>6</sub> H <sub>12</sub>	84	0.41
9	8.963	2,4-Dimethyl-1-heptene	C <sub>9</sub> H <sub>18</sub>	126	6.90
13	10.880	1,2,4,4-Tetramethylpentene	C <sub>9</sub> H <sub>16</sub>	124	0.20
18	18.507	1-Undecene, 8-methyl-	C <sub>12</sub> H <sub>24</sub>	168	0.11
20	19.892	1-Undecene, 4-methyl-	C <sub>12</sub> H <sub>24</sub>	168	0.46
22	20.993	2-Undecene,4,5-dimethyl-,[R*,S*-(Z)]-	C <sub>13</sub> H <sub>26</sub>	182	2.31
23	21.707	1-Dodecene	C <sub>12</sub> H <sub>24</sub>	168	0.47
25	23.149	1-Undecene,7-methyl-	C <sub>12</sub> H <sub>24</sub>	168	1.14
26	23.475	1-Decene,2,4-dimethyl-	C <sub>12</sub> H <sub>24</sub>	168	0.92
28	26.729	1-Dodecene	C <sub>12</sub> H <sub>24</sub>	168	0.62
33	31.471	1-Tridecene	C <sub>13</sub> H <sub>26</sub>	182	0.91
36	32.436	1-Undecene,7-methyl-	C <sub>12</sub> H <sub>24</sub>	168	5.70
42	35.940	1-Tridecene	C <sub>13</sub> H <sub>26</sub>	182	1.13
48	40.162	1-Tridecene	C <sub>13</sub> H <sub>26</sub>	182	0.61
57	44.141	9-Nonadecene	C <sub>19</sub> H <sub>38</sub>	266	1.10
60	47.915	3-Eicosene, (E)-	C <sub>20</sub> H <sub>40</sub>	280	0.50
71	54.910	10-Heneicosene (c,t)	C <sub>21</sub> H <sub>42</sub>	294	0.66
				<b>sum</b>	<b>25.23</b>
		<b>Halogen containing compounds</b>			
62	48.879	Tricosyl trifluoroacetate	C <sub>25</sub> H <sub>47</sub> F <sub>3</sub> O <sub>2</sub>	436	3.63
63	49.235	Tricosyl pentafluoropropionate	C <sub>26</sub> H <sub>47</sub> F <sub>5</sub> O <sub>2</sub>	486	0.97
67	51.070	Heneicosyl heptafluorobutyrate	C <sub>25</sub> H <sub>43</sub> F <sub>7</sub> O <sub>2</sub>	508	1.03
70	52.702	Tricosyl trifluoroacetate	C <sub>25</sub> H <sub>47</sub> F <sub>3</sub> O <sub>2</sub>	436	0.52
73	56.049	Hexacosyl trifluoroacetate	C <sub>28</sub> H <sub>53</sub> F <sub>3</sub> O <sub>2</sub>	478	1.30
74	56.946	Tetracosyl trifluoroacetate	C <sub>26</sub> H <sub>49</sub> F <sub>3</sub> O <sub>2</sub>	450	0.62
79	62.046	Octacosyl heptafluorobutyrate	C <sub>32</sub> H <sub>57</sub> F <sub>7</sub> O <sub>2</sub>	606	0.86
80	62.636	Tetracosyl heptafluorobutyrate	C <sub>28</sub> H <sub>49</sub> F <sub>7</sub> O <sub>2</sub>	550	0.54
84	66.452	Tetratriacontyl heptafluorobutyrate	C <sub>38</sub> H <sub>69</sub> F <sub>7</sub> O <sub>2</sub>	690	0.56
87	70.421	Tetratriacontyl heptafluorobutyrate	C <sub>38</sub> H <sub>69</sub> F <sub>7</sub> O <sub>2</sub>	690	0.24
				<b>Sum</b>	<b>10.27</b>
		<b>Esters</b>			
38	33.955	Pentadecafluorooctanoic acid, dodecyl ester	C <sub>20</sub> H <sub>25</sub> F <sub>15</sub> O <sub>2</sub>	582	0.33

51	41.262	Pentadecafluorooctanoic acid, tetradecyl ester	C <sub>22</sub> H <sub>29</sub> F <sub>15</sub> O <sub>2</sub>	610	1.37
52	41.573	Pentadecafluorooctanoic acid, tetradecyl ester	C <sub>22</sub> H <sub>29</sub> F <sub>15</sub> O <sub>2</sub>	610	0.77
53	41.966	Pentadecafluorooctanoic acid, tetradecyl ester	C <sub>22</sub> H <sub>29</sub> F <sub>15</sub> O <sub>2</sub>	610	1.71
54	42.359	Pentadecafluorooctanoic acid, tetradecyl ester	C <sub>22</sub> H <sub>29</sub> F <sub>15</sub> O <sub>2</sub>	610	0.76
				<b>sum</b>	<b>4.94</b>
		<b>Aldehydes, Ketones, Alcohol</b>			
10	9.512	2-Pentanone,4-hydroxy-4-methyl-	C <sub>6</sub> H <sub>12</sub> O <sub>2</sub>	116	1.56
14	11.327	2-Pentanone,3-[(acetyloxy)methyl]-3,4-dimethyl-, (+)-	C <sub>10</sub> H <sub>18</sub> O <sub>3</sub>	186	2.19
17	17.891	1-Pentanol, 2-ethyl-	C <sub>7</sub> H <sub>16</sub> O	116	0.20
21	20.769	1-Dodecanol, 3,7,11-trimethyl-	C <sub>15</sub> H <sub>32</sub> O	228	2.71
27	24.387	(2,4,6-Trimethylcyclohexyl) methanol	C <sub>10</sub> H <sub>20</sub> O	156	0.29
34	31.661	11-Methyldodecanol	C <sub>13</sub> H <sub>28</sub> O	200	6.92
35	32.060	11-Methyldodecanol	C <sub>13</sub> H <sub>28</sub> O	200	4.25
37	33.590	2-Hexyl-1-octanol	C <sub>14</sub> H <sub>30</sub> O	214	2.65
39	34.191	1-Heptanol, 2,4-diethyl-	C <sub>11</sub> H <sub>24</sub> O	172	0.27
40	34.585	2-Hexyl-1-octanol	C <sub>14</sub> H <sub>30</sub> O	214	2.43
41	34.807	Cyclododecanemethanol	C <sub>13</sub> H <sub>26</sub> O	198	0.64
50	40.857	1-Dodecanol, 2-hexyl-	C <sub>18</sub> H <sub>38</sub> O	270	1.94
55	42.513	1-Dodecanol, 2-hexyl-	C <sub>18</sub> H <sub>38</sub> O	270	0.49
56	43.667	(2,4,6-Trimethylcyclohexyl) methanol	C <sub>10</sub> H <sub>20</sub> O	156	0.42
64	49.544	1-Dodecanol, 2-hexyl-	C <sub>18</sub> H <sub>38</sub> O	270	0.40
65	49.935	1-Dodecanol, 2-hexyl-	C <sub>18</sub> H <sub>38</sub> O	270	2.75
66	50.347	1-Dodecanol, 2-hexyl-	C <sub>18</sub> H <sub>38</sub> O	270	0.71
68	51.499	E-14-Hexadecanal	C <sub>16</sub> H <sub>30</sub> O	238	0.17
75	57.375	1-Dodecanol, 2-octyl-	C <sub>20</sub> H <sub>42</sub> O	298	0.42
76	58.165	1-Heneicosanol	C <sub>21</sub> H <sub>44</sub> O	312	0.60
				<b>sum</b>	<b>32.01</b>

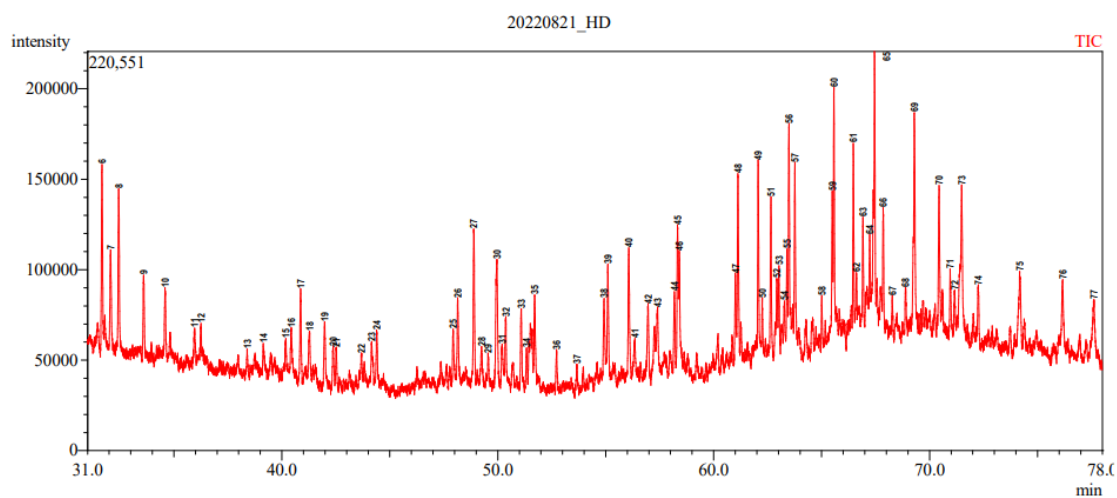
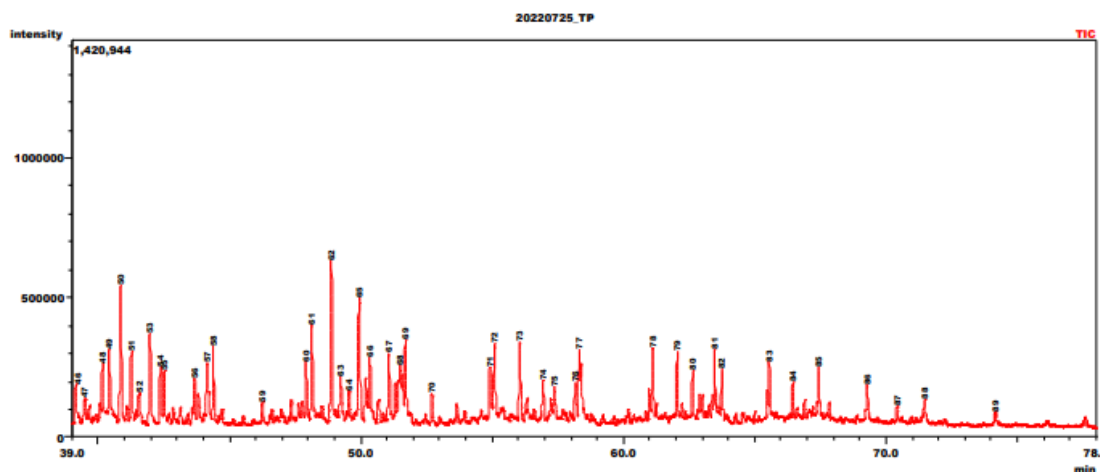
**Table C. 3: GC-MS Analysis of PLO obtained from catalytic pyrolysis**

Peak Number	Retention Time (min)	Organic Compound	Molecular Formula	Molecular Weight	Area (%)
		<b>Paraffin (n- and iso-paraffins)</b>			
1	2.342	Pentane, 2-methyl-	C <sub>6</sub> H <sub>14</sub>	86	0.63
3	2.597	n-Hexane	C <sub>6</sub> H <sub>14</sub>	86	1.92
8	6.029	Hexane, 2,3-dimethyl-	C <sub>8</sub> H <sub>18</sub>	114	1.61
10	8.076	Heptane, 2,4-dimethyl-	C <sub>9</sub> H <sub>20</sub>	128	0.51
11	8.558	2-Hexane, 4,4,5-trimethyl-	C <sub>9</sub> H <sub>18</sub>	126	0.29
18	11.798	Nonane	C <sub>9</sub> H <sub>20</sub>	128	0.42

20	16.917	Decane	C <sub>10</sub> H <sub>22</sub>	142	0.27
21	17.191	Decane, 4-methyl-	C <sub>11</sub> H <sub>24</sub>	156	1.18
22	17.415	Decane, 4-methyl-	C <sub>11</sub> H <sub>24</sub>	156	1.20
23	19.611	Decane, 3,7-dimethyl-	C <sub>12</sub> H <sub>26</sub>	170	0.26
28	22.096	Undecane	C <sub>11</sub> H <sub>24</sub>	156	0.40
33	27.083	Dodecane	C <sub>12</sub> H <sub>26</sub>	170	0.53
34	28.438	Dodecane,4,6-dimethyl-	C <sub>14</sub> H <sub>30</sub>	198	0.55
35	28.846	Dodecane,4,6-dimethyl-	C <sub>14</sub> H <sub>30</sub>	198	0.63
36	29.163	Dodecane,2,6,11-trimethyl-	C <sub>15</sub> H <sub>32</sub>	212	0.66
45	36.237	Tetradecane	C <sub>14</sub> H <sub>30</sub>	198	0.84
46	37.957	Dodecane,4,6-dimethyl-	C <sub>14</sub> H <sub>30</sub>	198	0.36
47	38.381	2,6,10-Trimethyltridecane	C <sub>16</sub> H <sub>34</sub>	226	0.63
48	39.140	Tetradecane, 4-methyl-	C <sub>15</sub> H <sub>32</sub>	212	0.75
51	40.422	Pentadecane	C <sub>15</sub> H <sub>32</sub>	212	1.11
60	44.387	Hexadecane	C <sub>16</sub> H <sub>34</sub>	226	1.21
61	46.258	Eicosane	C <sub>20</sub> H <sub>42</sub>	282	0.36
64	48.136	Eicosane, 10-methyl-	C <sub>21</sub> H <sub>44</sub>	296	2.21
71	51.697	Pentadecane	C <sub>15</sub> H <sub>32</sub>	212	1.46
74	55.081	Eicosane, 10-methyl-	C <sub>21</sub> H <sub>44</sub>	296	1.29
78	58.313	Hexadecane	C <sub>16</sub> H <sub>34</sub>	226	0.89
80	61.112	Heptadecane	C <sub>17</sub> H <sub>36</sub>	240	1.23
83	63.470	Heptadecane	C <sub>17</sub> H <sub>36</sub>	240	0.86
85	65.554	Heptadecane	C <sub>17</sub> H <sub>36</sub>	240	0.65
87	67.436	2-methyloctacosane	C <sub>29</sub> H <sub>60</sub>	408	0.58
88	69.282	Heneicosane	C <sub>21</sub> H <sub>44</sub>	296	0.41
90	71.470	Tetratetraacontane	C <sub>44</sub> H <sub>90</sub>	618	0.26
				<b>sum</b>	<b>26.16</b>
		<b>Naphthenes (cycloalkanes or cycloparaffins)</b>			
9	7.733	Cyclopentane, 1,1,3,4-tetramethyl-, cis-	C <sub>9</sub> H <sub>18</sub>	126	0.31
12	8.684	Cyclohexane, 1,3,5-trimethyl-	C <sub>9</sub> H <sub>18</sub>	126	0.71
15	9.774	Cyclohexane,1,3,5-trimethyl-,(1.alpha,3.alpha,5.beta.)	C <sub>9</sub> H <sub>18</sub>	126	0.97
16	10.478	1,2,4,4-Tetramethylcyclopentene	C <sub>9</sub> H <sub>16</sub>	124	0.31
19	16.530	Cyclopropane, 1-heptyl-2-methyl-	C <sub>11</sub> H <sub>22</sub>	154	0.24
79	58.389	Cyclooctane, 1-methyl-3-propyl-	C <sub>12</sub> H <sub>24</sub>	168	0.48
84	63.744	1-Cyclopentyleicosane	C <sub>25</sub> H <sub>50</sub>	350	0.55
				<b>sum</b>	<b>3.57</b>
		<b>Olefins (alkenes and iso-olefins)</b>			
2	2.522	1-Pentene, 2-methyl-	C <sub>6</sub> H <sub>12</sub>	84	1.10
4	2.687	2-Pentene, 4-methyl-	C <sub>6</sub> H <sub>12</sub>	84	0.27
5	3.097	4-Methyl-1,3-Pentadiene	C <sub>6</sub> H <sub>10</sub>	82	0.20
6	3.183	1-Pentene, 2,4-dimethyl-	C <sub>7</sub> H <sub>14</sub>	98	0.41
7	4.277	1,3-Pentadiene, 2,4-dimethyl-	C <sub>7</sub> H <sub>12</sub>	96	0.19

13	8.966	2,4-Dimethyl-1-heptene	C <sub>9</sub> H <sub>18</sub>	126	8.09
26	21.000	2-Undecene,4,5-dimethyl- ,[R*,S*-(Z)]-	C <sub>13</sub> H <sub>26</sub>	182	2.42
27	21.714	1-Undecene	C <sub>11</sub> H <sub>22</sub>	154	0.46
29	23.153	1-Decene,2,4-dimethyl-	C <sub>12</sub> H <sub>24</sub>	168	0.88
30	23.483	1-Decene,2,4-dimethyl-	C <sub>12</sub> H <sub>24</sub>	168	0.74
32	26.732	1-Dodecene	C <sub>12</sub> H <sub>24</sub>	168	0.63
37	31.477	1-Tridecene	C <sub>13</sub> H <sub>26</sub>	182	0.62
39	32.065	1-Undecene,7-methyl-	C <sub>12</sub> H <sub>24</sub>	168	3.61
40	32.440	1-Undecene,7-methyl-	C <sub>12</sub> H <sub>24</sub>	168	4.68
44	35.944	3-Hexadecene, (Z)-	C <sub>16</sub> H <sub>32</sub>	224	0.89
50	40.161	1-Tridecene	C <sub>13</sub> H <sub>26</sub>	182	0.73
59	44.142	3-Octadecene, (E)-	C <sub>18</sub> H <sub>36</sub>	252	1.20
63	47.919	3-Eicosene, (E)-	C <sub>20</sub> H <sub>40</sub>	280	0.96
73	54.902	1-Tricosene	C <sub>23</sub> H <sub>46</sub>	322	1.22
				<b>sum</b>	<b>29.3</b>
		<b>Halogenated containing compounds</b>			
53	41.266	Octadecyl trifluoroacetate	C <sub>20</sub> H <sub>37</sub> F <sub>3</sub> O <sub>2</sub>	366	1.46
56	42.365	Octadecyl trifluoroacetate	C <sub>20</sub> H <sub>37</sub> F <sub>3</sub> O <sub>2</sub>	366	1.21
65	48.881	Heneicosyl heptafluorobutyrate	C <sub>25</sub> H <sub>43</sub> F <sub>7</sub> O <sub>2</sub>	508	2.84
69	50.350	Tricosyl trifluoroacetate	C <sub>25</sub> H <sub>47</sub> F <sub>3</sub> O <sub>2</sub>	436	0.72
72	52.707	Hexacosyl trifluoroacetate	C <sub>28</sub> H <sub>53</sub> F <sub>3</sub> O <sub>2</sub>	478	0.45
75	56.054	Octacosyl trifluoroacetate	C <sub>30</sub> H <sub>57</sub> F <sub>3</sub> O <sub>2</sub>	506	1.40
76	56.945	Tricosyl pentafluoropropionate	C <sub>26</sub> H <sub>47</sub> F <sub>5</sub> O <sub>2</sub>	486	0.76
81	62.047	Triacontyl heptafluorobutyrate	C <sub>34</sub> H <sub>61</sub> F <sub>7</sub> O <sub>2</sub>	634	0.87
82	62.632	Octacosyl trifluoroacetate	C <sub>30</sub> H <sub>57</sub> F <sub>3</sub> O <sub>2</sub>	506	0.65
86	66.451	Tetratriacontyl heptafluorobutyrate	C <sub>38</sub> H <sub>69</sub> F <sub>7</sub> O <sub>2</sub>	690	0.38
89	70.428	Tetratriacontyl heptafluorobutyrate	C <sub>38</sub> H <sub>69</sub> F <sub>7</sub> O <sub>2</sub>	690	0.17
				<b>sum</b>	<b>10.91</b>
		<b>Esters and Ethers</b>			
24	19.900	Sulfurous acid, hexyl pentadecyl ester	C <sub>21</sub> H <sub>44</sub> O <sub>3</sub> S	376	0.52
49	39.484	Nonyl tetradecyl ether	C <sub>23</sub> H <sub>48</sub> O	340	0.65
54	41.580	Pentadecafluorooctanoic acid, tetradecyl ester	C <sub>22</sub> H <sub>29</sub> F <sub>15</sub> O <sub>2</sub>	610	0.69
62	47.612	Docosyl octyl ether	C <sub>30</sub> H <sub>62</sub> O	438	0.51
				<b>sum</b>	<b>2.37</b>
		<b>Aldehydes, Ketones, Alcohol</b>			
14	9.511	2-Pentanone,4-hydroxy-4- methyl-	C <sub>6</sub> H <sub>12</sub> O <sub>2</sub>	116	0.96
17	11.329	2-Pentanone,3- [(acetyloxy)methyl]-3,4- dimethyl-, (+)-	C <sub>10</sub> H <sub>18</sub> O <sub>3</sub>	186	2.29
25	20.773	1-Dodecanol, 3,7,11- trimethyl-	C <sub>15</sub> H <sub>32</sub> O	228	2.60

31	24.391	(2,4,6-Trimethylcyclohexyl) methanol	C <sub>10</sub> H <sub>20</sub> O	156	0.45
38	31.667	11-Methyldodecanol	C <sub>13</sub> H <sub>28</sub> O	200	5.60
41	33.592	2-Hexyl-1-octanol	C <sub>14</sub> H <sub>30</sub> O	214	2.13
42	34.589	2-Hexyl-1-octanol	C <sub>14</sub> H <sub>30</sub> O	214	1.77
43	34.807	Cyclododecanemethanol	C <sub>13</sub> H <sub>26</sub> O	198	0.57
52	40.857	1-Dodecanol, 2-hexyl-	C <sub>18</sub> H <sub>38</sub> O	270	2.27
55	41.966	1-Dodecanol, 2-hexyl-	C <sub>18</sub> H <sub>38</sub> O	270	1.75
57	42.509	1-Dodecanol, 2-hexyl-	C <sub>18</sub> H <sub>38</sub> O	270	0.70
58	43.667	(2,4,6-Trimethylcyclohexyl) methanol	C <sub>10</sub> H <sub>20</sub> O	156	0.58
66	49.239	1-Dodecanol, 2-hexyl-	C <sub>18</sub> H <sub>38</sub> O	270	0.70
67	49.942	1-Dodecanol, 2-hexyl-	C <sub>18</sub> H <sub>38</sub> O	270	2.82
68	50.192	1-Decanol, 2-octyl-	C <sub>18</sub> H <sub>38</sub> O		0.85
70	51.066	1-Dodecanol, 2-hexyl-	C <sub>18</sub> H <sub>38</sub> O	270	1.19
77	58.166	1-Heneicosanol	C <sub>21</sub> H <sub>44</sub> O	312	0.51
				<b>sum</b>	<b>27.74</b>

**Appendix D: GC-MS Spectra of heavy distillate and pyrolytic liquid oils****Figure D. 1: GC-MS Spectra of Heavy distillate****Figure D. 2: GC-MS Spectra of Pyrolytic liquid oil (without catalyst)**

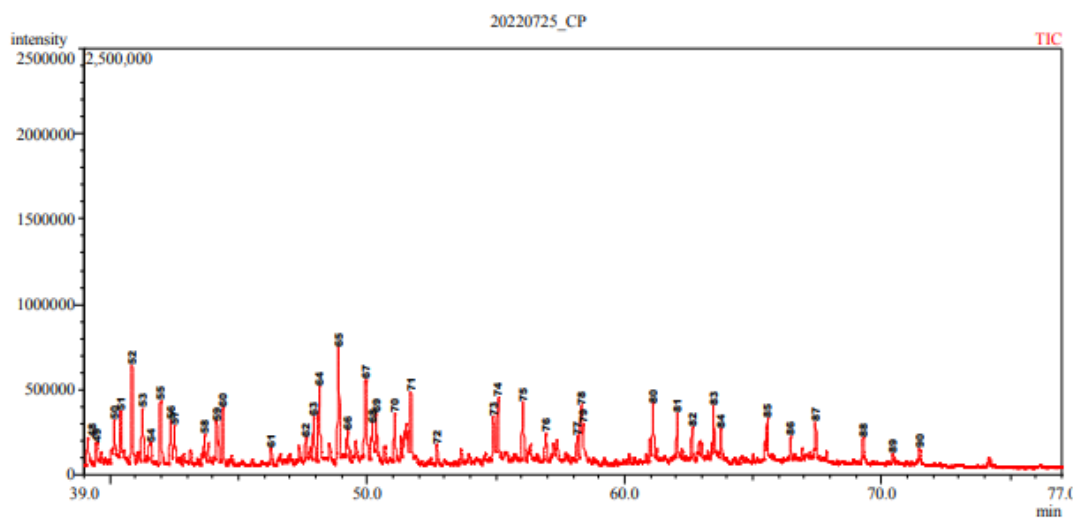


**Figure D. 3: GC-MS Spectra of Pyrolytic liquid oil (with catalyst)**

### Appendix E: Activation energy of HD with MCRM at various phases

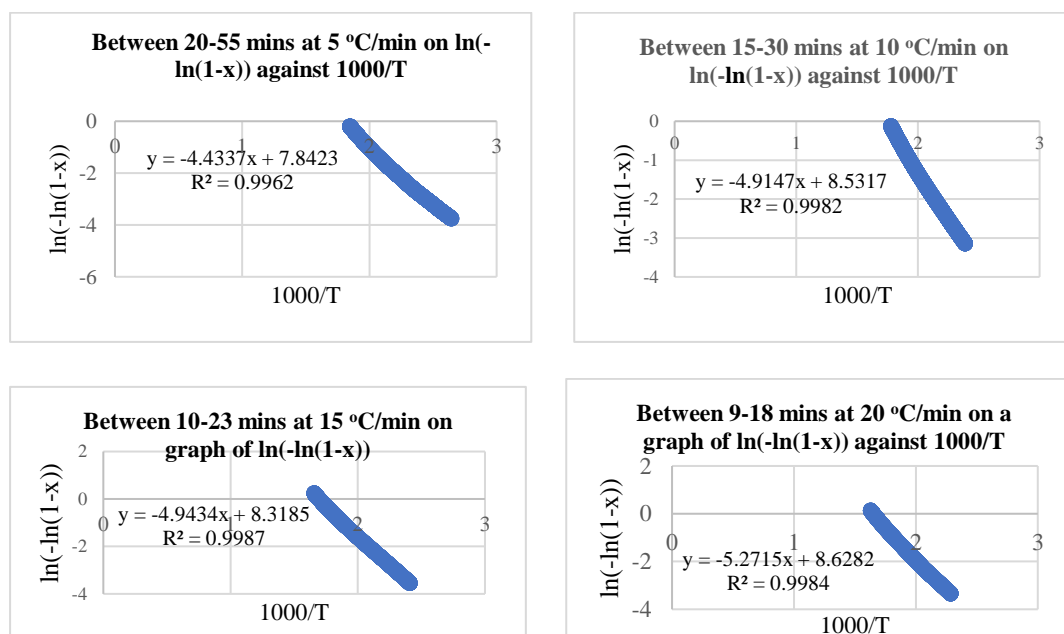


Figure E. 1: Dehydration phase of HD at various heating rates with MCRM

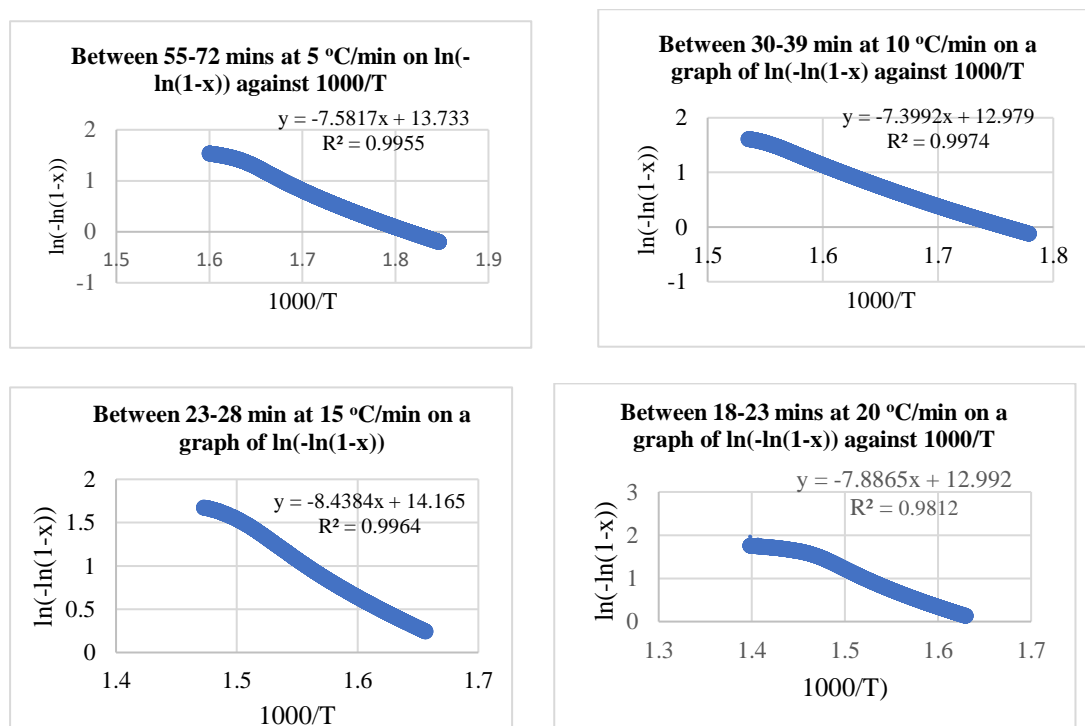
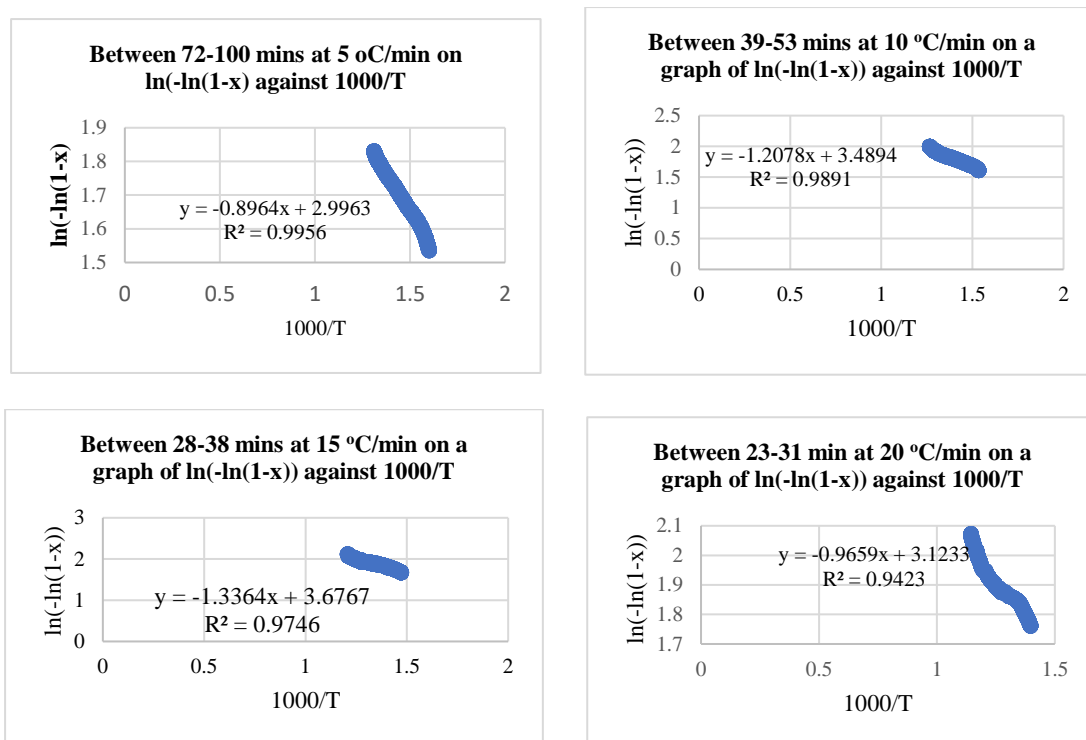


Figure E. 2: Decomposition phase of HD at various heating rates with MCRM





**Figure E. 3: Condensation phase of HD at various heating rates with MCRM**

### Appendix F: Rate constants of HD from slope of $\ln(1-x)$ against time

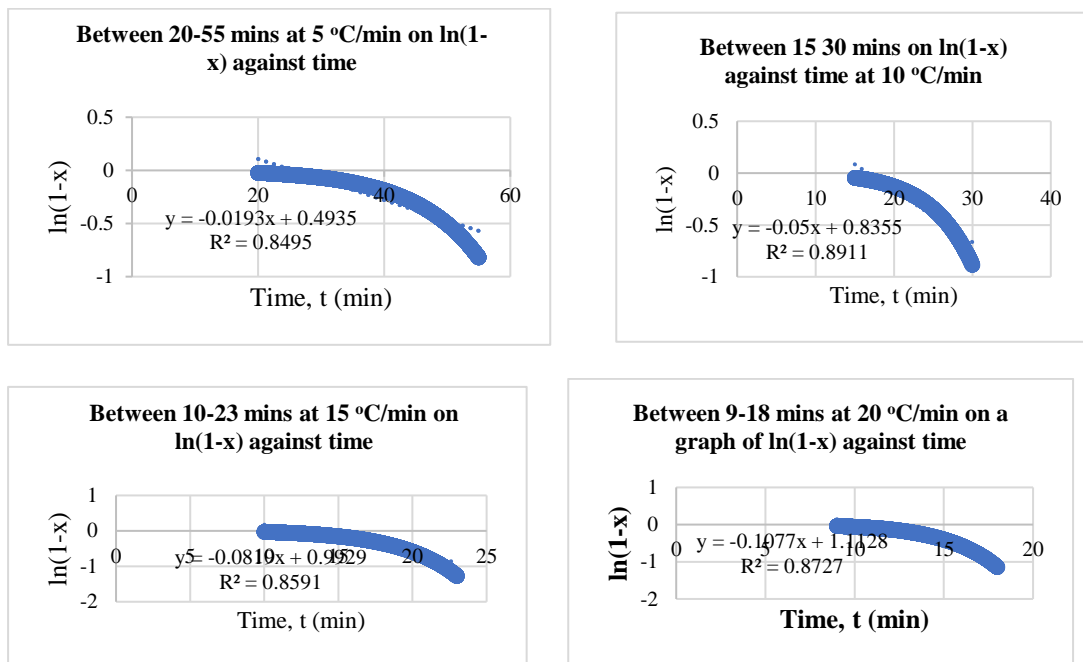


**Figure F. 1: Dehydration phase of HD from  $\ln(1-x)$  vs. time**

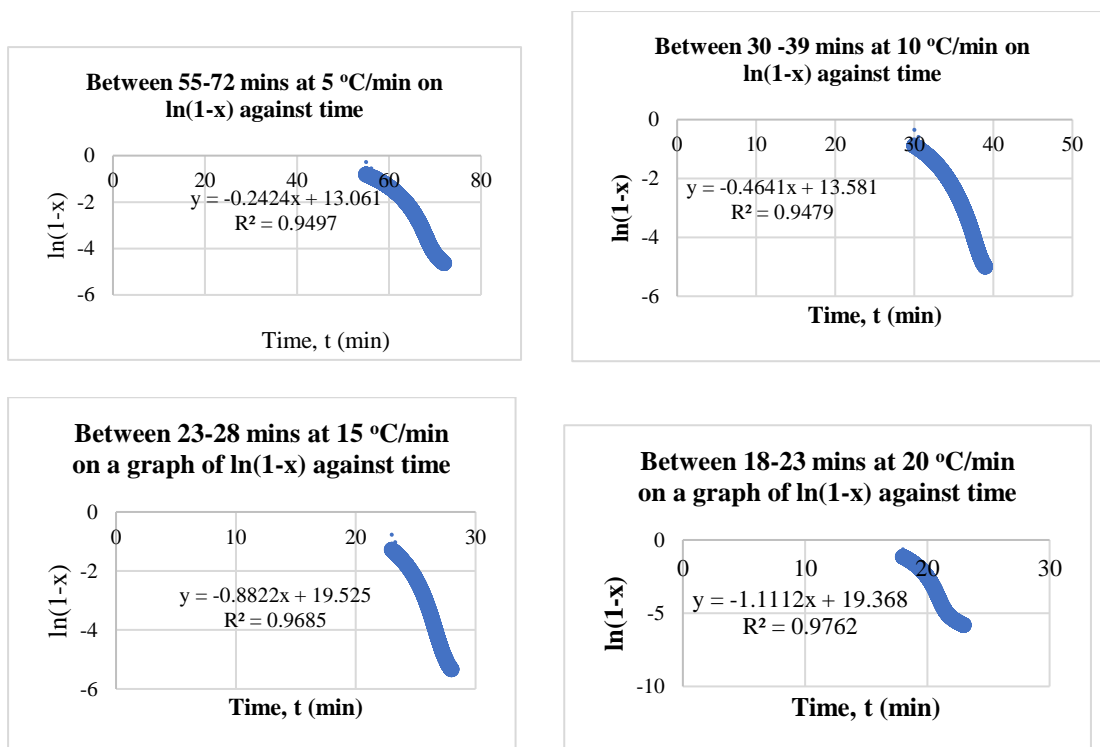


Figure F. 2: Decomposition phase of HD from  $\ln(1-x)$  vs. time

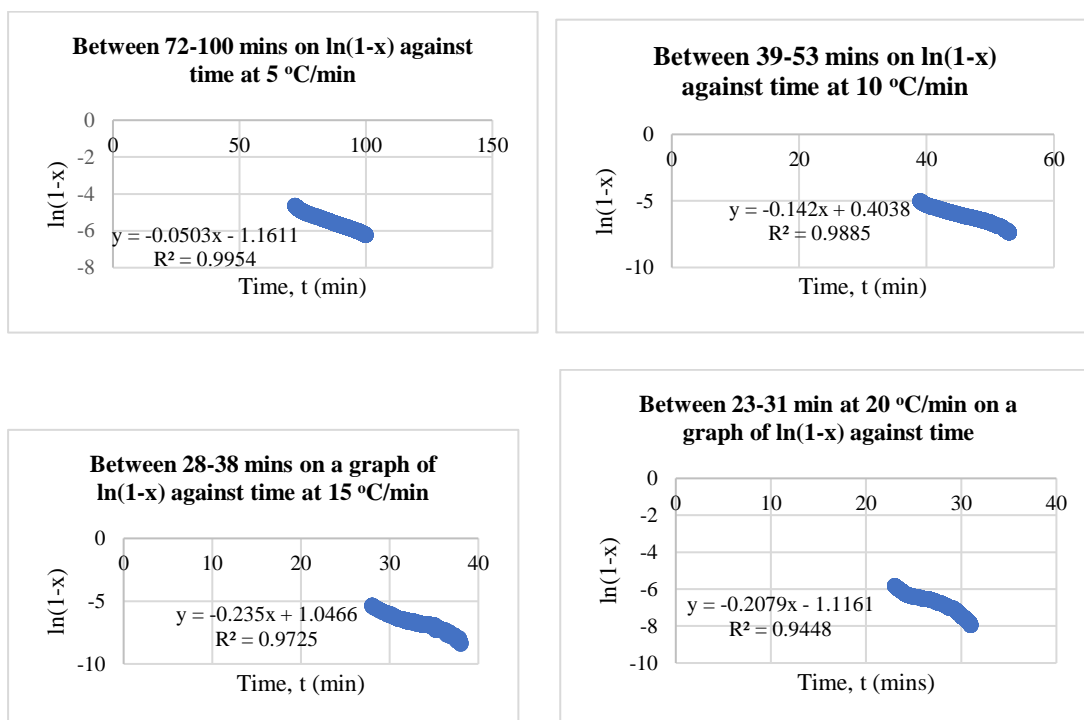


Figure F. 3: Condensation phase of HD from  $\ln(1-x)$  vs. time

## Appendix G: Calculation of thermodynamics parameters of HD

**Table G. 1: Activation energy of HD from MCRM at 5 oC/min**

phase	Temp (°C)	Temp (K)	T <sup>2</sup>	Slope from Graphs	Slope *1000	Coefficient of Determination, R <sup>2</sup>	E <sub>a</sub> (J/mol) (Slope*8.3143)
Dehydration	268	541	292681	4.4337	4433.7	0.9962	36863.11191
Decomposition	352	625	390625	7.5817	7581.7	0.9955	63036.52831
Condensation	490	763	582169	0.8964	896.4	0.9956	7452.93852

**Table G. 2: Frequency factor of HD at 5 °C/min from MCRM at respective phases**

Heating Rate (β) (K/min)	β*E <sub>a</sub>	RT <sup>2</sup>	βE <sub>a</sub> /RT <sup>2</sup>	Intercept	Exp (Intercept)	βE <sub>a</sub> /RT <sup>2</sup> * Exp (Intercept) = A (M min <sup>-1</sup> )	Frequency Factor, A (M sec <sup>-1</sup> )
5	184315.6	2433437.64	0.075743	7.8423	2546.05	192.8454486	3.21409081
5	315182.6	3247773.44	0.097046	13.733	920801.72	89359.90234	1489.331706
5	37264.69	4840327.72	0.007699	2.9963	20.01	0.154063348	0.002567722

**Table G. 3: Entropy changes of HD at 5 °C/min from MCRM at respective phases**

Planck's Constant (h)	Ah	Boltzmann's Constant (K)	KT	Ah/KT	ln(Ah/KT)	Entropy, S R*ln(Ah/KT)
6.63E-34	2.13E-33	1.38E-23	7.47E-21	2.85E-13	-28.8848	-240.1568051
6.63E-34	9.87E-31	1.38E-23	8.63E-21	1.14E-10	-22.8906	-190.3191791
6.63E-34	1.70E-36	1.38E-23	1.05E-20	1.62E-16	-36.3609	-302.3155034

**Table G. 4: Enthalpy and Gibbs Free Energy changes of HD at 5 °C/min**

RT	Enthalpy, J/mol		Gibbs Free Energy, J/mol
	$H = E_a - RT$	$T\Delta S$	$\Delta G = \Delta H - T\Delta S$
4498.036	32365.08	-129925	162289.9072
5196.438	57840.09	-118949	176789.5778
6343.811	1109.128	-230667	231775.8567

**Table G. 5: Activation energy of HD from MCRM at 10 °C/min**

phase	Temp (oC)	Temp (K)	T <sup>2</sup>	Slope	Slope *1000	Coefficient of Determination, R <sup>2</sup>	E <sub>a</sub> (J/mol) (Slope*8.3143)
Dehydration	289	562	315844	-4.9197	4919.7	0.9982	40903.86171
Decomposition	378	651	423801	-7.3992	7399.2	0.9974	61519.16856
Condensation	517	790	624100	-1.2078	1207.8	0.9891	10042.01154

**Table G. 6: Frequency factor of HD at 10 °C/min from MCRM**

Heating Rate ( $\beta$ ) (K/min)	$\beta * E_a$	RT <sup>2</sup>	$\beta E_a / RT^2$	Intercept	Exp (Intercept)	$\beta E_a / RT^2 * \text{Exp (Intercept)} =$ A (M min <sup>-1</sup> )	Frequency Factor A (M sec <sup>-1</sup> )
10	409038.6	2626022	0.155763605	8.5317	5073.06	790.19854	13.1699756
10	615191.7	3523609	0.174591377	12.979	433219.58	75636.40348	1260.6067
10	100420.1	5188955	0.019352668	3.4894	32.77	0.63411497	0.010569

**Table G. 7: Entropy changes of HD at 10 oC/min from MCRM**

Planck's Constant (h)	Ah	Boltzmann's Constant (K)	KT	Ah/KT	ln(Ah/KT)	R*ln(Ah/KT)
6.63E-34	8.73E-33	1.38E-23	7.76E-21	1.13E-12	-27.5125	-228.7470
6.63E-34	8.36E-31	1.38E-23	8.98E-21	9.30E-11	-23.0981	-192.0443
6.63E-34	7.01E-36	1.38E-23	1.09E-20	6.43E-16	-34.9808	-290.8410

**Table G. 8: Enthalpy and Gibbs Free Energy changes of HD at 10 oC/min**

RT	Enthalpy, J/mol		Gibbs Free Energy, J/mol	
	H = Ea-RT	TΔS	ΔG = ΔH - TΔS	
4672.6366	36231.22511	-128555.8065	164787	
5412.6093	56106.55926	-125020.8607	181127.4	
6568.297	3473.71454	-229764.3968	233238.1	

**Table G. 9: Activation energy of HD from MCRM at 15 °C/min**

phase	Temp (oC)	Temp (K)	T <sup>2</sup>	Slope	Slope (x1000)	Coefficient of Determination, R <sup>2</sup>	E <sub>a</sub> (J/mol) (Slope*8.3143), E <sub>a</sub> (J/mol)
dehydration	331	604	364816	4.9434	4943.4	0.9987	41101
Decomposition	406	679	461041	8.4384	8438.4	0.9964	70159
Condensation	555	828	685584	1.3364	1336.4	0.9746	11111

**Table G. 10: Frequency factor of HD at 15 °C/min from MCRM**

Heating Rate ( $\beta$ ) (K/min)	$\beta * E_a$	$RT^2$	$\beta E_a / RT^2$	Intercept	Exp (Intercept)	$\beta E_a / RT^2 * \text{Exp (Intercept) A}$ (M min <sup>-1</sup> )	Frequency Factor, A (M sec <sup>-1</sup> )
15	616513.7	3033190	0.203256	8.3185	4099.006884	833.1472838	13.88578806
15	1052391	3833233	0.274544	14.165	1418343.217	389397.4963	6489.958271
15	166668.5	5700151	0.029239	3.6767	39.51577661	1.155413863	0.019256898

**Table G. 11: Entropy changes of HD at 15 °C/min from MCRM**

Planck's Constant (h)	Ah	Boltzmann's Constant (K)	KT	Ah/KT	ln(Ah/KT)	Entropy, $\Delta S$ R*ln(Ah/KT)
6.63E-34	9.21E-33	1.38E-23	8.34E-21	1.10E-12	-27.5316	-228.9062
6.63E-34	4.30E-30	1.38E-23	9.37E-21	4.59E-10	-21.5015	-178.7701
6.63E-34	1.28E-35	1.38E-23	1.14E-20	1.12E-15	-34.4278	-286.2432

**Table G. 12: Enthalpy and Gibbs Free Energy changes of HD at 15 °C/min**

RT	Enthalpy, J/mol		Gibbs Free Energy, J/mol	
	H = Ea-RT	$T\Delta S$	$\Delta G = \Delta H - T\Delta S$	
5021.8372	36079	-138259	174338	
5645.4097	64514	-121385	185899	
6884.2404	4227	-237009	241236	

**Table G. 13: Activation energy of HD from MCRM at 20 °C/min**

phase	Temp (°C)	Temp (K)	T <sup>2</sup>	Slope	Slope*1000	Coefficient of Determination, R <sup>2</sup>	E <sub>a</sub> (J/mol) (Slope*8.3143)
Dehydration	341	614	376996	5.2715	5271.5	0.9984	43828.83
Decomposition	442	715	511225	7.8865	7886.5	0.9812	65570.73
Condensation	601	874	763876	0.9659	965.9	0.9423	8030.78

**Table G. 14: Frequency factor of HD at 20 °C/min from MCRM**

Heating Rate (β)	β*E <sub>a</sub>	RT <sup>2</sup>	βE <sub>a</sub> /RT <sup>2</sup>	Intercept	Exp (Intercept)	βE <sub>a</sub> /RT <sup>2</sup> * Exp (Intercept) A (M min <sup>-1</sup> )	Frequency Factor, A (M sec <sup>-1</sup> )
20	876576.649	3134457.843	0.279658	8.6282	5587.013	1562.453542	26.041
20	1311414.539	4250478.018	0.308533	12.992	438888.2	135411.6807	2256.861
20	160615.6474	6351094.227	0.025289	3.1233	22.72124	0.574607449	0.009576

**Table G. 15: Entropy changes of HD at 20 °C/min from MCRM**

Planck's Constant (h)	Ah	Boltzmann's Constant (K)	KT	Ah/KT	ln(Ah/KT)	Entropy, ΔS R*ln(Ah/KT)
6.63E-34	1.73E-32	1.38E-23	4.71E-21	3.67E-12	-26.3311	-218.9249
6.63E-34	1.50E-30	1.38E-23	6.10E-21	2.45E-10	-22.1285	-183.9829
6.63E-34	6.35E-36	1.38E-23	8.29E-21	7.66E-16	-34.8059	-289.3869

**Table G. 16: Enthalpy and Gibbs Free Energy changes of HD at 20 °C/min**

RT	Enthalpy, J/mol		Gibbs Free Energy, J/mol	
	H = Ea-RT	TΔS	ΔG = ΔH - TΔS	
2835.176	40993.66	-74653.4	115647.05	
3674.921	61895.81	-81320.5	143216.27	
4996.894	3033.89	-173922	176955.40	